Fault Tolerant Attitude Control of a Pico-Satellite Equipped with Reaction Wheels and Magnetorquers

Group 18gr1033

Aalborg University
Control & Automation
Fredrik Bajers Vej 7
DK-9220 Aalborg

AALBORG UNIVERSITY
STUDENT REPORT

10th Semester, Project

Technical Faculty of IT and Design

Department of Electronics Systems

Control and Automation

Fredrik Bajers Vej 7C

9220 Aalborg

en.aau.dk/education/master/control-automation

Title:
Fault Tolerant Attitude Control of a Pico-Satellite Equipped with Reaction Wheels and Magnetorquers

Theme:
Master thesis

Project Period:
P10, Spring 2018
01/02/2018 - 07/06/2018

Project Group:
18gr1033

Participants:
- Dániel Bolgár
- Nikolaos Biniakos
- Alexandru-Cosmin Nicolae

Supervisors:
Jesper Abilgaard Larsen

Pages:
Appendices: 2 (4 pages)
Attached: 1 zip file
Concluded: 07/06/2018

Synopsis

The thesis investigates actuator fault detection and fault tolerant control algorithms of a picosatellite equipped with reaction wheels and magnetorquers. The control scheme is developed and tested in a simulation environment instead of a real pico-satellite.

Preface

This report has been written by group 1033 during fourth semester in Control and Automation MSc in Aalborg University, Department of Electronic Systems during the period from February 2018 to June 2018. It is written as a Master's thesis for the Control and Automation Master's program.

A nomenclature is included presenting the acronyms, symbols and terminology used throughout the thesis. Quotes are inside quotation marks and are cursive.

The authors would like to thank Associate Professor Jesper Abilgaard Larsen for supervising. The authors furthermore would like to thank the students involved in the development of the AAUSAT Simulink Library.

Attached to report is a zip file with:

- The MATLAB code
- Simulink models

Report by:

Dániel Bolgár

Nikolaos Biniakos

Alexandru-Cosmin Nicolae

Contents

Nomenclature

Notations

Vectors used have a bold typeface.

$$\mathbf{v}$$

Matrices are underlined.

$$\underline{A}$$

The identity matrix is denoted as:

$$\underline{\mathbf{1}}$$

Cross product operations can be evaluated by taking the skew symmetric matrix of the left vector and executing a matrix multiplication. The skew symmetric matrix of $\mathbf{v}$ is denoted as $\underline{v}^{\times}$. The 4×4 skew symmetric matrix of quaternions are denoted as $\underline{q}^{\times}$ in a similar fashion.

$$\mathbf{w} = \mathbf{u} \times \mathbf{v} = \underline{u}^{\times}\mathbf{v}$$

Matrix transposition is denoted as

$$\underline{A}^T$$

If a non-square matrix has to undergo an operation similar to inversion, Moore-Penrose pseudoinverse is used. Pseudoinverse matrix is indicated as $\underline{A}^{\dagger}$. If the matrix satisfies $rank(\underline{A}) = min(m, n)$ and $m < n$, the left pseudoinverse is used as follows

$$\underline{A}^{\dagger} = (\underline{A}^T\underline{A})^{-1}\underline{A}^T$$

If $n < m$, the right pseudoinverse is used as follows

$$\underline{A}^{\dagger} = \underline{A}^T(\underline{A}\underline{A}^T)^{-1}$$

The majority of equations are expressed in satellite body reference frame (SBRF). Unless it is not explicitly noted, the matrices and vectors are expressed in SBRF. In case the expression is in Earth centered inertial frame (ECI), it is noted in the superscript as

$$\mathbf{XY}^{[I]}$$

The rotation quaternion and angular velocity between frames use the subscript to denote the frame where the transformation is done from, the superscript is the symbol of the frame being transformed into. In case the frame symbols are not present, it should be interpreted as a transformation from inertial frame to satellite body reference frame.

$${}^{\mathbf{s}}_{\mathbf{i}}\mathbf{q}(\mathbf{t})$$

Rotation matrix corresponding to rotation matrix ${}^{\mathbf{s}}_{\mathbf{i}}\mathbf{q}(\mathbf{t})$ is denoted as

$$\underline{R}({}^{\mathbf{s}}_{\mathbf{i}}\mathbf{q}(\mathbf{t}))$$

A subarray of an array is denoted as $\mathbf{a}_{4:7}$. When only the vector part of a quaternion is used, it is denoted as

$$\mathbf{q}_{1:3}$$

The scalar component of a quaternion is denoted as

$$\mathbf{q}_4$$

The complex of a quaternion is denoted as

$$\mathbf{q}^*$$

In sections using linearization, operating points of variables are denoted as

$$\bar{\mathbf{v}}$$

Deviations from the operating point are denoted as

$$\tilde{\mathbf{v}}$$

When discussing control schemes, a d in the superscript denotes the variable referring to a control demand. If the d is not present, the variable refers to the actual value. An e (as in error) in superscript denotes the difference between demand and actual value.

$$N^d$$

Faults in magnetorquers or reaction wheels are denoted as

$$\mathcal{F}_{MT} \text{ or } \mathcal{F}_{RW}$$

Acronyms

AAUSAT The name of the satellites developed at Aalborg University

ADCS Attitude Determination and Control System

AIS Automatic Identification System

COM Center of Mass

DaMSA Danish Maritime Safety Administration

ECEF Earth Centered Earth Fixed Frame

ECI Earth Centered Inertial Frame

FDI	Fault Detection and Isolation
FMEA	Failure Mode and Effects Analysis
LEO	Low Earth Orbit
OI	Occurrence Index
SBRF	Satellite Body Reference Frame
SI	Severity Index
SMC	Sliding Mode Control
SO	Severity and Occurrance
UIO	Unknown Input Observer

Symbols

$\underline{A}_{M,fi}$	Transformation matrix between axis oriented reaction wheel torque and torques in 3 dimensional body frame in case of faulty ith reaction wheel
$\underline{A}_M$	Transformation matrix between axis oriented reaction wheel torque and torques in 3 dimensional body frame
$\mathbf{B}$	local geomagnetic field in body fixed frame
$\mathbf{d}$	Disturbance input
$\mathbf{F_{MT}}$	The fault vector for the magnetorqers
$\mathbf{F_{RW}}$	The fault vector for the reaction wheels
$\mathbf{h_{ref}}$	The reference angular momentum vector of the reaction wheels
$\mathbf{h_{rw}}$	The angular momentum vector of the reaction wheels
$\mathbf{h_T}$	Total angular momentum of the satellite
$\mathbf{h_{sat}}$	Angular momentum of the satellite
$\underline{I}_s$	Satellite inertia matrix
I_w	Reaction wheel axial moment of inertia
$\mathbf{m}_{mt}$	The magnetic dipole moment
$\mathbf{m_{mt}}$	Magnetorquer magnetic moment

$\mathbf{N_M}$	4×1 vector containing the reaction wheel motor motor torques parallel to their axes
$\mathbf{N_{rw}}$	Reaction wheel torque in body frame
$\mathbf{N_{ctrl}}$	The torque from magnetorquers and the reaction wheels
$\mathbf{N_{dist}}$	Disturbance torque
$\mathbf{N_{mt}}$	The torque from magnetorquers
$\mathbf{q}_\omega$	The angular velocity quaternion
ω_o	Orbit angular velocity
$\bar{\mathbf{q}}$	The operating point of the quaternion
${}^{\mathbf{s}}_{\mathbf{i}}\tilde{\mathbf{q}}(\mathbf{t})$	The error quaternion
${}^{\mathbf{s}}_{\mathbf{i}}\dot{\mathbf{q}}(\mathbf{t})$	The rotation from ECI to SBRF using the quaterion $\mathbf{q}$
$\mathbf{u}$	Control input
$\boldsymbol{\omega}(\mathbf{t})$	Angular velocity
$\bar{\boldsymbol{\omega}}(\mathbf{t})$	The operating point of angular velocity
$\tilde{\boldsymbol{\omega}}(\mathbf{t})$	The error in the angular velocity

Terminology

Nadir	The axis pointing towards Earth's center of mass
Picosatellite	Picosatellites are small satellites with mass between 0.1 and 1 kg.
Precession	A rotating body can experience a change in the orientation around the rotational axis.
Vernal Equinox	The vernal equinox is the vector pointing towards the Sun's center during the equinox (20th of March in 2018). The x vector also keeps its direction relative to the stars.

1 | Introduction

Satellites are no longer the privilege of just a handful of economic powerhouses such as nations or mega companies. There are currently 1738 active satellites orbiting Earth, 129 of it is categorized as having civil uses, created mostly for educational purposes [2]. The ongoing AAUSAT project at Aalborg University is part of this educational effort. AAUSATs are mostly student built low-cost picosatellites, 5 of them already in orbit, the next one is currently in development [1]. The mission goal of each of them include taking pictures of Earth and celestial objects and downlink them, or even tracking objects on Earth's surface. These require precise attitude control of the satellite.

Satellite attitude control differs fundamentally from the attitude control of earthbound objects, and is more challenging, as there is no direct mechanical connection available to other objects. Thus attitude control can be achieved using different interactions, such as transferring angular momentum between components of the satellite, utilizing the magnetic field of Earth or solar sails, or in some cases rocket propellants.

While the satellites themselves can be chosen to be engineered relatively cheaply, there is no way of avoiding the high cost of putting the satellite into orbit. Many efforts were made recently to reduce this cost. Since the cost is highly dependent on the weight of the satellite, by minimizing the weight, a lot of money can be saved. The per kilogram cost of putting an object to Low Earth Orbit (LEO) in the case of Falcon Heavy, 1655 USD [24], however this price only applies for 54400 kg payload. There are rockets missions with the purpose of putting several satellites into orbit, thus reducing the cost for individual satellites. The sizing unit of the satellites involved in such missions is standardized. One unit is $10 \times 10 \times 10$ cm and 1 kg. AAU CUBESAT fits into one unit, thus costing 49000 USD to put in orbit [8].

The weight constraint had to be taken into account when designing each component of the satellite. For the attitude control system it means that using propellants excessively is not an option. To make quick attitude control possible, reaction wheels are used as actuators, supported by magnetorquers for desaturation.

Since putting satellites into orbit is quite costly, a lot of effort is made to prevent system failures. It is imperative to design the satellite in such a way that a fault in one of the modules does not lead to mission failure. The satellite is designed to withstand extreme temperature changes, large accelerations during launch etc. Every part is made to last as long as possible. Attitude estimation schemes are outside the scope of the thesis. In order to be able to handle faults in actuators, a fault-tolerant control scheme is implemented. This thesis explores several fault detection and fault handling schemes involved in fault tolerant attitude control.

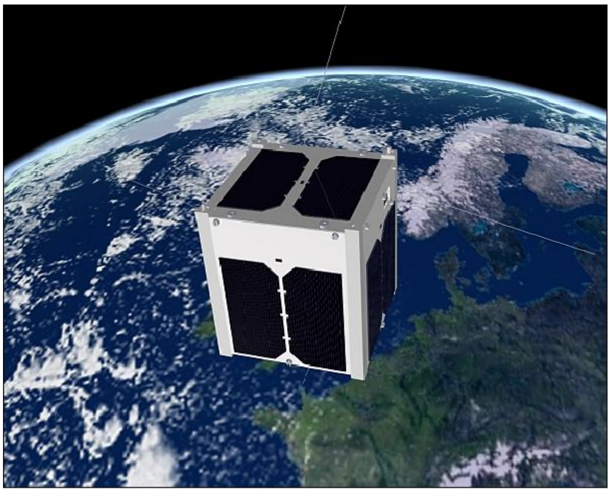

Figure 1.1: AAUSAT on Duty. An Illustration. [**imref**]

1.1 Problem statement

The objective of the present thesis is to implement a fault-tolerant attitude control scheme for a pico-satellite equipped with magnetorquers and reaction wheels. The fault tolerant control scheme isolates actuator faults.

1.2 Use-case

To further expand the problem statement stated above, a use case is conceived. In order to achieve the mission task, the use case is constructed for proving the system requirements.

The mission of AAUSAT-3 is used as a reference for establishing the use-case. One of the tasks of the pico-satellite is to track ships in arctic regions. This steams from the desire of the Danish Maritime Safety Administration (DaMSA) to improve naval safety by monitoring the ships. The test area would be around Greenland, where monitoring is lacking.

In order to achieve this objective, a Low Earth Orbit satellite is deployed and Automatic Identification System (AIS) signals are used for exchanging information with a ground station. As secondary mission the satellite has to gather pictures of the Arctic regions.

If the requirement for the satellite is tracking objects on Earth, the tracking torque demand can be calculated using knowledge about satellite altitude, orbit shape and the corresponding satellite speed, and satellite moment of inertia. For a circular orbit at 600 km altitude, the satellite speed would be $7.56km/s$ according to [22]. Appendix D presents the graphs used in deriving the torque demand for Earth station pointing. A maximum torque of $2.388 \cdot 10^{-7} Nm$ was calculated, which acts as a requirement for the actuators torque output.

2 | System Description

This chapter presents a description of the system configuration, which includes mechanical properties, sensors and actuators description and Attitude Determination and Control System (ADCS) approaches.

The satellite used as a reference in this thesis is a CubeSat, depicted in figure 2.1, a pico-satellite that has been designed by California Polytechnic State University. This concept of satellite impose a few constrains. The dimensions of a 1U CubeSat is $10 \times 10 \times 10$ cm with a mass of 1kg, giving the advantage of having a light weight leading to a low power consumption, and a drawback of limited space. In order to enlarge the space within the satellite, the dimensions could be changed when designing it, such that a 3U design might be suitable for a satellite that will contain solar arrays or thrusters.

From figure 2.1 it can be seen that the satellite contains three magnetorquers shown as an example, but for the scope of the current thesis a pico-satellite equipped with three doubled and orthogonal magnetorquers is used. Also the CubeSat image shows the solar panels with on board electronics.

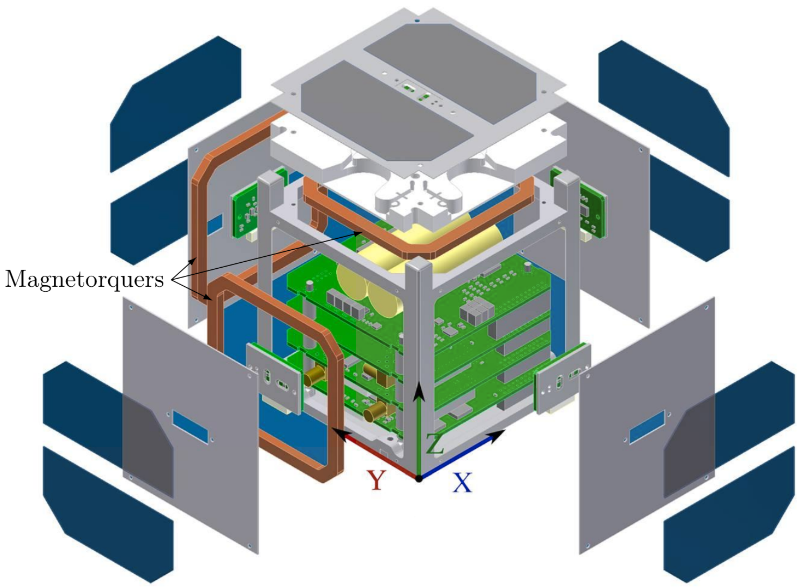

Figure 2.1: CubeSat exploded view [9]

The satellite is equipped with two types of attitude actuators, magnetorquers and reaction wheeels. In order to keep the reaction wheels controllable, desaturation is performed using magnetorquers.

ADCS approaches

The objective of the ADCS system illustrated in figure 2.2 will be to control the angular velocity of the satellite and also to point to a specific target located on Earth. Therefore, a few procedures can be taken into account:

Detumbling is the phase right after the satellite is deployed from the device called P-POD. The control goal during this phase is to decrease the angular velocity of the satellite.

Desaturation means decreasing reaction wheel angular velocity in order to keep the wheels from saturation, thus keeping the wheels controllable in both directions.

Pointing pointing involves keeping the satellite attitude stabilized at the reference attitude.

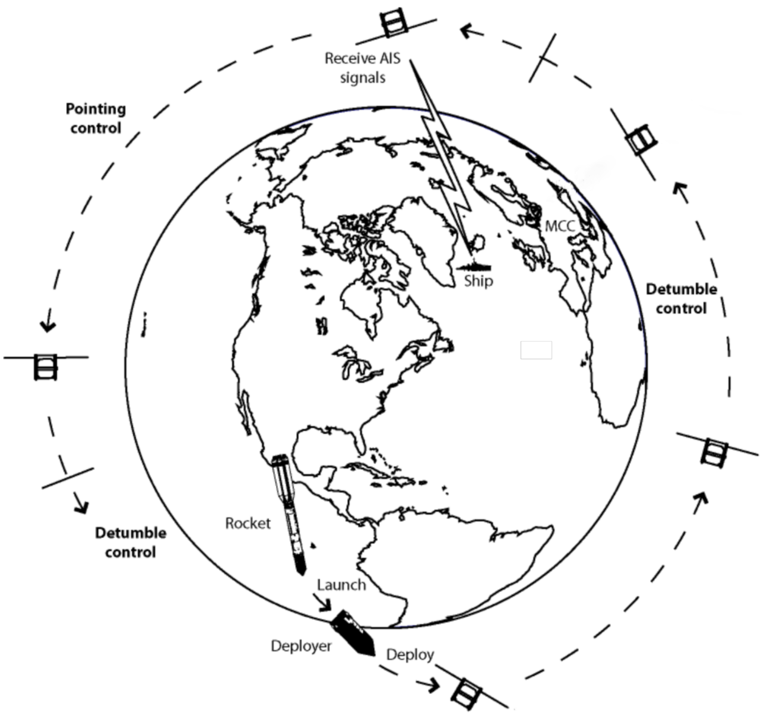

Figure 2.2: ADCS system description [11]

2.1 Sensors

This section presents an overview about the various types of sensors the satellite contains on board and has been used for attitude determination.

Magnetometer

The orbit of the satellite is predictable, the satellite's location can be described as a function of time. Earth's magnetic field can also be quite accurately modeled. This means that by using magnetometer, the orientation of the satellite can be approximated by comparing Earth's magnetic field model at the satellite's current location and the direction of the magnetic field in the SBRF attributed to Earth following the magnetometer measurements. To address the noise in the measurement, including the noise arising from inside the satellite, Kalman or particle filtering, along with sensor fusion can be used, however this is outside of the scope of the thesis.

Sun Sensor

Sun trackers can be much easier to develop than star trackers. They measure the Sun's orientation in relation to the satellite frame. By using it alongside other sensors, higher accuracy attitude estimation can be achieved. However when Earth is obstructing the sun rays, it is unable to provide attitude data, thus it is not sufficient to only use a sun tracking sensor.

Gyroscope

The gyroscope is another type of attitude determination sensor, used for measuring the rate of change of the satellite orientation. Thus, a gyroscope is measuring the angular velocity of the satellite.

2.2 Actuators

This section describes the attitude actuators that the satellite is equipped with.

Reaction Wheels

One method of controlling a spacecraft's attitude is by using either reaction or momentum wheels attached to the spacecraft's body. The difference between momentum and reaction wheels is that the nominal angular velocity of momentum wheels is high in order to store angular momentum, while for reaction wheels, low. By controlling the wheel's angular velocity using a motor, the amount of angular momentum stored in the wheel can be controlled. If there are no external forces involved, the sum of angular momentum in the system made up by the spacecraft's body and the reaction wheels is constant. This means that by increasing the angular velocity of the wheels, the satellite body's angular momentum can be reduced. This angular momentum transfer can be used to control the attitude of the satellite. If the goal is to change the angular momentum of the whole satellite, actuators that are capable of external interaction should be used, such as magnetorquers or solar sails.

In some satellites, the reaction wheels nominal speed is set higher than zero in order to avoid static friction in the bearings. Reaction wheels usually make up only a small fraction of a satellite's weight. They rely on being able to run at high speeds, making their angular momentum significant. The small weight ratio makes precise controlling easier.

Reaction wheels have an angular velocity limitation. This means that if a reaction wheel reaches its maximum angular velocity, it can no longer generate a torque on the satellite's body in one direction. In this scenario the system's controllability decreases, thus it should be avoided. An angular momentum unloading strategy should be designed to avoid it. Instead of returning the angular momentum to the satellite's body, unloading the angular momentum through other methods is preferred. Magnetorquers can be used for such purposes.

Moving parts are usually prone to failures. Reaction wheels are expected to occasionally run at high angular velocities, which wears down the lubrication and the bearings. Reaction wheels equipped with active magnetic bearings are in development [16]. These can eliminate friction from the system and by controlling the bearing, can even reduce micro-vibrations, increasing the durability of the system. AAUSAT-II itself however uses mechanical wheel bearings.

Magnetorquer

Magnetorquers are special coils that can control the satellite's attitude by creating a magnetic momentum that interacts with Earth's magnetic field. It is capable of changing the total angular momentum of the satellite. Magnetorquers can only exert torque in two dimensions at any given moment, however over one orbit, three dimensional control can be achieved. In the investigated satellite they function as secondary actuators, with their purpose being the desaturation of the reaction wheels. Precise torque control can be achieved by setting up coaxial magnetorquers, one of which equipped with an iron core for larger magnetic field, the other lacking an iron core for finer magnetic field control.

3 | Requirements

Based on the use-case introduced and the available system, a set of requirements are formulated.

System requirements

1. **The satellite shall track the nadir within 1°.**
2. **The satellite should be able to track the Earth station within 1°.**
3. **The satellite shall detect certain actuator faults.**
4. **The satellite should be able to reconfigure the control scheme in order to handle faults.**

4 | Satellite Modeling

In the following chapter the modeling of the satellite is described. First, different reference frames are introduced for describing the attitude of the satellite. Next, the equations governing satellite rotation dynamics and kinematics are derived and linearized for the purpose of designing a linear controller. Finally, the main disturbances that a satellite can encounter in LEO are identified.

4.1 Reference Frames

Using different reference frame for different calculations can simplify equations. Values in one reference frame can be converted into the other by using the proper transformations. Inertial frames of reference are frames where Newton's three laws of dynamics apply. The most used reference frames for Earth-orbiting satellites are Earth Centered Inertial Frame (ECI), Earth Centered Earth Fixed Frame (ECEF), Orbit Frame, Satellite Body Reference Frame (SBRF) [7] [14]. Figure 4.1 provides a visualization of the frames.

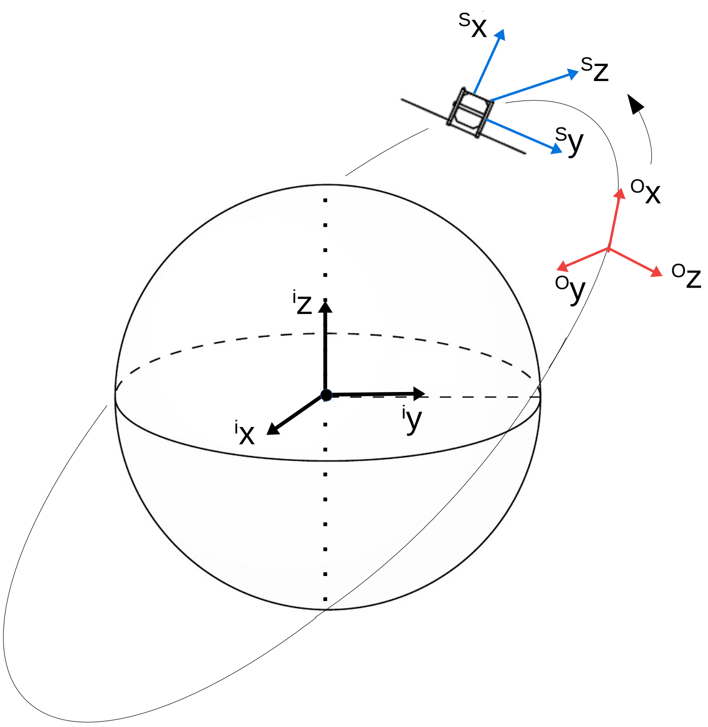

Figure 4.1: Reference frame axes. Superscripts: i - ECI, o - Orbital, s - Satellite Body Frame [21].

Earth Centered Inertial Frame (ECI)

Earth is rotating and is orbiting the Sun, it accelerates in the direction of the Sun's center of mass, the Sun is orbiting the center of the Milky Way, etc. Thus there is no frame fixed to Earth's center that is an inertial frame *per definitionem*. But in the case of earth orbiting satellites, there exists a coordinate system attached to Earth's center that out of practical considerations can be treated as one, the Earth Centered Inertial Frame (ECI). As the name suggests, the origin of the coordinate system is the center of earth. Inertial means that the frame does not rotate, the direction of stars remain the same. ECI is a cartesian coordinate system. Its ${}^{i}z$ vector points in the direction of the northern axis of rotation, while the ${}^{i}x$ axis towards the vernal equinox. The ${}^{i}y$ axis completes the triad of the right-handed Cartesian coordinate system.

Earth Centered Earth Fixed Frame (ECEF)

ECEF, similarly to ECI is centered at the Earth's origin. Its z vector points towards the north parallel to the rotational axis. Its x axis points at 0 deg latitude and 0 deg longitude on the Earth's surface, thus following Earth's rotation. This makes ECEF non-inertial. y axis completes the right-handed triad.

Orbital Frame

The Orbital Frame is centered at the center of mass of the satellite. The ${}^{o}z$ axis points towards the center of Earth, ${}^{o}x$ points in the direction of the satellite's velocity, while ${}^{o}y$ is the normal vector for the orbital plane. The 3 axes make up an orthogonal triad.

Local Vertical, Local Horizontal Frame (LVLH)

The ${}^{lvlh}x$ axis is parallel to the vector pointing from the center of the Earth to the satellite. ${}^{lvlh}z$ is parallel to the orbit normal. ${}^{lvlh}y$ is assigned to complete the right-handed orthogonal triad.

Satellite Body Reference Frame (SBRF)

Body-fixed frames are attached to the satellite's body, but the orientation of the frame in relation to the body is arbitrary. Due to practical considerations the axes of the SBRF are chosen to line up with the principal axes of inertia of the body.

4.2 Satellite equations of motion

The satellite equations of motion is split into a kinematic and dynamic model. The kinematic model describes the relation between the orientation of the satellite and the time derivative of the orientation using the rotation of the ECI and SBRF frame. A dynamic model is established in order to relate the torques which influence the satellite and the angular velocity.

The derivation of the satellite equations of motion is presented in appendix C, therefore, putting together both dynamic and kinematic equation derived in the appendix, the system equations of the satellite will be non-linear and can be combined into one equation as follows:

$$\begin{bmatrix} {}^{\mathbf{s}}_{\mathbf{i}}\dot{\mathbf{q}}(\mathbf{t}) \\ \dot{\boldsymbol{\omega}}(\mathbf{t}) \end{bmatrix} = \begin{bmatrix} \frac{1}{2}\underline{\omega}^{\times}{}^{\mathbf{s}}_{\mathbf{i}}\mathbf{q}(\mathbf{t}) \\ -\underline{I}_s^{-1}\underline{\omega}^{\times}\underline{I}_s\boldsymbol{\omega}(t) - \underline{I}_s^{-1}\underline{\omega}^{\times}\mathbf{h_{rw}} + \underline{I}_s^{-1}[\mathbf{N_{rw}}(t) + \mathbf{N_{mt}}(\mathbf{t}) + \mathbf{N_{dist}}(t)] \end{bmatrix} \tag{4.1}$$

where,
- ${}^{\mathbf{s}}_{\mathbf{i}}\mathbf{q}(\mathbf{t}) = [q_1\ q_2\ q_3\ q_4]^T$ is the attitude quaternion
- $\boldsymbol{\omega}(\mathbf{t}) = [\omega_1\ \omega_2\ \omega_3]^T$ is the angular velocity vector relative to the ECI
- $\mathbf{h_{rw}}$ is the angular momentum of the reaction wheels
- $\underline{I}_s$ is the inertia matrix
- $\mathbf{N_{dist}}$ is the disturbance torque
- $\mathbf{N_{rw}}$ is the torque from reaction wheels
- $\mathbf{N_{mt}}$ is the torque from magnetorquers

Linearized equation of motion

For the purpose of designing a linear controller as can be seen in section 5.3 the equations of motion of the satellite need to be linearized. The whole process of linearization is presented in appendix C.

Using the results from appendix C the linear equation of motion can be combined in a state-space form as:

$$\begin{bmatrix} {}^{\mathbf{s}}_{\mathbf{i}}\dot{\tilde{\mathbf{q}}}(\mathbf{t}) \\ \dot{\tilde{\boldsymbol{\omega}}}(\mathbf{t}) \end{bmatrix} = \begin{bmatrix} -\underline{\bar{\omega}}^{\times} & \frac{1}{2}\underline{\mathbf{1}}_{(3\times3)} \\ \underline{0}_{(3\times3)} & \underline{I}_s^{-1}(\underline{I}_s\bar{\boldsymbol{\omega}})^{\times} - \underline{I}_s^{-1}\underline{\bar{\omega}}^{\times}\underline{I}_s \end{bmatrix} \begin{bmatrix} \tilde{\mathbf{q}}(\mathbf{t}) \\ \tilde{\boldsymbol{\omega}}(t) \end{bmatrix} - \begin{bmatrix} \underline{\mathbf{0}}_{(3\times3)} \\ \underline{I}_s^{-1} \end{bmatrix} \tilde{\mathbf{N}}_{\mathbf{ctrl}} \tag{4.2}$$

where,
- $\tilde{\mathbf{N}}_{\mathbf{ctrl}}$ is the torque from magnetorquers and the reaction wheels and is defined as: $\tilde{\mathbf{N}}_{\mathbf{ctrl}} = \mathbf{N_{mt}} + \mathbf{N_{rw}}$
- ${}^{\mathbf{s}}_{\mathbf{i}}\tilde{\mathbf{q}}(\mathbf{t})$ is the error quaternion
- $\tilde{\boldsymbol{\omega}}$ is the error in the angular velocity
- $\bar{\boldsymbol{\omega}}$ is the operating point of angular velocity

4.3 Environmental disturbances

The environmental disturbances can cause a change in the total angular momentum of the spacecraft. The following section will elaborate on the main environmental disturbances that includes aerodynamic, solar radiation, gravity gradient and magnetic disturbance torque, as well as the J_2 orbital perturbation due to oblateness of the Earth. The order of the magnitudes is 10^{-9}.

Orbit perturbation - J_2

Due to Earth's spin, its shape is oblate rather than spherical. This non-spherical mass distribution of the Earth affects a satellite motion in LEO. The gravitational potential is corrected using spherical harmonics which depend only on the latitude. These harmonics affect the satellite, determining its orbit difference compared to ideal mathematical models. An approximation of the gravitational potential of the Earth is [28][21]:

$$U \approx -\frac{\mu}{r}\left[1 - \sum_{n=2}^{\infty}\left(\frac{R_e}{r}\right)^n J_n P_n cos(\theta)\right] = \frac{\mu}{r}[U_0 + U_{J_2} + ...] \tag{4.3}$$

describing deviations of the potential to the South and North direction, with $\mu = GM$, G being the gravitational constant and M the Earth's mass, P_n be Legendre polynomial, θ be a spherical polar coordinate, $R_e = 6.3781 \cdot 10^6 m$ is the mean radius of the Earth at the equator, r is the distance between the earth and the satellite, U_0 = -1, $U_{J_2} = \left(\frac{R_e}{r}\right)^2 J_2 \frac{1}{2}(3cos^2\theta - 1)$ and $J_2 = 1.0826 \cdot 10^{-3}$ be a zonal numerical coefficient and the other terms $(J_3, J_4, ...)$ been discarded since are less significant compared to J_2. The force caused by the J_2 term is written as

$$\mathbf{F}_{J_2} = -m\nabla U \tag{4.4}$$

with the vector $\mathbf{F}_{J_2}$ expand to the force components [26][21] :

$$F_x = -\frac{\partial U}{\partial x} = \mu\left[-\frac{x}{r^3} + A_{J_2}\left(15\frac{xz^2}{r^7} - 3\frac{x}{r^5}\right)\right] \tag{4.5}$$

$$F_y = -\frac{\partial U}{\partial y} = \mu\left[-\frac{y}{r^3} + A_{J_2}\left(15\frac{yz^2}{r^7} - 3\frac{y}{r^5}\right)\right] \tag{4.6}$$

$$F_z = -\frac{\partial U}{\partial z} = \mu\left[-\frac{z}{r^3} + A_{J_2}\left(15\frac{z^3}{r^7} - 3\frac{z}{r^5}\right)\right] \tag{4.7}$$

where $A_{J_2} = \frac{1}{2}J_2 R_e^2$.

Aerodynamic disturbance torque

Gas molecules, in a Low Earth Orbit collide with the surface of the satellite causing a force which direction opposes the direction of the satellites velocity vector. This Aerodynamic force can be modeled as [28, 21]

$$\mathbf{F_A} = -\frac{1}{2}\rho\ C_D\ A_\perp \mathbf{v}^2 \tag{4.8}$$

where ρ is the atmospheric density is chosen to be constant and equal to $1.454 \cdot 10^{-13} Kg/m^3$ based on the Committee on Space Research[19], $\mathbf{v}$ is the satellite velocity vector, $A_\perp$ is

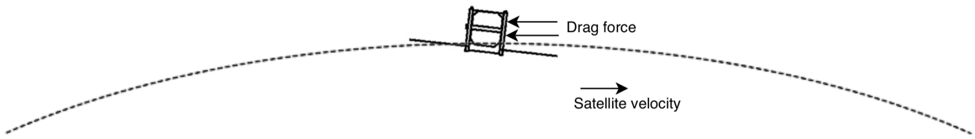

Figure 4.2: Aerodynamic disturbance force action on a orbiting satellite

the area perpendicular to the velocity and C_D is the drag coefficient and is chosen to be equal to 1.5 [28][21] for simulation purposes. If the calculation of the lifetime of the satellite is of great importance a more accurate drag coefficient should be used.

Using the equation 4.8, the aerodynamic torque acting on the satellite can be written as

$$\mathbf{N}_{drag} = \mathbf{r}_s \times \mathbf{F}_A \tag{4.9}$$

where $\mathbf{r}_s$ is the vector from the center of mass of the satellite to the geometric center of the exposed area

Solar radiation disturbance torque

Solar radiation pressure is caused by photons coming from various sources, such as reflection from the Earth's atmosphere, from solar wind and direct radiation from the Sun to the surface of the satellite[28][21] . Direct radiation is larger and only this source will be taken into account.

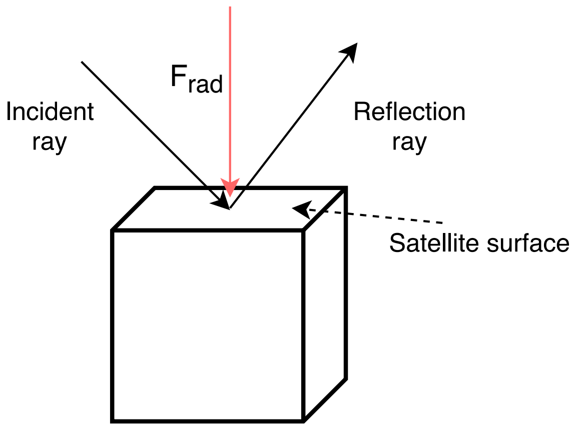

Figure 4.3: Solar radiation acting on satellite surface

The solar flux is given as

$$P = \frac{F_s}{c} \tag{4.10}$$

where F_s is the intensity or mean energy flux given as 1358 $[W/m^2]$ and c is the speed of light. The solar radiation force $\mathbf{F}_{rad}$ can be expressed as

$$\mathbf{F_{rad}} = C_a P A \ \hat{S} \tag{4.11}$$

where $C_a \in [0, 2]$ is the absorption coefficient which depends on the material of the satellite with 2 be the value of totally reflected beam and for simulation purposes is chosen to be 1.5, P is the solar flux, A is the radiated surface area, and $\hat{S} = \frac{\mathbf{r_{sun,sat}}}{||\mathbf{r_{sun,sat}}||}$ is the unit vector from the satellite to the sun. The solar radiation torque can be computed as

$$\mathbf{N}_{rad} = \mathbf{r}_s \times \mathbf{F}_{rad} \tag{4.12}$$

where $\mathbf{r}_s$ is the vector from the center of mass of the satellite to the center of pressure.

Gravity Gradient disturbance torque

Contrary to J_2 effect, in order to derive an expression for the gravitational torque exerted about the mass center of the satellite, it is assumed symmetrical and spherical Earth's mass distribution [28]. The gravity gradient effect about the center of mass of the satellite is a consequence of the non-uniform gravitational field of the Earth. If the gravitational field was uniformly distributed no such torque would be present. The force to an infinitesimal element $d\mathbf{F_i}$ at a distance R_i from the center of the Earth can be written

$$d\mathbf{F}_i = \frac{-\mu \mathbf{R_i} dm_i}{R_i^3} \tag{4.13}$$

as it can be seen in *figure 4.4*. The torque about the geometric center of the satellite can be written as

$$\mathbf{N}_{gra}^i = \mathbf{r}_i \times d\mathbf{F}_i \tag{4.14}$$

Assuming that the center of mass is aligned with the geometric center, the torque about the center of mass of the satellite can be expressed as[28][21]

$$\mathbf{N}_{gg} = \frac{3\mu}{\mathbf{R}_{sc}^3} [\hat{\mathbf{R}}_{\mathbf{sc}} \times (\mathbf{I_s} \ \hat{\mathbf{R}}_{\mathbf{sc}})] \tag{4.15}$$

where $\hat{\mathbf{R}}_{\mathbf{sc}}$ is the unit vector from center of mass the Earth to the satellite's center of mass, $\mu = Gm_{earth}$ with G be the gravitational constant 6.674010^{-11} $[m^3 kg^{-1} s^{-2}]$ and $\underline{I}_s$ is the inertia matrix of the satellite.

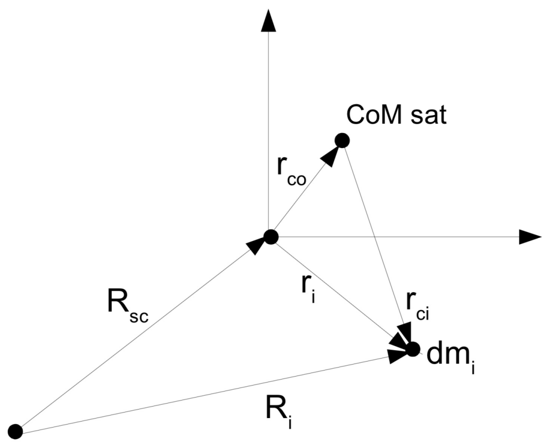

Figure 4.4: Gravity gradient torque computation using the coordinate system

Magnetic residual

When the satellite orbits the Earth, due to the interference of the magnetic field of the Earth and the satellite magnetic residual, an extra disturbance torque is generated. Because the magnetic residual can not be perfectly decreased to zero, the actuators and sensors will produce a residual magnetic moment. Similarly like magnetorqers, the torque generated by the magnetic residual can be computed using:

$$\mathbf{N}_{mr} = \mathbf{m} \times \mathbf{B} \tag{4.16}$$

where $\mathbf{m}$ is the magnetic moment and $\mathbf{B}$ is the magnetic field of the Earth.

The magnetic field of the Earth can be approximated using [29]:

$$B = \frac{2M}{R^3} \tag{4.17}$$

where M is the Earth magnetic moment and R is the distance from the Earth to the center of the satellite.

The International Geomagnetic Reference Field (IGRF) consists of a selection of data added by different observatories. It represents an approximation of the Earth magnetic field compared with the measured magnetic field.

5 | Control Schemes

The satellite control schemes are introduced starting from the top of the hierarchy. The chosen reaction wheel desaturation control scheme determines the overall control structure, while allowing modification of other control blocks, making the system modular. Three different main attitude controllers are discussed.

When developing complex systems, using a modular design, setting up a hierarchy between elements, and using abstractions can be very helpful in keeping the complexity at a manageable level. They can also prove to be useful during debugging or finding faults in the system. The proposed control scheme utilizes these tools. Figure 5.1 introduces the high-level control scheme used in the thesis. The scheme is inspired by the control scheme proposed by Trégouët et al. in their paper concerning a new desaturation control scheme [27].

The main attitude controller outputs a torque reference for the actuators, which is then distributed by lower level controllers. This means that the attitude controller can be swapped without having to modify the lower level controllers. The desaturation controller distributes the torque between the reaction wheels and magnetorquers. The reaction wheel subsystem executes local fault detection and fault isolation. It receives a three dimensional torque demand and distributes it between the individual reaction wheel motors. The reaction wheel subsystem checks fault residual signals and adjusts torque distribution between reaction wheels accordingly. These will be elaborated in subsequent sections.

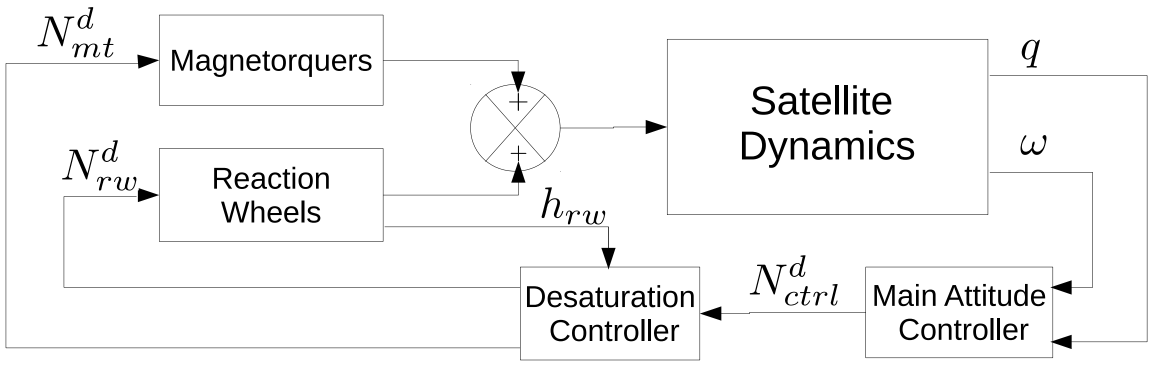

Figure 5.1: Main Control Loop.

$$\underline{I}_s\dot{\boldsymbol{\omega}} + \underline{\omega}^{\times}\underline{I}_s\boldsymbol{\omega} = -\dot{\mathbf{h}}_{rw} - \underline{\omega}^{\times}\mathbf{h}_{rw} + \mathbf{N_{mt}} + \mathbf{N_{dist}} = -\underline{\omega}^{\times}\mathbf{h}_{rw} + \mathbf{N_{rw}} + \mathbf{N_{mt}} + \mathbf{N_{dist}} \quad (5.1)$$

5.1 Desaturation

The reaction wheel DC motors and bearings have a limited angular velocity range they can operate in. When the velocity reaches the limit, the motor can no longer accelerate the wheel further in one of the two directions, thus reducing controllability. To avoid this, the wheel velocity should be kept near a small reference angular velocity. Usually the speed is above zero to avoid static friction in the bearings. Decreasing the reaction wheel speed by transferring its angular momentum is called desaturation. Desaturation also decreases the reaction wheels' gyroscopic term's effect on the overall satellite dynamics.

Reaction wheels are used to control the attitude of the satellite by controlling its angular momentum. This is done by transferring angular momentum between the reaction wheels and the satellite body. This leaves the sum of the satellite body's and wheels' angular momentum unchanged. Desaturation, i.e. decreasing the angular momentum of the reaction wheels can be done by transferring the angular momentum back to the satellite, however this would jeopardize the satellite attitude control goal. Angular momentum should be discarded in a different way. Magnetorquers are capable of desaturation since they can interact with the Earth's magnetic field and are able to transfer angular momentum of the satellite system to Earth. Since the Earth's magnetic field is quite weak, the torque produced by magnetorquers are small compared to the torque of the reaction wheels. A further drawback of magnetorquers is that even if they are set up in an orthogonal configuration, they can only assert torques in a two dimensional plane at any given moment, the plane perpendicular to Earth's magnetic field. Reaction wheels can be used for fast attitude control while magnetorquers are good for gradually desaturating the reaction wheels over several orbits.

The angular momentum transfer happens through the satellite's body, but with the right control scheme. The desaturation can be completely decoupled from attitude control. Trégouët et al. [27] developed a cascaded control method for reaction wheel desaturation. The method is a revised version of the so-called cross-product control law.

Classical Cross Product Control Law

The cross product control law achieves desaturation by using two control loops that are designed separately. The **attitude control loop** treats the reaction wheel torque as control input, the magnetorquer torque as disturbance, according to equation 5.2.

$$\underline{I}_s\dot{\boldsymbol{\omega}} + \underline{\omega}^{\times}(\underline{I}_s\boldsymbol{\omega} + \mathbf{h_{rw}}) = \overbrace{\mathbf{N_{rw}}}^{\mathbf{u}} + \overbrace{\mathbf{N_{mt}}}^{\mathbf{d}} \tag{5.2}$$

If the control goal is to rotate the satellite, it might be desired to make the apparent satellite dynamics independent of reaction wheel angular momenta. This can be achieved by using the actuators to counteract the effect of the gyroscopic term $\underline{\omega}^{\times}\mathbf{h_{rw}}$. This is a form of state compensation. Equation 5.3 presents the attitude control loop terms corresponding to $\mathbf{u}$ control input and to $\mathbf{d}$ disturbance. $\mathbf{N_{dist}}$ is discarded from the discussion of the desaturation scheme.

$$\underline{I}_s\dot{\boldsymbol{\omega}} + \underline{\omega}^{\times}\underline{I}_s\boldsymbol{\omega} = \overbrace{-\underline{\omega}^{\times}\mathbf{h_{rw}} + \mathbf{N_{rw}}}^{\mathbf{u}} + \overbrace{\mathbf{N_{mt}}}^{\mathbf{d}} \tag{5.3}$$

Equation 5.3 implies that the task state compensation is assigned to the reaction wheels according to 5.4.

$$\mathbf{N_{rw}} = -\dot{\mathbf{h}}_{\mathbf{rw}} = \mathbf{u} + \underline{\omega}^{\times}\mathbf{h_{rw}} \tag{5.4}$$

The goal of the **momentum dumping loop** is to track the reference angular momenta of the reaction wheels. The dynamics of the momentum dumping loop is described by equation 5.5. Introducing a constant angular velocity reference in the equation can be utilized to design a reference tracking control law subsequently.

$$\dot{\mathbf{h}}_{\mathbf{rw}} = \frac{d}{dt}(\mathbf{h_{rw}} - \mathbf{h_{ref}}) = -\underline{B}^{\times}(t)\mathbf{m_{mt}} \tag{5.5}$$

where $\mathbf{m_{mt}}$ is the magnetic moment of the magnetorquers, $\mathbf{B}$ is the local geomagnetic field in SBRF, $\mathbf{h_{rw}}$ is the angular momentum vector of the reaction wheels, $\mathbf{h_{ref}}$ is the reference reaction wheel angular momentum for desaturation.

Using the dynamics in equation 5.5, the momentum dumping control law can be designed to stabilize around $\mathbf{h_{ref}}$. The original cross product control does exactly that. The cross-product control law controls the magnetorquers' magnetic momentum using a negative feedback on the difference between the angular momentum of the reaction wheels and their reference angular momentum, as shown in equation 5.6.

$$\mathbf{m_{mt}} = -\frac{\underline{B}^{\times}(t)}{|\mathbf{B}(t)|^2}k_p\left(\mathbf{h_{rw}} - \mathbf{h_{ref}}\right) \tag{5.6}$$

where k_p is an adjustable proportional gain.

Recognizing that the reaction wheels cannot change $\mathbf{h_T}^{[I]}$ total angular momentum, a step can be taken towards detaching the effect of the magnetorquers and the reaction wheels. Substituting $\mathbf{h_{rw}} = \underline{R}({}^s_i\mathbf{q})\mathbf{h_T^{[I]}} - \underline{I}_s\boldsymbol{\omega}$. Using this, equation 5.6 can be rewritten according to equation 5.7.

$$\mathbf{m_{mt}} = -\frac{\underline{B}^{\times}(t)}{|\mathbf{B}(t)|^2}k_p\left(\underline{R}({}^s_i\mathbf{q})\mathbf{h_T^{[I]}} - \underline{I}_s\boldsymbol{\omega} - \mathbf{h_{ref}}\right) \tag{5.7}$$

Momentum dumping and attitude control can potentially be opposing goals, since attitude control changes the reaction wheel velocity to produce the required torque, while the desaturator tries to keep the angular velocity close to the reference. Further analysis made by Trégouët et al. [27] found that the classical cross product control law can be interpreted as having a quasi-cascaded structure with the momentum dumping loop including the magnetorquers as the upper subsystem and the attitude control loop with the reaction wheels being the lower subsystem. The problem is that there's a feedback involved from the lower subsystem to the upper one, making $\frac{d}{dt}(\mathbf{h_{rw}} - \mathbf{h_{ref}})$ dependent on the attitude parameters, as shown in equation 5.8.

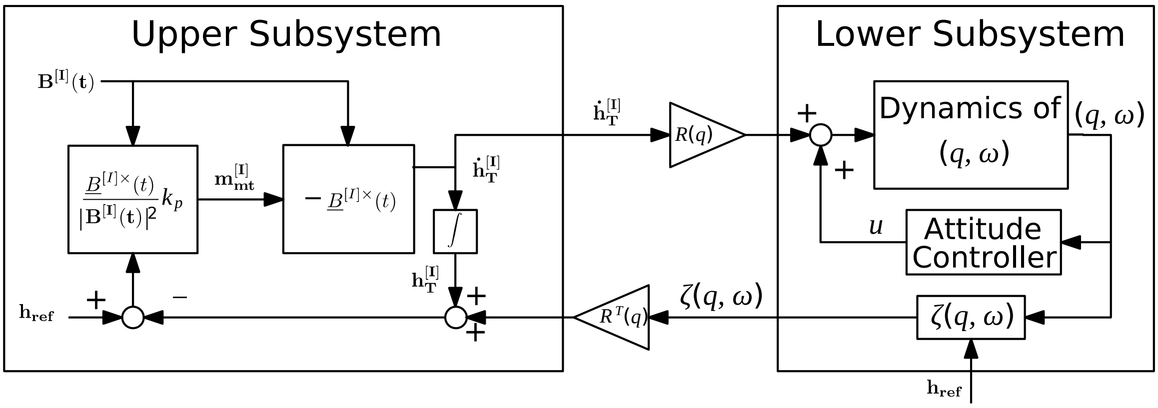

Figure 5.2: Quasi cascaded desaturation control scheme [27, Fig. 2.]

$$\begin{aligned}
\mathbf{m_{mt}} &= -\frac{(\underline{R}({}^s_i\mathbf{q})\underline{B}^{[I]}(t))^\times}{|\mathbf{B}(t)|^2}k_p\left(\underline{R}({}^s_i\mathbf{q})\mathbf{h}_\mathbf{T}^{[\mathbf{I}]} - \underline{I}_s\boldsymbol{\omega} - \mathbf{h_{ref}}\right) \\
&= -\underline{R}({}^s_i\mathbf{q})\frac{\underline{B}^{[I]\times}(t)}{|\mathbf{B^{[I]}}(t)|^2}k_p\left(\mathbf{h}_\mathbf{T}^{[\mathbf{I}]} - \mathbf{h_{ref}} + \underline{R}^T({}^s_i\mathbf{q})\overbrace{\left(\left(\underline{R}({}^s_i\mathbf{q}) - \underline{1}_3\right)\mathbf{h_{ref}} - \underline{I}_s\boldsymbol{\omega}\right)}^{\xi(\mathbf{q},\boldsymbol{\omega})}\right) \\
&= -\underline{R}({}^s_i\mathbf{q})\frac{\underline{B}^{[I]\times}(t)}{|\mathbf{B^{[I]}}(t)|^2}k_p\left(\mathbf{h}_\mathbf{T}^{[\mathbf{I}]} - \mathbf{h_{ref}} + \underline{R}^T({}^s_i\mathbf{q})\boldsymbol{\xi}(\mathbf{q},\boldsymbol{\omega})\right)
\end{aligned} \tag{5.8}$$

where $\underline{1}_{3\times3}$ is a 3×3 identity matrix, $\boldsymbol{\xi}(\mathbf{q},\boldsymbol{\omega})$ is the notation for the term related satellite dynamics states that affect the desaturation dynamics.

Remapping equation 5.8 to inertial frame results in equation 5.9. Figure 5.2 illustrates the system according to equations 5.3 and 5.9.

$$\mathbf{m_{mt}^{[I]}} = -\frac{\underline{B}^{[I]\times}(t)}{|\mathbf{B^{[I]}}(t)|^2}k_p\left(\mathbf{h}_\mathbf{T}^{[\mathbf{I}]} - \mathbf{h_{ref}} + \underline{R}^T({}^s_i\mathbf{q})\xi(\mathbf{q},\boldsymbol{\omega})\right) \tag{5.9}$$

Revised cross product control law

In cascaded structure, the upper subsystem can undesirably disturb the lower one. Since attitude control is more crucial than desaturation, it would be more desirable to use the attitude control loop as the upper subsystem and the momentum dumping loop as the lower one, as opposed to the reverse. This arrangement can be obtained by applying input allocation, i.e. 'suitably assigning the low level actuators' input, based on a higher level control effort requested by the control system' [13]. From the point of view of the desaturation controller, the control goal is to keep the reaction wheels' angular momentum as close to the reference momentum as possible. By using a modified version of the cross product control law, the desaturation controller dynamics can be decoupled from the attitude control loop, this way the desaturator can achieve its control goal independently from the attitude control law. The control scheme is presented in Figure 5.3.

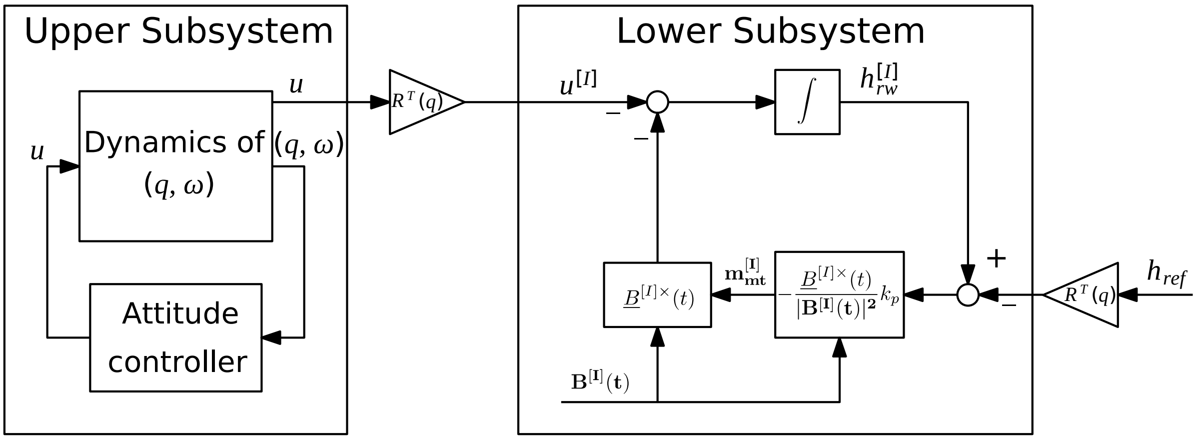

Figure 5.3: Cascaded desaturation control scheme [27, Fig. 4.]

The momentum dumping control law for the reverse cascade is derived in two steps. First, the control law for the original cascade scheme presented in 5.9 in ECI frame is revised to discard the feedback connection corresponding to $\boldsymbol{\xi}(\mathbf{q}, \boldsymbol{\omega})$, as presented in this subsection, second, input allocation is used to reverse the order of the cascade, as presented in the following section. The system can be turned into a cascade if the term $\boldsymbol{\xi}(\mathbf{q}, \boldsymbol{\omega})$ is eliminated from equation 5.9. The resulting control law is presented in equation 5.10.

$$\mathbf{m}_{\mathbf{mt}}^{[\mathbf{I}]} = -\frac{\underline{B}^{[I]\times}(t)}{|\mathbf{B}^{[\mathbf{I}]}(t)|^2} k_p \left(\mathbf{h}_{\mathbf{T}}^{[\mathbf{I}]} - \underline{R}^T({}_i^s\mathbf{q})\mathbf{h}_{\mathbf{ref}} \right) \tag{5.10}$$

The dynamics of the total angular momentum and the satellite's angular velocity can be described according to equations 5.11 and 5.12, where the total angular momentum dynamics is described in ECI frame, while the satellite angular velocity dynamics is described in SBRF frame. The magnetorquer torque is considered a disturbance, which is altering the total angular momentum of the system.

$$\dot{\mathbf{h}}_{\mathbf{T}}^{[I]} = -\underline{B}^{[I]}(t)^{\times}\mathbf{m}_{\mathbf{mt}}^{[\mathbf{I}]} \tag{5.11}$$

$$\underline{I}_s\dot{\boldsymbol{\omega}} + \underline{\omega}^{\times}\underline{I}_s\boldsymbol{\omega} = \mathbf{u} + \underline{R}^T({}_i^s\mathbf{q})\dot{\mathbf{h}}_{\mathbf{T}}^{[I]} \tag{5.12}$$

Static allocation

Equation 5.12 suggests that the desaturation loop can have an effect on the attitude control loop, as mentioned above. That is undesired, since the attitude control loop is of higher importance than desaturation. To reverse the cascade arrangement corresponding to control law 5.10, the grouping of the terms need to be revised first. For the reverse cascade scheme, the control input $\mathbf{u}$ is modified to include the magnetorquer torque, according to equation 5.13. The magnetorquer torque is no longer handled as a disturbance, instead it is explicitly a term in the control input. If $\mathbf{u}$ actuation tracking $\mathbf{u}$ demand well, the main attitude dynamics becomes independent of the magnetorquer torque output.

$$\underline{I}_s\dot{\boldsymbol{\omega}} + \underline{\omega}^{\times}\underline{I}_s\boldsymbol{\omega} = \overbrace{-\underline{\omega}^{\times}\mathbf{h}_{\mathbf{rw}} + \mathbf{N}_{\mathbf{rw}} + \mathbf{N}_{\mathbf{mt}}}^{\mathbf{u}} \tag{5.13}$$

With the new grouping, the reaction wheel torque reference can be expressed according to equation 5.14. The equation suggests that if the in some cases the magnetorquers can 'help out' the reaction wheels, decreasing reaction wheel torque demand, thus decreasing reaction wheel acceleration.

$$\mathbf{N}_{\mathbf{rw}} = \mathbf{u} - \mathbf{N}_{\mathbf{mt}} + \underline{\omega}^{\times}\mathbf{h}_{\mathbf{rw}} \tag{5.14}$$

The momentum dumping dynamics becomes what is presented in SRBF by equation 5.15, in ECI frame by equation 5.16. Transformation to inertial frame eliminates the gyroscopic term from the equation. Equation 5.16 suggests that the desaturation dynamics is affected by the main attitude control input.

$$\frac{d}{dt}(\mathbf{h}_{\mathbf{rw}} - \mathbf{h}_{\mathbf{ref}}) = -\mathbf{u} - \underline{\omega}^{\times}\mathbf{h}_{\mathbf{rw}} - \left(\underline{R}({}_i^s\mathbf{q})\mathbf{B}^{[\mathbf{I}]}(t)\right)^{\times}\mathbf{m}_{\mathbf{mt}} \tag{5.15}$$

$$\dot{\mathbf{h}}_{\mathbf{rw}}^{[\mathbf{I}]} = -\underline{R}^T({}_i^s\mathbf{q})\mathbf{u} - \mathbf{B}^{[\mathbf{I}]}(t)^{\times}\mathbf{m}_{\mathbf{mt}}^{[\mathbf{I}]} \tag{5.16}$$

The new magnetorquer magnetic moment control law is established for dynamics presented by equation 5.16, ignoring $\mathbf{u}$. The control law is given by equation 5.17. The control system consisting of equations 5.17 and 5.14 are illustrated by figure 5.3. Since the main attitude control loop is unaffected by the desaturation control loop, the main attitude controller can be considered as the upper subsystem of the cascade. The control law suggests that the sum of magnetorquer magnetic moments $\mathbf{m}_{\mathbf{mt}}^{[\mathbf{I}]}$ has no component in the direction of $\mathbf{B}^{[\mathbf{I}]}$, since that would be a waste of energy.

$$\mathbf{m}_{\mathbf{mt}}^{[\mathbf{I}]} = -\frac{\underline{B}^{[I]}(t)^{\times}}{|\mathbf{B}^{[\mathbf{I}]}(t)|^2} k_p \left(\mathbf{h}_{\mathbf{rw}}^{[\mathbf{I}]} - \underline{R}^T ({}^s_i\mathbf{q}) \mathbf{h}_{\mathbf{ref}} \right) \tag{5.17}$$

Figures 5.4 and 5.5 present desaturation over several orbits. The attitude controller control goal is nadir pointing, in the very beginning the attitude and angular velocity of the satellite differs from nadir pointing. The error is handled by quick reaction wheel torque action, then the wheels are desaturated over several orbits. The graphs show a semi-periodic magnetorquer behavior, corresponding to the periodic nature of Earth's magnetic field. By adjusting k_p control gain in the magnetorquer control law, the speed of desaturation can be adjusted as well.

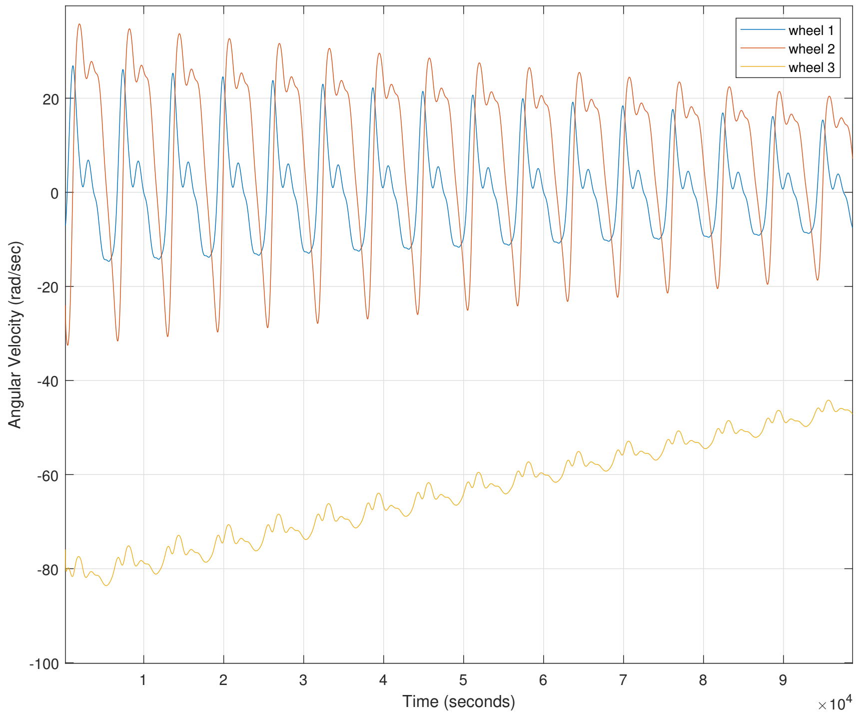

Figure 5.4: Angular velocity of reaction wheels in orthogonal configuration, during desaturation

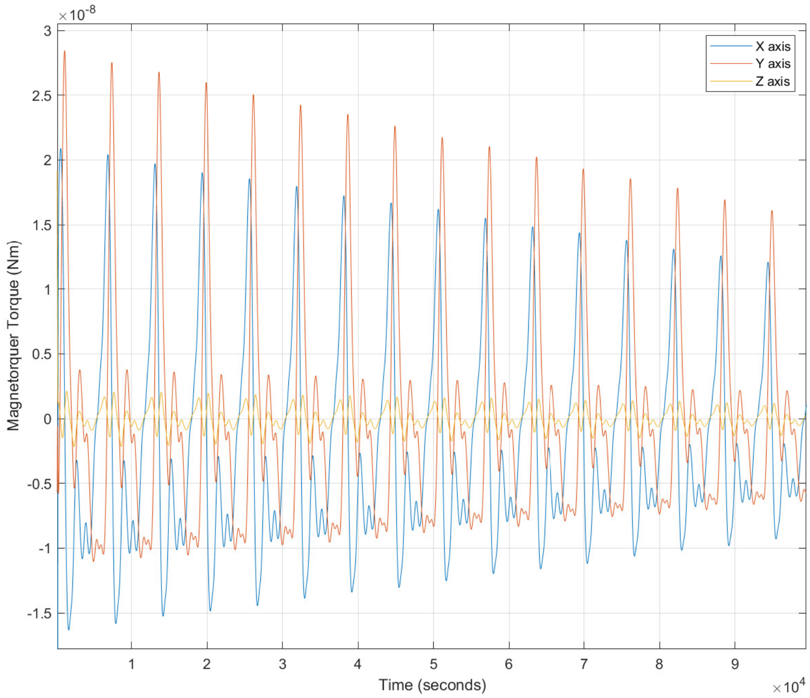

Figure 5.5: Magnetorquer torque $\mathbf{N_{mt}}$ during desaturation

5.2 Attitude Reference

The main attitude controllers require an attitude reference quaternion and a reference angular velocity to track. In the simulation environment, the attitude reference quaternion is given in orbit frame, the angular velocity reference in ECI frame. As discussed above, two attitude control goals are distinguished: nadir pointing and Earth station tracking. For nadir pointing, the attitude reference quaternion is simply assigned as $[0\ 0\ 0\ 1]^T$ and the angular velocity reference is identical to the orbit angular velocity. Creating the references for Earth station tracking are not as trivial.

For Earth station tracking, the reference quaternion can be calculated using the positions of the satellite, the station, and the center of Earth. The unit rotation axis of the attitude quaternion is $\mathbf{e} = \frac{{}^{sat}\mathbf{R}_o \times {}^{sat}\mathbf{R}_{st}}{||{}^{sat}\mathbf{R}_o \times {}^{sat}\mathbf{R}_{st}||}$, where ${}^{sat}\mathbf{R}_o$ is the distance from center of Earth to the satellite and ${}^{sat}\mathbf{R}_{st}$ is the distance from station to the satellite.

The angle between the nadir pointing and the station pointing vectors can be calculated using the law of cosines. The attitude quaternion in orbit frame is calculated using the quaternion rotation formula $\mathbf{q} = e^{\frac{\Phi}{2}(e_1\mathbf{i}+e_2\mathbf{j}+e_3\mathbf{k}+e_4)} = \cos\frac{\Phi}{2} + (e_1\mathbf{i} + e_2\mathbf{j} + e_3\mathbf{k})\sin\frac{\Phi}{2}$, as described in appendix A. The corresponding angular velocity reference can be calculated using the equation described in appendix C.13.

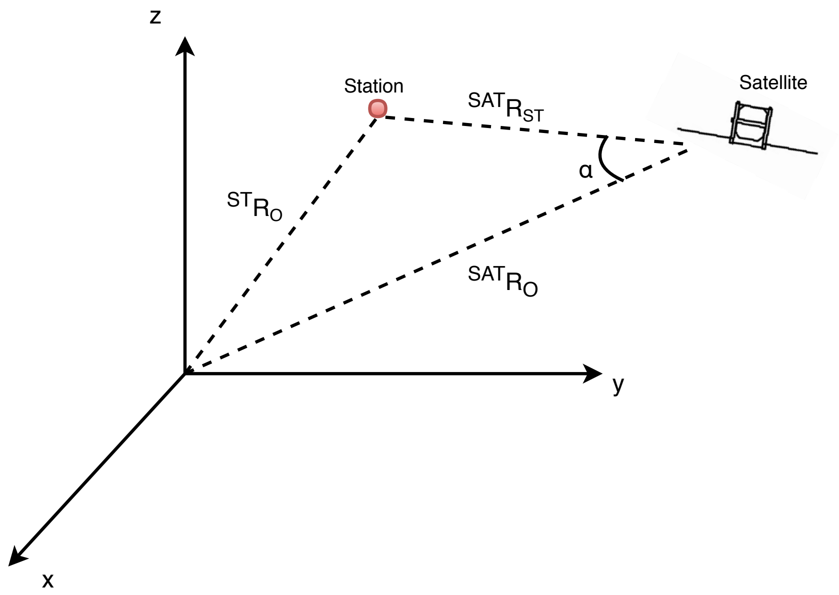

Figure 5.6: Tracking a target on Earth

5.3 Main Attitude Controller

Previously the main attitude controller was treated as a black box. The current and subsequent sections discuss several satellite attitude controllers.

Sections concerning linear and sliding mode attitude controllers, describe control methods used previously in [21]. A hybrid attitude controller is newly implemented in the simulation environment.

Hybrid Attitude Controller

Dynamic discontinuous hybrid controller, global asymptotic stability, local exponential stability, state feedback for ω and q. Capable of detumbling. [20]

There are different ways to describe the rotation of a 3D object. One of them is by using Euler sequences consisting of three rotational values. Euler rotation sequences can use combinations of roll, pitch and yaw. There's an inherent problem with Euler rotation, that makes controlling Euler rotation based models an issue, i.e. they are susceptible to singularities. Certain orientations might have an infinite amount of corresponding Euler angles. This can arise when the rotations are made in such a way that some rotation axes align with each other. This issue is commonly known as the gimbal lock. The result of a gimbal lock is that given an attitude, the corresponding Euler rotations cannot be unambiguously deducted, unless extra constraints are introduced.

Quaternion based rotation representation are more appropriate for control. Quaternions are not susceptible to singularities. The only problem with quaternion representation is the so-called double coverage, i.e. rotation by $-\mathbf{q}$ represents the same rotation as rotation by $-\mathbf{q}$. This becomes obvious from the rotation equation 5.18.

$$\mathbf{q}\mathbf{v}\mathbf{q}^{-1} = (-\mathbf{q})\mathbf{v}(-\mathbf{q}^{-1}) \tag{5.18}$$

The attitude control goal can be described as tracking the orientation demand $\mathbf{q}$. According to [20], it is impossible to design a globally stabilizing quaternion based state feedback that is robust to measurement noise. The quaternion-based robust hysteretic feedback controller which is capable of globally asymptotically stabilizing a rigid body is described subsequently, according to [20]. It can be considered as a more robust extension of classical state feedback controller.

The dynamics of a rigid body is described in equation 5.19. For clarity of the control method, disturbance torques are emitted from the equation. Since the control system compensates for the gyroscopic term, it is omitted as well from the discussion .

$$\underline{I}_s\dot{\boldsymbol{\omega}} = \underline{\omega}^{\times}\underline{I}_s\boldsymbol{\omega} + \mathbf{N_{ctrl}} \tag{5.19}$$

The control goal can be clearly described with rotation matrices. Rotation matrices use 9 variables to describe a rotation, but they have the advantage of being non-ambiguous. The rotation error can be described using equation 5.20.

$$\underline{R}(\mathbf{q^e}) = \underline{R}(\mathbf{q^d})^T\underline{R}(\mathbf{q}) \tag{5.20}$$

The goal is to align $\underline{R}(\mathbf{q})$ with $\underline{R}(\mathbf{q^d})$ orientation demand. If that demand is satisfied, $\underline{R}(\mathbf{q^e})$ orientation error becomes $\underline{I}$ identity matrix. In quaternion representation, this goal corresponds to having a unit quaternion with the scalar element being ± 1, according to equation 5.21.

$$\underline{R}(\mathbf{q^e}) = \underline{R}(\mathbf{q^e}) = \underline{1} \xrightarrow{equivalent} \mathbf{q^e} = \pm \begin{bmatrix} 0 \\ 0 \\ 0 \\ 1 \end{bmatrix} \tag{5.21}$$

Because of the double coverage property of quaternions, stabilizing an attitude, stabilization has to be done on a two equilibrium points corresponding to $\mathbf{q^e}$ in equation 5.21. If a feedback controller is used in the form of $\mathbf{N_{ctrl}} = f(\mathbf{q^e})$, $\mathbf{q^e}$ and $-\mathbf{q^e}$ might result in different torque demand, even though they both represent the same rotation. Out of the double covering quaternions $[0,0,0,1]^T$ and $-[0,0,0,1]^T$, one might be a stable, the other an unstable equilibrium point. The hybrid controller addresses this issue. According to [20], robust and global stabilization on this set is impossible to achieve using non-hybrid discontinuous state feedback in the presence of sensor noise. The paper proposes a hybrid, discontinuous, hysteretic, robust, globally asymptotically stabilizing attitude control method instead. A system is considered a hybrid system in the subsequent discussion if the state changes can vary between being continuous or discrete.

The state changes are controlled by the following rules. Controller state storing information about which of the double covering quaternions should be tracked is introduced as $x_c \in \{-1, 1\}$. x_c decides which of the two double covering quaternions should be tracked. If $x_c = signum(q_4)$ rule is followed, the controller becomes sensitive to measurement noise. To avoid that, a hysteresis introduced, with an adjustable $\delta \in (0,1)$ hysteresis threshold parameter. The rule for choosing between discrete or continuous control mode is presented in equation 5.22.

$$
\begin{aligned}
C &:= \left\{(\mathbf{q}, \boldsymbol{\omega}, x_c) \in \mathbb{S}^3 \times \mathbb{R}^3 \times \{-1, 1\} : x_c q_4 \geq -\delta\right\} \\
D &:= \left\{(\mathbf{q}, \boldsymbol{\omega}, x_c) \in \mathbb{S}^3 \times \mathbb{R}^3 \times \{-1, 1\} : x_c q_4 \leq -\delta\right\}
\end{aligned}
\tag{5.22}
$$

If $(\mathbf{q}, \boldsymbol{\omega}, x_c) \in C$, i.e. the controller is running in continuous mode, the governing equations are according to equation 5.23. When $(\mathbf{q}, \boldsymbol{\omega}, x_c) \in D$, x_c controller state swaps sign instantaneously. Because of the δ thresholding, two swaps don't happen in infinitesimally small time.

$$\dot{x}_c = 0, (\mathbf{q}, \boldsymbol{\omega}, x_c) \in C \tag{5.23}$$

$$x_c^+ = -x_c, (\mathbf{q}, \boldsymbol{\omega}, x_c) \in D \tag{5.24}$$

where x_c^+ is the next value of x_c during discrete time state change.

Equation 5.25 describes the generated negative feedback control signal. K_q is the adjustable orientation error gain, K_e is an also adjustable parameter for angular velocity gain.

$$\mathbf{u} = -K_q x_c \mathbf{q^e}_{1:3} - K_\omega \boldsymbol{\omega}^\mathbf{e} \tag{5.25}$$

Detumbling

After a satellite is ejected from its rocket, it might be rotating quite fast. The first task of the satellite attitude controller is detumbling the satellite, preparing for normal operation. The hybrid attitude controller is capable of doing that. This means that the hybrid attitude controller is a good nominee for being the attitude controller for every operation mode. A simulation was made where the satellite's initial angular velocity is unrealistically high, while the control goal is stabilizing the satellite to point at the nadir. Actuator saturation is omitted in order to present the dynamics of the control law more clearly. Figures 5.7a and 5.8 present the torque demand and the angular velocity during detumbling. At 4 seconds, the input quaternion is negated in order to present the controller handling the double coverage of the quaternion. Figure 5.7b presents x_c during the detumbling maneuver.

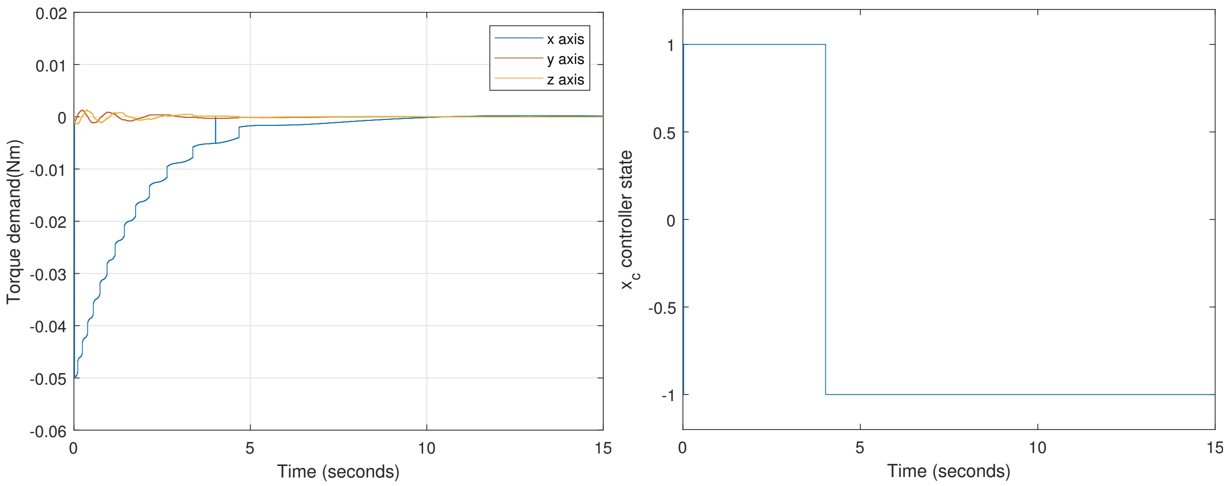

(a) **(b)**

Figure 5.7: Figure a) shows the hybrid controller detumbling torque demand while figure b) illustrates x_c controller state during detumbling maneuver using the hybrid controller. The quaternion error is negated at 4 seconds.

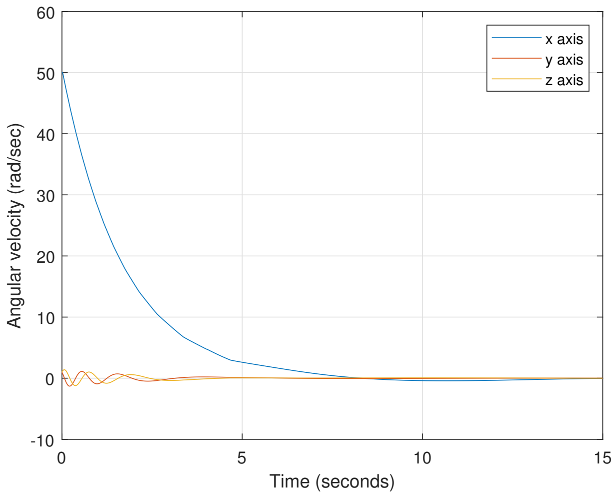

Figure 5.8: Satellite angular velocity during detumbling maneuver using the hybrid controller

Linear attitude controller

The operating point during nadir pointing is defined between the orbit frame and the body frame. In the operating point the angular rate between the frames should be zero ${}^{\mathbf{s}}_{\mathbf{o}}\boldsymbol{\omega} = 0$ and the two frames should be aligned, thus the relative attitude quaternion is $[0\ 0\ 0\ 1]^T$. Therefore, $||\bar{\boldsymbol{\omega}}||$ is equal to the orbital angular velocity, and equation 4.2 following [10] can be written as

$$\begin{bmatrix} \dot{\tilde{\mathbf{q}}}(\mathbf{t}) \\ \dot{\tilde{\boldsymbol{\omega}}}(\mathbf{t}) \end{bmatrix} = \begin{bmatrix} 0 & 0 & 0 & \frac{1}{2} & 0 & 0 \\ 0 & 0 & \omega_o & 0 & \frac{1}{2} & 0 \\ 0 & -\omega_o & 0 & 0 & 0 & \frac{1}{2} \\ -2\sigma_x & 0 & 0 & 0 & 0 & 0 \\ 0 & 2\sigma_y & 0 & 0 & 0 & \omega_o\sigma_y \\ 0 & 0 & 0 & 0 & \omega_o\sigma_z & 0 \end{bmatrix} \begin{bmatrix} \tilde{\mathbf{q}}(\mathbf{t}) \\ \tilde{\boldsymbol{\omega}}(t) \end{bmatrix} - \begin{bmatrix} \underline{\mathbf{0}}_{(3\times3)} \\ \underline{I}_s^{-1} \end{bmatrix} \tilde{\mathbf{N}}_{\mathbf{ctrl}} \tag{5.26}$$

with $\sigma_x = \frac{I_y - I_z}{I_x}, \sigma_y = \frac{I_z - I_x}{I_y}, \sigma_z = \frac{I_x - I_y}{I_z}$ and $I_x = 0.0017$, $I_y = 0.0022$, $I_z = 0.0022$ been the values of the inertia matrix and $\omega_o \approx 0.0011$ is the orbital angular rate. Moreover, by comparing the values of matrix *equation (5.26)* it can be seen that the value $\frac{1}{2}$ is larger compared to the other values thus *equation (5.26)* can be simplified to

$$\begin{bmatrix} \dot{\tilde{\mathbf{q}}}(\mathbf{t}) \\ \dot{\tilde{\boldsymbol{\omega}}}(\mathbf{t}) \end{bmatrix} = \begin{bmatrix} \underline{0}_{(3\times3)} & \frac{1}{2}\underline{\mathbf{1}}_{(3\times3)} \\ \underline{0}_{(3\times3)} & \underline{0}_{(3\times3)} \end{bmatrix} \begin{bmatrix} \tilde{\mathbf{q}}(\mathbf{t}) \\ \tilde{\boldsymbol{\omega}}(t) \end{bmatrix} - \begin{bmatrix} \underline{\mathbf{0}}_{(3\times3)} \\ \underline{I}_s^{-1} \end{bmatrix} \tilde{\mathbf{N}}_{\mathbf{ctrl}} \tag{5.27}$$

Three equal subsystems can be derived from *equation (5.27)* as

$$\begin{bmatrix} \dot{\tilde{q}}_i \\ \dot{\tilde{\omega}}_i \end{bmatrix} = \begin{bmatrix} 0 & \frac{1}{2} \\ 0 & 0 \end{bmatrix} \begin{bmatrix} \tilde{q}_i(t) \\ \tilde{\omega}_i(t) \end{bmatrix} - \begin{bmatrix} 0 \\ I_{i,s}^{-1} \end{bmatrix} \tilde{N}_i \tag{5.28}$$

with $i = 1, 2, 3$. The control torque was defined by the state feedback law as

$$N_i^d = - \begin{bmatrix} k_1 & k_2 \end{bmatrix} \begin{bmatrix} \tilde{q}_i(t) \\ \tilde{\omega}_i(t) \end{bmatrix} \tag{5.29}$$

leading to a second order closed loop system calculated as $det(s\underline{I} - (\underline{A} - \underline{BK}))$. Identifying this with a general second order equation $s^2 + 2\zeta\omega_n s + \omega_n^2$, with ζ be the dumping factor which was chosen to be equal to 1 and ω_n the natural frequency $\omega_n = \frac{2\pi}{60/0.35}$ with 60 being the chosen rise time value. The controller gains were derived as

$$k_1 = -2I_{i,s}\omega_n^2$$

$$k_2 = -2\zeta I_{i,s}\omega_n^2$$

Since the matrix $\underline{A}$ is affine, stability analysis was made for all the values of $\bar{\boldsymbol{\omega}}$ evaluated on the vertices of the convex polyhedron for the all values of $\bar{\boldsymbol{\omega}}$[21] giving maximum eigenvalue -0.0308. In the figure 5.9 it is seen the torque demand from the linear controller for nadir pointing reference.

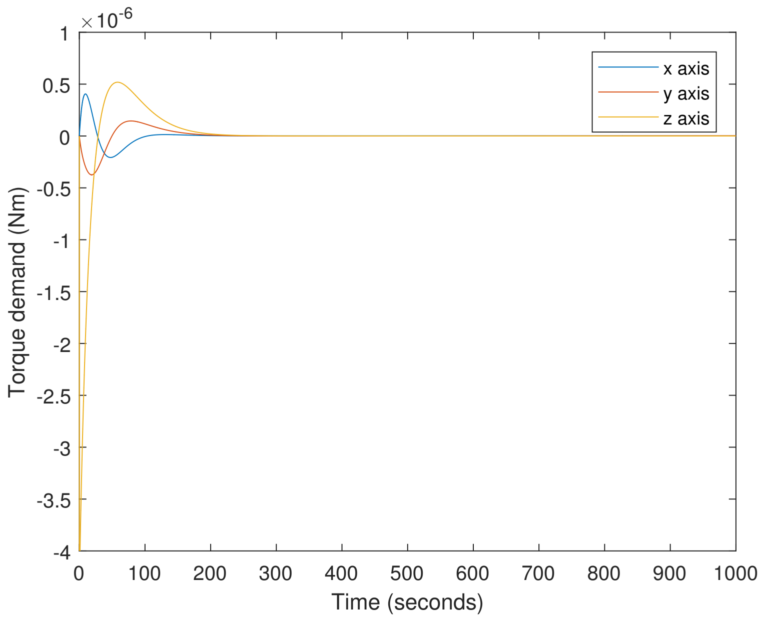

Figure 5.9: Linear controller Nadir pointing torque demand

Sliding mode control

As described previously, the sliding mode control scheme belongs to the class of non-linear control designs. The objective of the SMC is the design, from a geometrical point of view, of a manifold in the state space, denoted as s. When the state trajectory is on the manifold ($s = 0$) it is constraint such that the behavior of the system will meet the specifications it is designed for, i.e convergence to the desired reference. In figure 5.10 it can be seen how the states slide on the hyperplane towards origin.

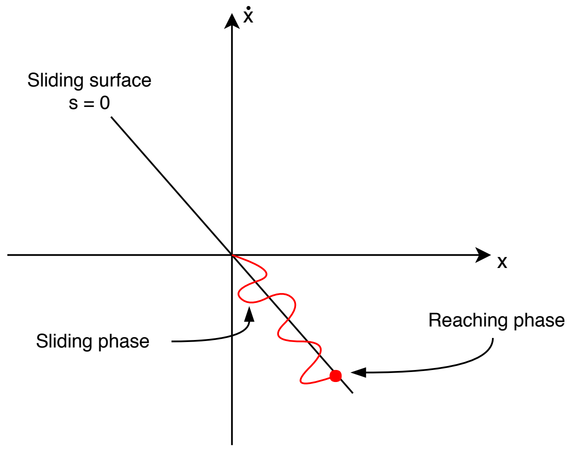

Figure 5.10: Sliding mode behavior

Sliding variable design

Small signal deviation i.e. the quaternion error can be described as

$$\tilde{\mathbf{q}} = \bar{\mathbf{q}}^{-1} \otimes \mathbf{q} \tag{5.30}$$

with $\bar{\mathbf{q}}^{-1}$ be the desired reference quaternion and $\mathbf{q}$ be the measured, and for the angular velocity as

$$\tilde{\boldsymbol{\omega}} = \boldsymbol{\omega} - \bar{\boldsymbol{\omega}} \tag{5.31}$$

with $\bar{\boldsymbol{\omega}}$ be the nominal value of the angular velocity. The sliding variable can now be written in terms of the error signals as

$$s = \underline{F}\tilde{\mathbf{q}} + \tilde{\boldsymbol{\omega}} \tag{5.32}$$

with $\underline{F} = \alpha\underline{\mathbf{1}}_{3\times3}$ be a positive definite matrix. It can be seen that for $s = 0$, the motion on the sliding surface is governed by $\tilde{\boldsymbol{\omega}} = -\alpha\tilde{\mathbf{q}}_{\mathbf{1:3}}$, where $\tilde{\mathbf{q}}_{\mathbf{1:3}}$ denotes the vector part of the quaternion, and α is chosen appropriately through trial and error to give the desired convergence for $\tilde{\mathbf{q}}$, leading to the desired alignment $[0\ 0\ 0\ 1]^T$ between frames. In order to prove this, differentiation of equation 5.30 following [11] is written as

$$\dot{\tilde{\mathbf{q}}} = \frac{1}{2}(-\mathbf{q}_{\bar{\omega}} \otimes \tilde{\mathbf{q}} + \tilde{\mathbf{q}} \otimes \mathbf{q}_{\bar{\omega}} + \tilde{\mathbf{q}} \otimes \mathbf{q}_{\tilde{\omega}}) \tag{5.33}$$

with $\mathbf{q}_{\bar{\omega}} = \bar{\omega_1}i + \bar{\omega_2}j + \bar{\omega_3}k + 0$ and $\mathbf{q}_{\tilde{\omega}} = \tilde{\omega_1}i + \tilde{\omega_2}j + \tilde{\omega_3}k + 0$. From equation 5.33 the real part of the quaternion error can be written as

$$\dot{\tilde{q_4}} = -\frac{1}{2}\tilde{\boldsymbol{\omega}}\tilde{\mathbf{q}}_{\mathbf{1:3}} = \frac{\alpha}{2}\|\tilde{\mathbf{q}}_{\mathbf{1:3}}\|^2 = \frac{\alpha}{2}(1 - \tilde{q_4}^2) \tag{5.34}$$

It can be seen that $\tilde{\mathbf{q}} \longrightarrow [0\ 0\ 0\ 1]^T$ with a desired rate given by α. Figure 5.11 showing the $\tilde{\mathbf{q}}$ converging with rate given by $\alpha = 0.035$

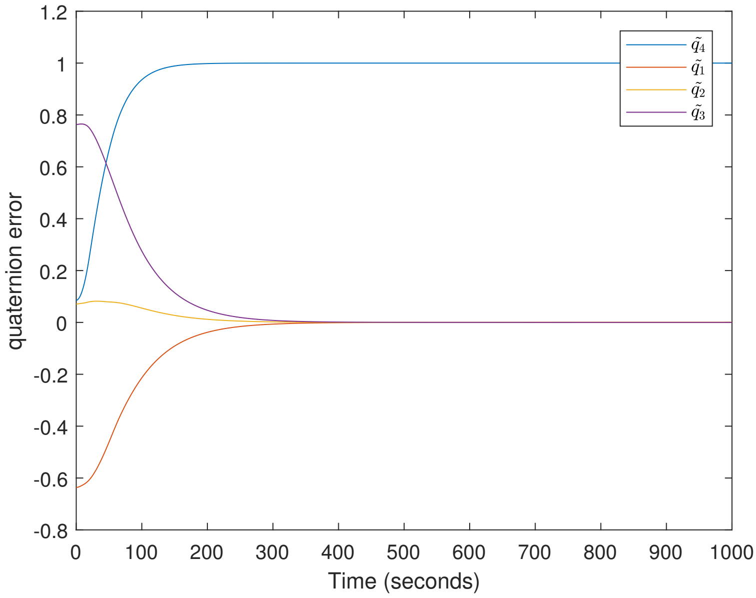

Figure 5.11: Shows the quaternion error converging with $\alpha = 0.035$

Sliding condition - Control law

The variable s can be driven to 0 by making use of a Lyapunov candidate function as

$$V = \frac{1}{2}\mathbf{s}^T\mathbf{s} \tag{5.35}$$

and in order to prove stability around $s = 0$ a necessary condition is $\dot{V} < 0$ for each $s \neq 0$. The time derivative of equation 5.35 is written as

$$\dot{V} = \frac{1}{2}(\dot{\mathbf{s}^T}\mathbf{s} + \mathbf{s}^T\dot{\mathbf{s}}) \tag{5.36}$$

showing that $\mathbf{s}^T\dot{\mathbf{s}} < 0\ \forall s \neq 0$ the condition may be satisfied. Substituting equation 5.32 is obtained

$$\dot{V} = \mathbf{s}^T\dot{\mathbf{s}} = \mathbf{s}^T(\underline{F}\dot{\tilde{\mathbf{q}}} + \dot{\tilde{\boldsymbol{\omega}}}) \tag{5.37}$$

and thus replacing the dynamic equation 4.1, equation 5.37 may be written as

$$\dot{V} = \mathbf{s}^T \underline{I}_s^{-1}(-\underline{\omega}^{\times}\underline{I}_s\boldsymbol{\omega} - \underline{\omega}^{\times}\mathbf{h_{rw}} + \mathbf{N^d_{rw}} + \mathbf{N_{mt}} + \mathbf{N_{dis}} - \underline{I}_s\dot{\tilde{\omega}} + \underline{I}_s\underline{F}\dot{\tilde{\mathbf{q}}}) \tag{5.38}$$

designing the control as

$$\mathbf{N^d_{rw}} = \underline{\omega}^{\times}\underline{I}_s\boldsymbol{\omega} + \underline{\omega}^{\times}\mathbf{h_{rw}} + \underline{I}_s\dot{\omega} - \underline{I}_s\underline{F}\dot{\tilde{\mathbf{q}}} - \underline{I}_s\lambda sign(\mathbf{s})) \tag{5.39}$$

equation 5.38 is written as

$$\dot{V} = -\mathbf{s}^T(-\dot{\tilde{\boldsymbol{\omega}}} + \lambda sign(\mathbf{s}) - \mathbf{N_{mt}} - \mathbf{N_{dist}}) \tag{5.40}$$

Eventually, it can be seen that choosing $\lambda > \|\dot{\tilde{\boldsymbol{\omega}}}_{\mathbf{max}}\| + \|\mathbf{N_{mt}}\| + \|\mathbf{N_{dist}}\|$ the condition $\dot{V} < 0$ is satisfied. Sign function presents chattering around the manifold which is undesirable, thus the sign function is replaced with the hyperbolic tangent function *tanh* which is smoother. In the figure 5.12 is depicted the torque demand the sliding mode controller outputs.

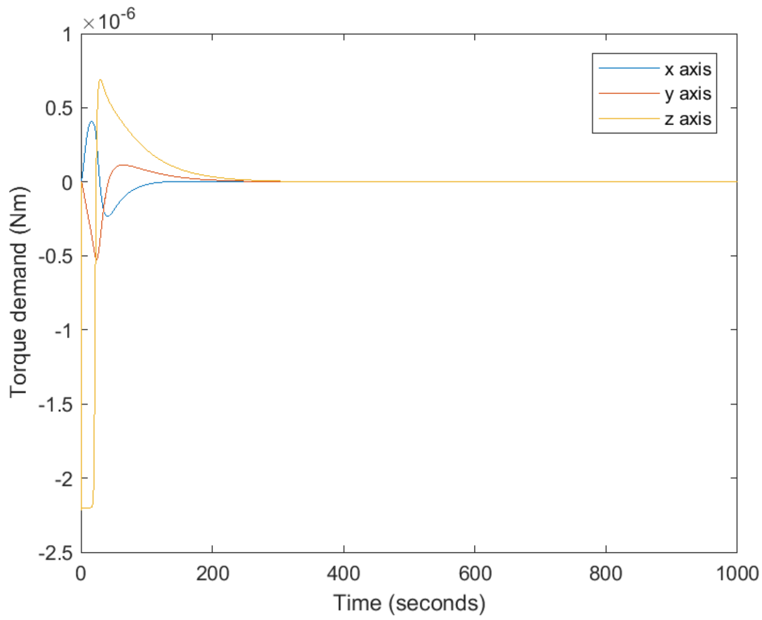

Figure 5.12: Sliding Mode controller nadir pointing torque demand

6 | Actuators modelling and control

This chapter will describe the chosen reaction wheels and BLDC motors along with the electrical and mechanical modelling of the motors.

6.1 Reaction wheels

The satellite should be capable of tracking an Earth station in order to be able to downlink data effectively. Tracking a ship requires similar control capability, since the velocity of the wheel is practically zero compared to the velocity of the satellite. Directing the satellite to the nadir continuously only requires keeping a satellite angular velocity equal to the orbit's angular velocity. Pointing the antennas to the Earth station requires torque from the actuators, the torque demand can be calculated based on the angular acceleration demand for Earth station tracking.

The wheel moment of inertia is [6] $I_w = 2.456[gcm^2]$ and the weight is $m_w = 4.201[g]$ compared to the motor weight $m_{motor} = 8[g]$ and the motor shaft moment of inertia $I_{motor} = 0.0249[gcm^2]$. The characteristics of the selected motor can be found in appendix B. The maximal speed of the motor is $\omega_{max} = 20000[rpm]$ and thus the maximum angular momentum that the system wheel-motor can provide can be found as

$$h_{max} = J_{wheel}\omega_{max}$$

which is found to be $5.1438 \cdot 10^{-4}[Kgm^2/s]$ for each wheel. For three axis stabilization, three wheels each orthogonal to the principal axis, are efficient but in case of one actuator failure it jeopardizes controllability of the satellite. To avoid this, redundancy is desired, requiring four wheels in tilted positions. The configuration of the wheels is chosen to be in tetrahedron shape giving rise to more reliable and robust system. The tetrahedron configuration will be discussed in section 6.1.

BLDC motor model

In order to make the system more reliable, brush-less DC motors are chosen as actuators. BLDC motors are lighter compared to brushed with the same power output and do not causing sparking thus can be used in operations that demand long life and reliability. Each motor consists of an electrical part and a mechanical part. The electrical part of the motor can be modeled using Kirchhoff's Voltage Law as

$$V_a - V_R - V_L - V_e = 0 \tag{6.1}$$

where V_a is the voltage source, V_R is the voltage drop across the resistance, V_L is the voltage drop across the inductance and V_e is the back emf. Equation 6.1 can be re written as

$$V_a = R_a i + L_a \frac{di}{dt} + k_e \omega \tag{6.2}$$

where R_a [Ohm] is the armature resistance, L_a [H] is the armature inductance and k_e is the back emf coefficient as it can be seen in the *figure 6.1* .

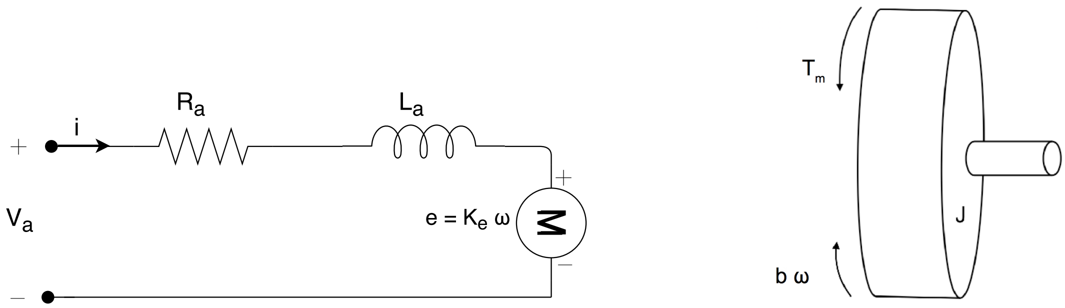

Figure 6.1: Electrical and mechanical part of the motor

The mechanical part of the motor can be modelled as

$$k_t i = J \frac{d\omega}{dt} + b\omega \tag{6.3}$$

where J is the rotor moment of inertia, k_t [Nm/A] is the motor torque coefficient and b [Nm s/rad] is the viscous friction coefficient. Equation 6.3 can be solved for i and replaced in 6.2[32]

$$i = \frac{J}{k_t} \frac{d\omega}{dt} + \frac{b}{k_t}\omega \tag{6.4}$$

$$V_a = \frac{LJ}{k_t} \frac{d^2\omega}{dt^2} + \frac{RJ + Lb}{k_t} \frac{d\omega}{dt} + \frac{Rbk_e}{k_t}\omega \tag{6.5}$$

by Laplace transformed 6.5, the second order transfer function from V_a to ω can be written as

$$\frac{\omega(s)}{V_a(s)} = \frac{k_t}{LJs^2 + (RJ + Lb)s + (Rb + k_e k_t)} \tag{6.6}$$

following [32] the electrical time constant τ_e and mechanical time constant τ_m can be written respectively $\tau_e = \frac{LJ}{RJ+Lb}$ and $\tau_m = \frac{RJ+LB}{RB+k_e k_t}$, the values for the two time constants are found to be $\tau_e = 1.2709 \cdot 10^{-10}$[s] and $\tau_m = 8.4102 \cdot 10^{-4}$[s] thus since the τ_e is very small compared to τ_m, the effect of inductance can be neglected thus the transfer function from V_a to ω is reduced to a first order transfer function as

$$\frac{\omega(s)}{V_a(s)} = \frac{k_t}{R(Js + b) + k_e k_t} \tag{6.7}$$

the block diagram of the system can be seen in figure 6.2 along with PI velocity controller which will be discussed in the next section.

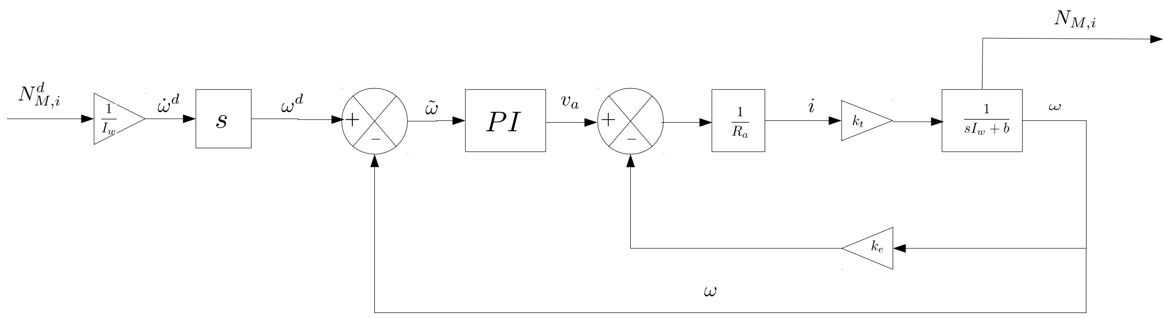

Figure 6.2: Angular velocity controlled DC motor

Angular velocity control

The higher level controllers give a control demand to the reaction wheels, this torque demand is transformed to angular velocity demand in motor frame. A *PI* controller has been designed to control the angular velocity of the motor as seen in the *figure 6.2*: The PI controller gains are chosen by trial and error in order to achieve faster closed loop response, zero steady state error and stable system. The gains are chosen to be:

$$k_p = 0.006$$
$$k_i = 6$$

The root locus of one motor with PI controller is seen in figure 6.3

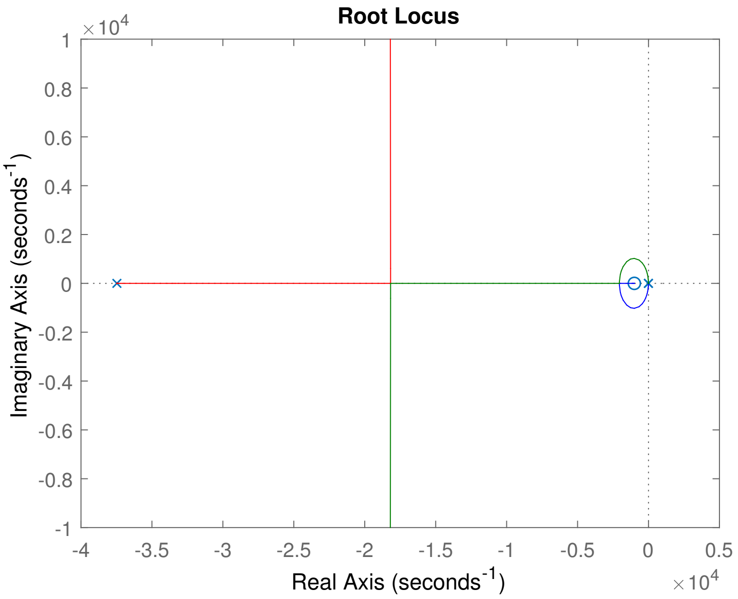

Figure 6.3: Root locus of one motor with PI controller

Furthermore, it is worth showing how the poles moving when the motor reach saturation mode and thus the gain becomes 0 which can be seen in figure 6.4.

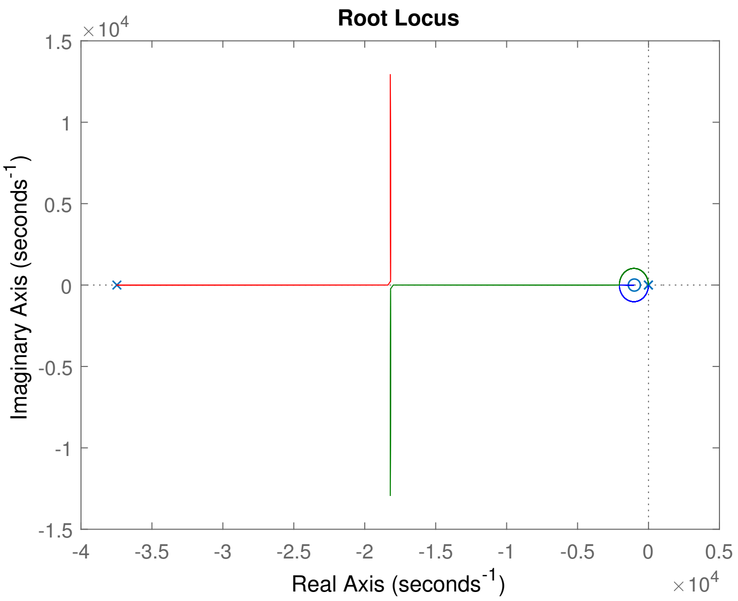

Figure 6.4: Root locus of one motor with PI controller when the gain K becomes 0

Reaction Wheel Configuration

Studies have been conducted on what is the best configuration of redundant reaction wheels. The optimal configuration can of course depend on the requirements. If the requirement is to have the same controllability for reaction wheels in case of fault, and six reaction wheels are available, orthogonally configured double reaction wheels can be used. Minimizing energy consumption is normally the goal in deciding on a configuration. Ismail et al. [30] investigated several configurations by running simulations with the configuration being the only difference. The tetrahedron configuration of four reaction wheels has been chosen as the default configuration in the present thesis, which is quite widespread in the field [5], and is redundant with an excess of one wheel. The tetrahedron configuration is visualized in Figure 6.5. In tetrahedron configuration the four wheel orientations are evenly distributed, unlike the also widespread pyramid configuration.

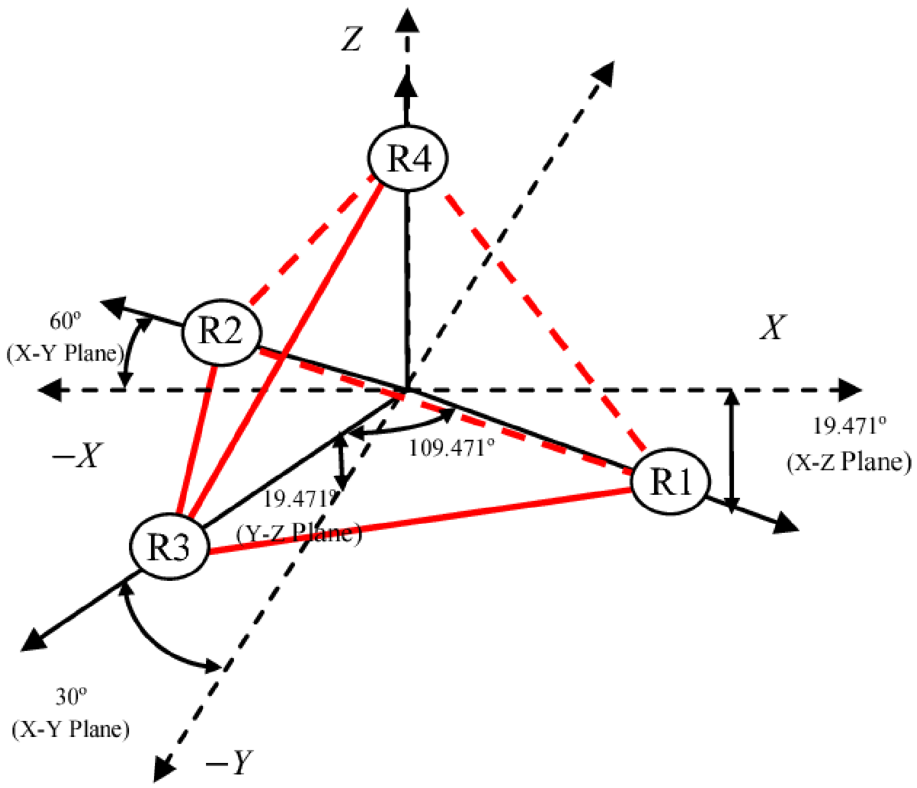

Figure 6.5: Geometry of the tetrahedron configuration [18]

Transformation Between Body & Reaction Wheel Space

The main attitude controller sends torque demand signal to the actuators. The reaction wheel torque demand has to be converted from body frame to torques parallel to reaction wheel axes. This transformation is nontrivial. Transforming back from reaction wheel space to body frame is quite intuitive. Knowing the orientation, the mounting angle of each motor axis and the corresponding motor torque, the torque in body frame for tetrahedral configuration can be derived according to equation 6.8 - 6.9. The matrix for tetrahedron configuration is given by [15].

$$\mathbf{N_{rw}} = \underline{A}_M \mathbf{N_M} = \begin{bmatrix} \mathbf{Axis_1^M} & \mathbf{Axis_2^M} & \mathbf{Axis_3^M} & \mathbf{Axis_4^M} \end{bmatrix} \mathbf{N_M} \tag{6.8}$$

$$\underline{A}_M \mathbf{N_M} = \begin{bmatrix} \cos(19.47) & -\cos(19.47)\cos(60) & -\cos(19.47)\cos(60) & 0 \\ 0 & \cos(19.47)\cos(30) & -\cos(19.47)\cos(30) & 0 \\ -\sin(19.47) & -\sin(19.47) & -\sin(19.47) & 1 \end{bmatrix} \mathbf{N_M} \tag{6.9}$$

where $\mathbf{N_{rw}}$ is the reaction wheel torque in body frame, $\mathbf{N_M}$ is the vector containing the reaction wheel DC motor torques parallel to their axes, $\mathbf{Axis_i^M}$ are the reaction wheel motor orientation in body frame, $\underline{A}_M$ is the transformation matrix between axis oriented reaction wheel torque and torques in 3 dimensional body frame.

The transformation matrix for orthogonal configuration is quite trivial, and is presented in equation 6.10.

$$\underline{A}_{M,orth} = \begin{bmatrix} 1 & 0 & 0 \\ 0 & 1 & 0 \\ 0 & 0 & 1 \end{bmatrix} \tag{6.10}$$

The nontrivial body frame to motor frame transformation can be derived by reordering equation 6.8. Since $\underline{A}_M$ is a 4×3 matrix, a pseudo inverse has to be used when reordering the equation, as presented in equation 6.11.

$$\mathbf{N_M} = \underline{A}_M^{\dagger} \mathbf{N_{rw}} = \underline{A}_M^T (\underline{A}_M \underline{A}_M^T)^{-1} \mathbf{N_{rw}} \tag{6.11}$$

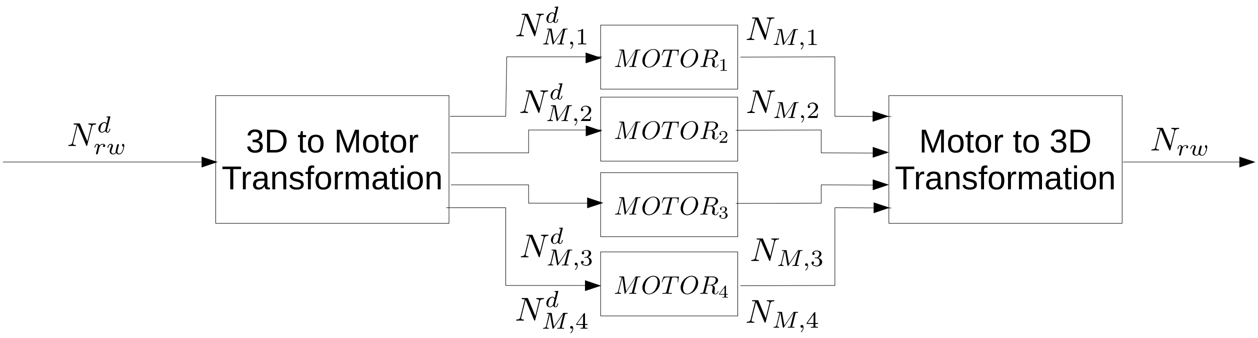

Figure 6.6: Reaction wheel torque distribution

In case there's a demand to adjust the torque distribution between the wheels, an extra vector can be included, as shown in equation 6.12 [28, equation 18.41-42]. If k is set to 0, the norm of wheel torques are minimized.

$$\mathbf{N_M} = \underline{A}_M^{\dagger}\mathbf{N_{rw}} + k\,[1, -1, -1, 1]^T \tag{6.12}$$

6.2 Magnetorquer model

The magnetorquer system is made up of six magnetorquers set up in three orthogonal pairs.

The magnetic moment of the magnetorquer is controlled according to the desaturation torque demand. The interaction of the dipole with the magnetic field of the Earth will result in a torque that will be perpendicular to the magnetic field vector according to the following equation [28]:

$$\mathbf{N}_{mt} = \mathbf{m}_{mt} \times \mathbf{B} \tag{6.13}$$

where $\mathbf{N}_{mt}$ is the torque produced by the magnetorquer, $\mathbf{B}$ is the vector of the magnetic field of the Earth and $\mathbf{m}_{mt}$ is the magnetic dipole moment of the magnetorquer.

The magnetic moment $\mathbf{m}_{mt}$ is given by [31]:

$$\mathbf{m}_{mt} = n_{coil}\ I_{coil}\ \mathbf{A}_{coil} \tag{6.14}$$

where n_{coil} is the number of the coil windings, I_{coil} is the electric current flowing through the coil and $\mathbf{A}_{coil}$ is the area vector of the magnetorquer.

The resistance of the magnetorquer which is a function of the temperature of the coil, can be computed as

$$R_{mt} = \frac{n_{coil} C \rho_{mt}}{A_{wire}} = \frac{n C \rho_0 (1 + \alpha_0 (T_{mt} - T_0))}{A_{wire}} \tag{6.15}$$

where
R_{mt} is the resistance of the magnetorquer
n_{coil} is the number of windings
C is the wire circumference
A_{wire} is the wire cross-sectional area
ρ_0 is the resistivity of copper
α_0 is the coefficient of resistivity temperature
T_{mt} is the temperature given as an input
T_0 is the resistivity base temperature

The inductance in the simulation is neglected and the the current has been calculated based on resistance.

The characteristics of the magnetorquer is described in appendix F.

Magnetorquers open-loop control

In the simulation, the magnetorquer has no state, open loop control is used to calculate the control voltage needed to output the desired magnetic moment. The open loop gain is calculated using equation 6.14 as follows

$$\mathcal{K} = \frac{R_{mt}}{n_{coil}\mathbf{A}_{coil}} \tag{6.16}$$

$\mathcal{K}$ is the gain. The maximum voltage is 1.25[V].

The magnetorquer open loop control can be seen in figure 6.7:

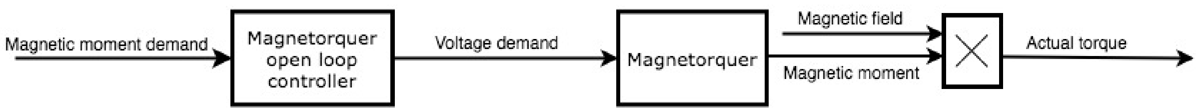

Figure 6.7: Magnetorquer open loop control

Relation between the coil current and generated magnetic field

The knowledge about the relation between coil current and generated magnetic field in any given point in space, can be used for fault detection. The magnetic field in the center of a square coil is computed using the law of Biot-Savart [25]:

$$d\mathbf{B}_{mt} = \frac{\mu_0 I}{4\pi}\frac{d\mathbf{s}\times\hat{\mathbf{r}}}{r^2} \tag{6.17}$$

where
$\mathbf{B}_{mt}$ is the magnetic field generated by magnetorquer

μ_0 is a constant called permeability of free space and is equal with $4\pi \times 10^{-7}\ Tm/A$
I is the current
$d\mathbf{s}$ is a length element in the direction of current
$\hat{\mathbf{r}}$ is the direction from $d\mathbf{s}$ to a particular position
r is the distance from $d\mathbf{s}$ to a particular position

Equation 6.17 represents an infinitesimal element, thus integrating the equation over the whole coil gives the generated magnetic field.

7 | Fault Analysis

Probable faults in the system are examined using a Failure Mode and Effects Analysis (FMEA). In order to decide the importance of handling each fault, the severity and occurrence (SO) of faults is analyzed. It was decided that the fault analysis is focused on actuators fault detection.

A fault in a system can be seen as a sudden shift in the system functionality, however, it might not mean a total shutdown of the system. The faults can be considered as a disturbance in the system, some of which might cause performance loss while others serious deterioration to the system. Failures are distinguished from faults since can cause a total shutdown of the system component.

In figure 7.1 a fault tolerant system is shown, which contains an autonomous supervisor that has the ability to switch between various controllers taking into account the type of fault that a component has. The spacecraft block illustrated in the picture is composed of a plant, actuators and sensors and is monitored by the fault detection and isolation (FDI) system, which include detectors that will feed informations to the supervisor in the eventuality of a fault. Based on the information received, the supervisor will establish if a fault occurred or not and in case of a fault the effectors will handle it. Furthermore figure 7.1 shows the procedure of how faults are handled with various methods. The first step in Fault Analysis is fault modeling which uses a procedure called FMEA.

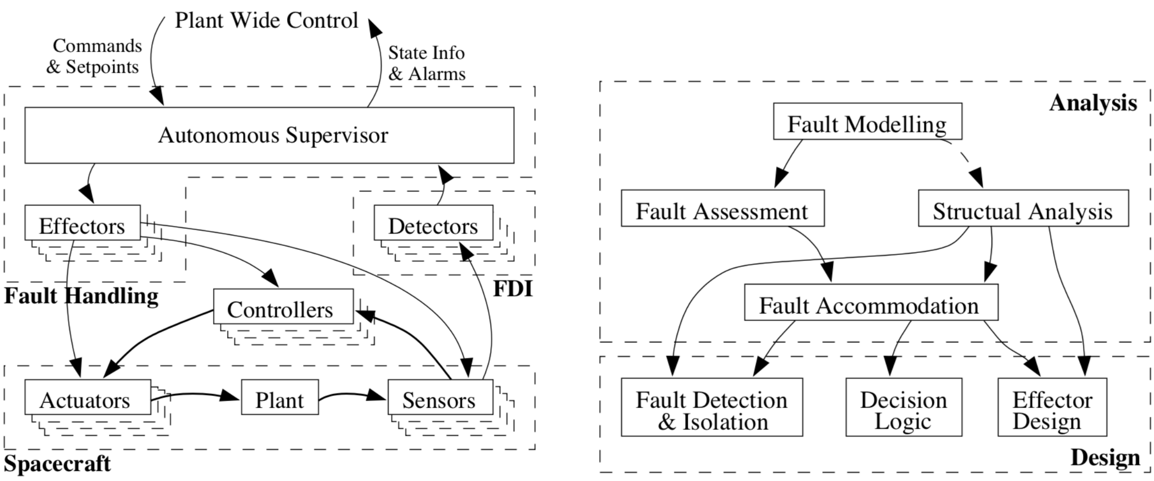

Figure 7.1: Fault tolerant system architecture and fault handling using different methods [23]

7.1 Failure Mode and Effects Analysis

A FMEA analysis which is a bottom-up analysis method is performed for the components of the satellite. The main goal of FMEA is to identify possible faults and their effects on components. Another aspect of FMEA analysis is that, the severity of a fault can be determined, offering the opportunity to prioritize the faults by severity and in this way focus on the important faults.

In order to control the attitude of the satellite, two types of actuators are used: magnetorquers and reaction wheels. Potential faults are gathered into tables 7.1 and 7.2 describing the effect and cause on the satellite in orbit.

Magnetorquers

Magnetorquers		
Creates a magnetic field that interacts with Earth's magnetic field		
Reference	**Failure Effect**	**Failure Cause**
$MT1$	Low magnetic field	1) Broken wire or bad soldering 2) Component burned
$MT2$	Maximum magnetic field power	Short circuit to the power voltage
$MT3$	Wrong direction of the magnetic moment	1) Misalignment of the magnetorquer 2) Short circuit between the magnetorquer and the power voltage
$MT4$	Wrong magnetic field magnitude	Faulty supply voltage

Table 7.1: Potential faults in the magnetorquers

Description of faults in the magnetorquers:

$\mathcal{F}_{MT1}$: The coil might have a broken wire or bad soldering, which can lead to the weakening of the magnetorqer magnetic field. The same effect can arise if an electric component is burned from large currents caused by a fault in the voltage regulator.

$\mathcal{F}_{MT2}$: A short circuit in the power supply can lead to maximum magnetic field output.

$\mathcal{F}_{MT3}$: A misalignment of the magnetorquer due to transportation or a sudden shift during the launch, could affect the direction of the magnetorquer magnetic field, leading to wrong magnetorquer magnetic moment output.

$\mathcal{F}_{MT4}$: A fault supply voltage that could mean lead to uncontrollable magnetorquer magnetic field.

Reaction wheels

Reaction wheels		
Produces a torque in order to rotate the satellite		
Reference	**Failure Effect**	**Failure Cause**
$RW1$	Faulty torque orientation	Shifting of the flywheel
$RW2$	Uncontrollable rotation	A short-circuit in the power supply
$RW3$	Low motor power	Short circuit
$RW4$	No torque exerted	A fault in windings
$RW5$	Higher power requirement	A fault in bearings

Table 7.2: Potential faults in the reaction wheels

Description of faults in the reaction wheels:

$\mathcal{F}_{RW1}$: A displacement of the flywheel during launch or transportation could result in an error in the controlled torque orientation.

$\mathcal{F}_{RW2}$: A short-circuit in the power supply could influence the control of the flywheel by decreasing the range of the control voltage.

$\mathcal{F}_{RW3}$: A short circuit to the ground due to a broken wire or bad soldering will result in low torque output.

$\mathcal{F}_{RW4}$: Due to a fault in the windings, the flywheel is uncontrollable since the motor can not exert torque.

$\mathcal{F}_{RW5}$: If the motor bearings fail, then the motor will need to generate more torque than usual in order to compensate, therefore more power is required.

In appendix H a severity and occurrence evaluation is performed.

7.2 Fault Detection

Fault detection deals with detecting system discrepancies and abnormal behavior. Some of the methods require sensor data filtering or threshold adjustment to handle signal noise. Fault detection is the first step towards handling faults. It does not necessarily identify the source of the fault, just establishes the fact that a fault has occurred in the system. In redundant systems, fault handling can be achieved by shutting down the actuator affected by the fault and redistributing the control tasks between the functioning actuators.

Accuracy of general fault detection methods can be improved by filtering the signals used in the fault detector. When observer is used filtering is not needed. Filtering methods are outside of the scope of the thesis. Observer theory is well developed for linear systems however, observers for nonlinear systems is a field under development [3].

Detectability of potential faults

The possible detection methods for the faults discussed above are discussed. The methods are described in more detail in subsequent sections.

Decreasing control voltage range: Detection does not require more in depth knowledge of the system. The fault detector needs to receive control voltage measurement, control voltage demand and needs to be aware of the normal voltage range. If the voltage demand is below the normal range, but the measured voltage does not match with the demand, a power supply related problem can be suspected.

Sensor fault: Some of the sensor faults can be detected through the discontinuities they cause in the signal.

Discrepancy between estimated and actual actuator torques: Observer based fault detection methods can help in exposing wrong torque estimates. The estimated torque is fed to the simulated observer system. If the system states of the observer and the real satellite have a substantial mismatch, a fault can be suspected.

Reaction wheel or magnetorquer axis displacement: The reaction wheel system has voltage, current, angular velocity sensors, but none of these local sensors are able to detect the displacement of the axis. However fault detectors taking into account the satellite dynamics using attitude measurements can register the difference between actuator torque demand and actuator torque output, which can indicate a misalignment. During normal operation, when all actuators are working, finding the actuator with misaligned axis can be quite problematic. Isolation of this type of fault can be done by turning off the main attitude controller, then one by one giving torque demand to each actuator. If the actuator has an unexpected effect on the satellite dynamics, the actuator can be deemed faulty.

Winding fault leading to zero torque output: Reaction wheel winding fault can not be directly detected, since there is no direct measurement available of the output torque. Residuals based on structural analysis can detect a discrepancy between winding current and torque output. Similarly, structural analysis based residual can be established for the magnetorquers using magnetic field and current measurement.

Reaction wheel bearing fault: If the bearing of a reaction wheel is faulty, the friction increases, changing the dynamics of the motor. This can be detected through the structural analysis based residual signal.

Motor fault detection

Model-free fault detection

Gradient anomaly detection: Some faults can cause anomalies in signals that are easy to notice by simply analyzing the signal shape they produce. Discontinuities for example often hint at a fault. Since most signals are sampled discretely, discontinuities appear as large signal steps. For example, if the angular velocity sensor in the reaction wheel motors fall to zero instantaneously, there's a good chance that a sensor fault has just occurred. Detecting faults through such anomalies require no knowledge of the system dynamics, thus they can be deemed as model free fault detection.

A reconfiguration scheme using anomaly detection in angular velocity sensors has been implemented in the simulation environment. The detection checks the magnitude of the angular velocity gradient, and if it's above the threshold, the fault detector module sends a fault signal to the reaction wheel supervisor system, which can decide to reconfigure the reaction wheel torque distribution. The signal equation is given by equation 7.1, where $\dot{\omega}_{thresh}$ denotes the threshold for fault signal generation, Δt denotes the sampling time. $\dot{\omega}_{thresh}$ can be set according to maximum reaction wheel torque, maximum reaction wheel angular velocity and wheel friction. $\dot{\omega}_{thresh}$ should at least be $\dot{\omega}_{thresh} > \frac{b\omega_{max}+\tau_{max}}{J_{motor}}$ if false fault signals are to be avoided.

$$FaultSignal_i = |\omega_{w,i}(k) - \omega_{w,i}(k-1)| > \dot{\omega}_{thresh}\Delta t \tag{7.1}$$

Structural Analysis

Structural analysis studies the interrelation between parameters and variables of the system by establishing constraints. The constraints can be obtained from the equations describing the system model. Structural analysis distinguishes known and unknown variables. The unknown variables are expressed using the known ones and the constraints. Structural analysis based residual signal generation requires that the unknown variables can be expressed redundantly. One of the constraints is used to express the unknown variable, the other to verify it. If there's a mismatch between the two, a fault is detected.

When looking for sensor faults, one constraint is between the measured and the actual values of a variable. When a sensor fault occurs, there can be a considerable difference between the measured and the actual value of a variable. Assuming that only one fault occurs at any given time, faults cannot mutually neutralize each other. The following structural analysis based residual generator is able to detect both actuator and sensor faults.

The constraints being used to detect faults in the motor are derived from the equations in section 6.1 and are listed in equations 7.2 to 7.5. C_i represents constraint relations, d_i represent differential relations. The relation between the constraints and the variables are illustrated by figure 7.2.

$$C_1(\omega, v) = V_a = R_a i + k_e \omega \tag{7.2}$$

$$C_2(\omega, \dot{\omega}, i) = k_t i = J\frac{d\omega}{dt} + b\omega \tag{7.3}$$

$$C_2(\tau, i) = \tau = k_t i \tag{7.4}$$

$$d_1(\omega, \dot{\omega}) \tag{7.5}$$

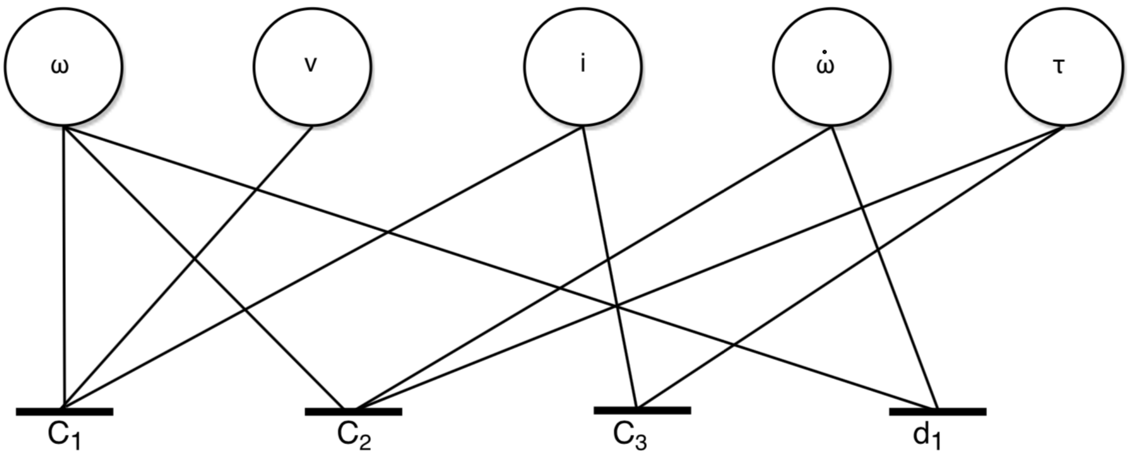

Figure 7.2: Structural graph of reaction wheel motor

ω and i can be measured, so the residual signal can be derived according to 7.6. In absence of fault, the residual should be close to zero.

$$residual = -k_t i + J\frac{d\omega}{dt} + b\omega \tag{7.6}$$

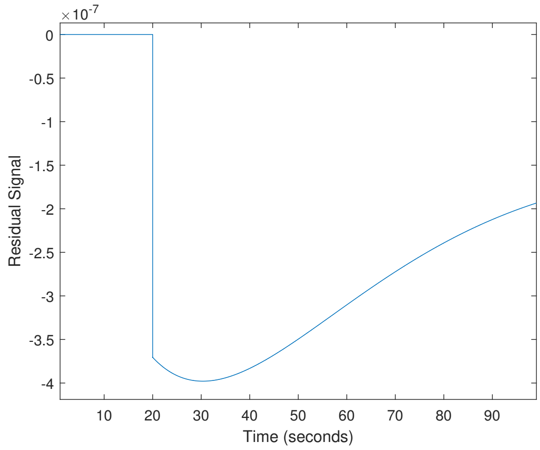

(a)

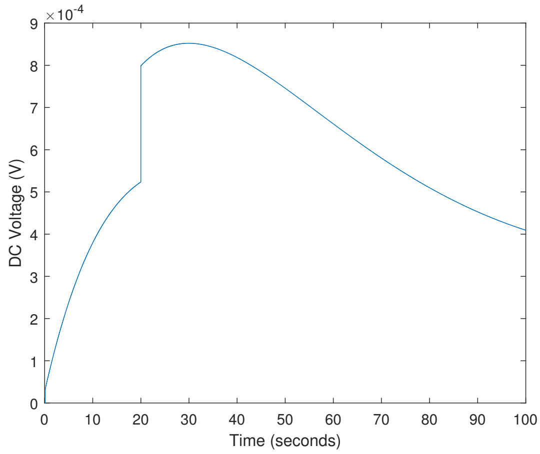

(b)

Figure 7.3: Figure 7.3a: Residual signal in scenario where at 20 s the reaction wheel friction doubles. Figure 7.3b: DC control voltage signal of angular velocity controlled reaction wheel in scenario where at 20 s the reaction wheel friction doubles

The friction model is quite accurate at high speeds, not so much for low speeds. This needs to be addressed by a higher threshold fault signal threshold at low speeds. Figures 7.3 - 7.4 show the effect of a bearing fault on the residual, when the fault doubles the reaction wheel friction.

When a residual indicates a fault, the supervisor system can decide to change the mode of torque distributor, shutting down the faulty wheel. There's a short term error in the reaction wheel subsystem's torque output, but then the angular velocity reference tracking normalizes the output quite quickly. This might jeopardize a downlink operation, but this kind of fault rarely occurs, and might only require downlinking to be postponed for the next orbit.

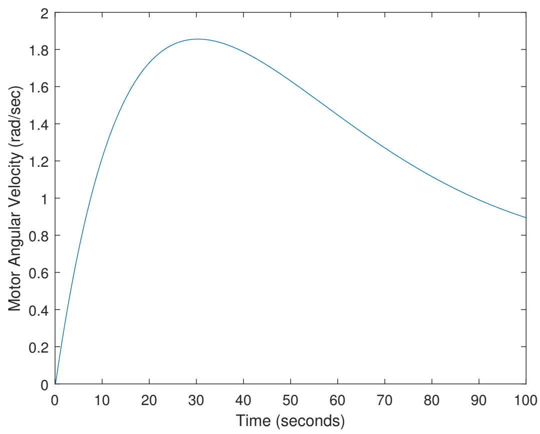

Figure 7.4: Angular velocity in scenario where at 20 s the reaction wheel friction doubles

Magnetorquer fault detection

Model based methods have been used for fault detection in magnetorquer actuators. Structural analysis based methods will be discussed first that have been implemented locally in the magnetorquer system and subsequently two observer based designs.

Magnetorquer local structural analysis

Using the Biot-Savar law from equation 6.17, the residual for the magnetorquer is generated using the following equation:

$$residual = B_{mt} - \frac{4\mu_0}{\sqrt{2}\pi L} I \tag{7.7}$$

where
B_{mt} is the magnetic field of the magnetorquer
μ_0 is a constant called permeability of free space
I is the current
L is the length of the coil

The Biot-Savart is applied for the magnetometer located at the center of the square coil.

The magnetometers measure the combined magnetic field from Earth and all the magnetorquers, the magnetic field generated by the examined magnetorquer has to be decoupled through sensor fusion.

Luenberger Observer

Parallel to structural analysis method an observer based method have been designed for fault detection in magnetorquer based actuators. Here will be discussed a Luenberger-like form which is based directly on the non-linear dynamics. In previous chapter has been discussed that for each axis there is a pair of magnetorquers. The redundant magnetic actuators are used for reconfiguration in the presence of a fault or failure.
The Luenberger-like observer is based on the dynamic equation 4.1 and for the sake of brevity is rewritten here as

$$\dot{\boldsymbol{\omega}} = -\underline{I}_s^{-1}\underline{\omega}^{\times}\underline{I}_s\boldsymbol{\omega} - \underline{I}_s^{-1}\underline{\omega}^{\times}\mathbf{h_{rw}} + \underline{I}_s^{-1}[\mathbf{N_{rw}} + \mathbf{N_{mt}} + \mathbf{N_{dist}}] \tag{7.8}$$

where the time dependency of the variables has been suppressed for clarity. Rearranging the above equation and by adding the fault vector $\mathbf{F_{MT}}$ it can obtained

$$\dot{\boldsymbol{\omega}} = \underbrace{-\underline{I}_s^{-1}[(\underline{I}_s\boldsymbol{\omega})^{\times} - (\mathbf{h_{rw}})^{\times}]}_{\underline{A}}\boldsymbol{\omega} + \underbrace{\underline{I}_s^{-1}}_{\underline{B}}\underbrace{[\mathbf{N_{rw}} + \mathbf{N_{mt}}]}_{\mathbf{u}} + \underline{I}_s^{-1}\mathbf{N_{dist}} + \mathbf{F_{MT}} \tag{7.9}$$

where $\underline{A} = -\underline{I}_s^{-1}[(\underline{I}_s\boldsymbol{\omega})^\times - (\mathbf{h_{rw}})^\times]$ is the system matrix, $\underline{B} = \underline{I}_s^{-1}$ is the input matrix, $\mathbf{N_{actual}} = \mathbf{N_{rw}} + \mathbf{N_{mt}}$ is the input vector and $\mathbf{N_{dist}} = \mathbf{d}$ is the disturbance vector. The system can now be written in Luenberger-like form as

$$\dot{\hat{\boldsymbol{\omega}}} = \underline{A}\hat{\boldsymbol{\omega}} + \underline{B}\mathbf{u} + \underline{B}\mathbf{d} + \underline{LC}(\boldsymbol{\omega} - \hat{\boldsymbol{\omega}}) \tag{7.10}$$

with $\underline{L}$ be the observer gain and the output vector can be written as

$$\mathbf{y} = \underline{C}\hat{\boldsymbol{\omega}} \tag{7.11}$$

with $\underline{C}$ be identity matrix. The matrix $\underline{A}$ is found by using the maximum values of $\boldsymbol{\omega}$ and $\mathbf{h_{rw}}$ which were obtained by running the simulation over one period, and thus the gain matrix is obtained by pole placement as

$$\underline{L} = \begin{bmatrix} -3.0000 & -0.0014 & 0.0004 \\ 0.0011 & -4.0000 & -0.0163 \\ -0.0003 & 0.0163 & -5.0000 \end{bmatrix} \tag{7.12}$$

Residual generation

Assuming that the motors are fault free a residual can be generated from the Luenberger-like observer. By denoting $\mathbf{N_{obs}} = \mathbf{I_s}\dot{\hat{\boldsymbol{\omega}}}$ where I is the inertia of the satellite then a residual can be generated as

$$residual = \mathbf{N_{actual}} - \mathbf{N_{obs}} \tag{7.13}$$

thus if $\|\mathbf{residual}\| \geq threshold$ a fault has been occurred. The structure of Luenberger-like observer can be seen in *figure 7.5* and the generated residual signal in *figure 7.6* .

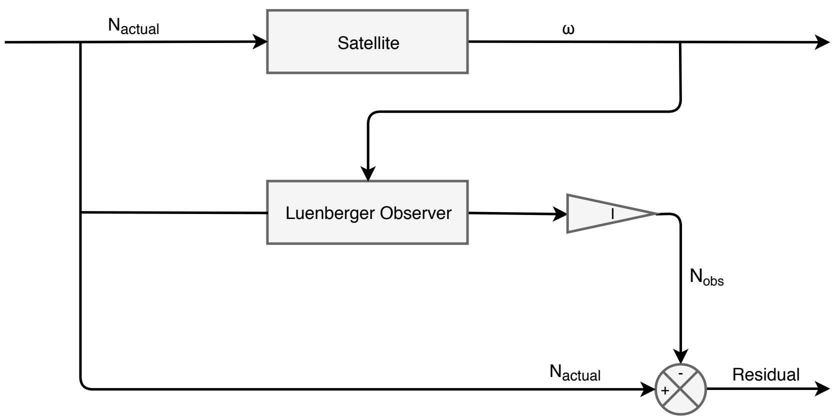

Figure 7.5: Luenberger-like observer structure and residual generation

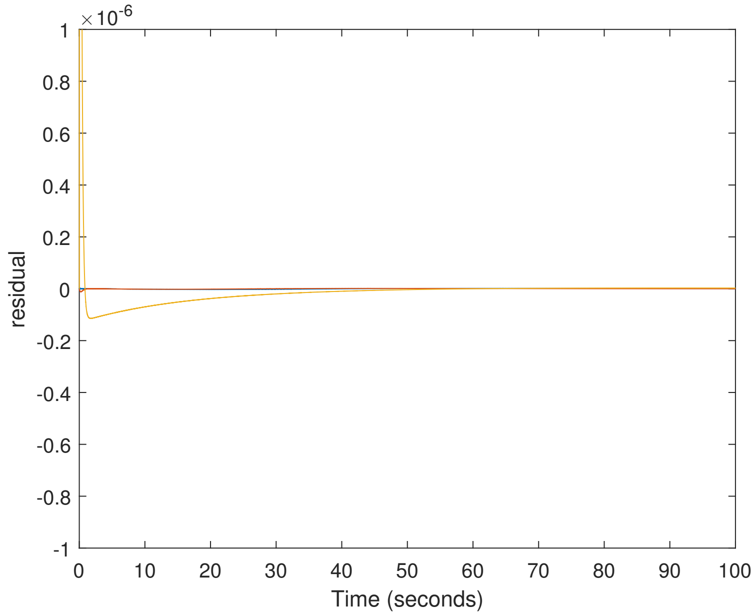

Figure 7.6: Luenberger-like Observer residual signal

Even the Luenberger-like observer is able to detect certain faults, is not robust in the sense of isolation. In order to isolate the faulty component the Luenberger-like observer can be combined with the local structural analysis based residual which have been discussed in 7.2 and together by combining their flags can reconfigure the magnetorquer scheme by shutting off the faulty component and turning on the healthy one which will be discussed in chapter 8. In the *figure 7.7* it can be seen the flag from the observer with a fault in the voltage supply of the first magnetorquer component at 200[s].

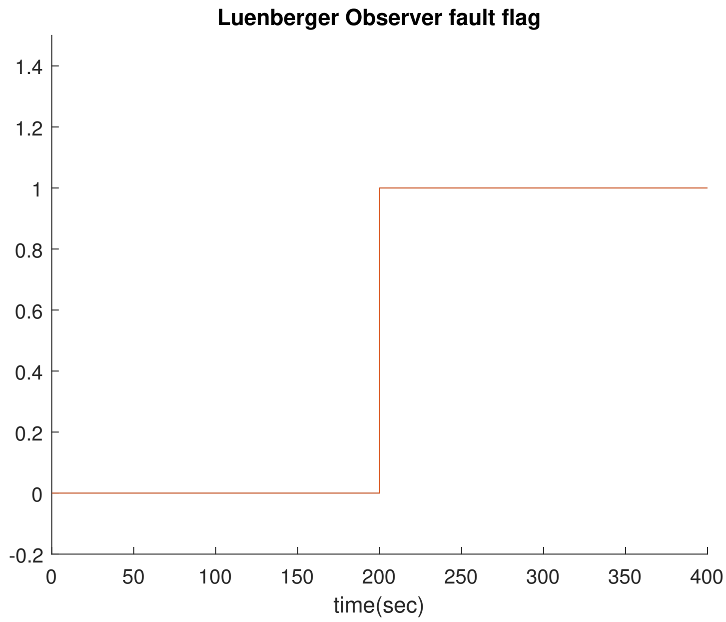

Figure 7.7: Luenberger-like Observer flag with a fault in the voltage supply occurring at 200 seconds

Unknown Input Observer (UIO)

Disturbances and modeling errors may cause discrepancies between the actual system and the descriptor mathematical model. Linearization and simplifications which make the system more manageable may lead to such uncertainties. Uncertainties can have an effect on the system dynamic behavior. During observer design, these uncertainties can be considered as unknown inputs. The observer can be designed to make the system state estimate error converge to zero in the presence of such unknown inputs. The linearized system dynamics is described according to equations 7.14 and 7.15.

$$\dot{\mathbf{x}} = \underline{A}\mathbf{x} + \underline{B}\mathbf{u} + \underline{E}\mathbf{d} \tag{7.14}$$

$$\mathbf{y} = \underline{C}\mathbf{x} \tag{7.15}$$

where $\underline{A}$,$\underline{B}$ and $\underline{C}$ are the system matrix, input and output matrix respectively and $\underline{E}$ is the distribution matrix of the unknown input (disturbance) $\mathbf{d}$. Furthermore, $\mathbf{x}$ is the state vector, $\mathbf{u}$ is the input vector and $\mathbf{y}$ is the output vector. The time dependency of the variables has been suppressed in order to relax the notation. Following [12],
An observer is defined as Unknown Input Observer for a system described by equation (7.14) *if the state estimation error vector e approaches zero asymptotically regardless of the presence of the unknown input*
The full order observer dynamics is set up according to equations 7.16 and 7.17.

$$\dot{\mathbf{z}} = \underline{F}\mathbf{z} + \underline{TB}\mathbf{u} + \underline{K}\mathbf{y} \tag{7.16}$$

$$\hat{\mathbf{x}} = \mathbf{z} + \underline{H}\mathbf{x} \tag{7.17}$$

with $\hat{\mathbf{x}}$ being the state estimate and $\mathbf{z}$ the state of the observer. When *equation (7.16)* is an observer for the system given by *equation (7.14)* the dynamics of the error vector ($\mathbf{e} = \mathbf{x} - \hat{\mathbf{x}}$) can be written according to equation 7.18 [12].

$$\dot{\mathbf{e}} = (\underline{A} - \underline{HCA} - \underline{K}1\underline{C})\mathbf{e} + (\underline{A} - \underline{HCA} - \underline{K}1\underline{C} - \underline{F})\mathbf{z} + ((\underline{A} - \underline{HCA} - \underline{K}1\underline{C})\underline{H} - \underline{K}2)\mathbf{y} \tag{7.18}$$

$$+(\underline{I} - \underline{HC} - \underline{T})\underline{B}\mathbf{u} + (\underline{I} - \underline{HC})\underline{E}\mathbf{d}$$

in the above equation the utility of $\mathbf{x} = \mathbf{e} + \hat{\mathbf{x}} = \mathbf{e} + \underline{H}\mathbf{y} + \mathbf{z}$ is used. The estimation error may converge to zero if the following conditions hold true:

$$\underline{F} = \underline{A} - \underline{HCA} - \underline{K}1\underline{C} \tag{7.19}$$

$$(\underline{I} - \underline{HC})\underline{E} = 0 \tag{7.20}$$

$$\underline{T} = (\underline{I} - \underline{HC}) \tag{7.21}$$

$$\underline{K} = \underline{K}_1 + \underline{K}_2 \tag{7.22}$$

$$\underline{K}_2 = \underline{FH} \tag{7.23}$$

where $\underline{K}_1$ is designed freely by pole placement to give desired eigenvalues of the observer. The error dynamics if equations 7.20-7.23 hold true can now be written as

$$\dot{\mathbf{e}} = \underline{F}\mathbf{e} \tag{7.24}$$

consequently if the eigenvalues of $\underline{F}$ are to the left half plane, the error converges exponentially to zero.

A solution to *equation (7.20)* is given by making use of the Moore-Penrose pseudo-inverse as

$$\underline{H} = \underline{E}(\underline{CE})^{\dagger} \tag{7.25}$$

with $(\underline{CE})^{+} = [(\underline{CE})^{T}(\underline{CE})]^{-1}\underline{CE})^{T}$. A sufficient and necessary condition for the UIO existence is that the number of independent unknown inputs can not be larger than the number of independent measurements which leads to

$$rank(\underline{CE}) = rank(\underline{E}) \tag{7.26}$$

and by denoting $\underline{A}_1 = \underline{A} - \underline{HCA}$ that the pair $(\underline{CA}_1)$ is detectable and thus F can have stable roots.

Residual Generation

In order to be able to detect faults, a residual signal is set up. The residual should converge to zero in the presence of $\mathbf{d}$ unknown input and the absence of faults. In order to make the faults strong detectable, the residual should not converge to zero in the presence of faults. The residual is defined as

$$\mathbf{r} = \mathbf{y} - \underline{C}\hat{\mathbf{x}} == \mathbf{y} - \underline{C}(\mathbf{z} + \underline{H}\mathbf{y}) = (\underline{I} - \underline{CH})\mathbf{y} - \underline{C}\mathbf{z}$$

which does not depend on the disturbance vector. Residual thresholding can be applied to detect faults. Figure 7.8. illustrates the nominal unknown input observer with a block diagram.

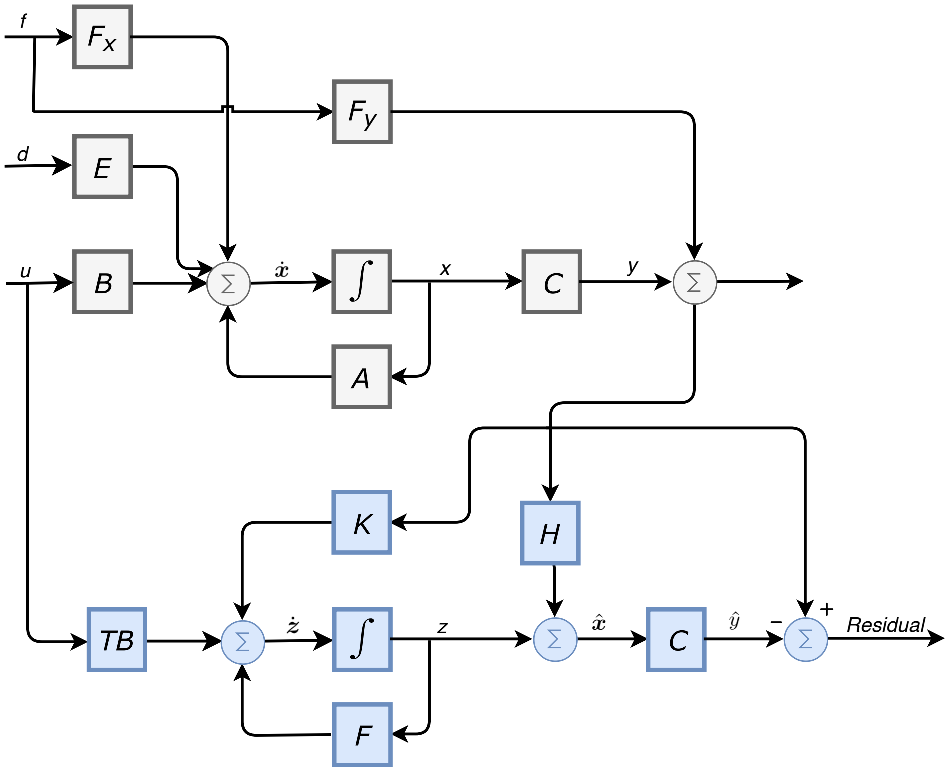

Figure 7.8: Observer based residual generator

Actuator fault isolation is possible assuming that all the sensors are fault free. Sensor fault isolation is possible assuming that the actuators are fault free. A descriptor model of the overall system with actuator fault can be written as given in equation 7.14.

$$\dot{\mathbf{x}} = \underline{A}\mathbf{x} + \underline{B}\mathbf{u} + \underline{E}\mathbf{d} + \underline{B}\mathbf{f_{act}} \tag{7.27}$$

where $\mathbf{f_{act}}$ represents the actuator faults.

Application of Unknown Input Observer

The present chapter discusses how to apply unknown input observer (UIO) theory to the satellite functioning in nadir pointing control goal. The regular UIO uses linear model, however the satellite system is highly nonlinear. During one orbit, the orientation of the nadir pointing satellite rotates by 360^o. By choosing the appropriate reference frame, this rotation can be eliminated from attitude dynamics. In local vertical, local horizontal frame (LVLH), the nadir pointing satellite keeps its attitude. This opens an opportunity to use linear approximation of the trigonometric nonlinearities in the satellite dynamic equations. The operating point should be chosen as nadir pointing, and if the attitude stays near enough to the operating point, the model stays quite accurate.

Yang's article on desaturation [33] describes a model that can be effective for UIO. The $\underline{A}$ matrix of the model is constant, so the UIO matrices can be derived as described in 7.2. The model detaches the orbit angular velocity from the dynamics according to equation 7.28.

$$\boldsymbol{\omega} = {}^{\mathbf{lv}}_{\mathbf{I}}\boldsymbol{\omega} + {}^{\mathbf{s}}_{\mathbf{lv}}\boldsymbol{\omega} \tag{7.28}$$

where ${}^{\mathbf{lv}}_{\mathbf{I}}\boldsymbol{\omega}$ is the angular velocity of the LVLH frame compared to the inertial frame and ${}^{\mathbf{s}}_{\mathbf{lv}}\boldsymbol{\omega}$ is the angular velocity of the body frame compared to the LVLH frame. $\underline{B}(t)$ includes Earth's local magnetic field, so it has to be updated at every sample. The model has been altered to include the unknown inputs and faults, furthermore the gravity gradient torque is handled outside of the system matrix $\underline{A}$.

$$\dot{\mathbf{x}} = \underline{A}\mathbf{x} + \underline{B}(t)\mathbf{u} + \underline{E}\mathbf{d} + \underline{F}_x\mathbf{f_y} \tag{7.29}$$

$$\mathbf{y} = \underline{C}\mathbf{x} + \underline{F}_y\mathbf{f_y} \tag{7.30}$$

For the detailed matrices of the model used for designing the observer, please refer to appendix I.

where I_w is the reaction wheel axial moment of inertia, ω_o is the angular velocity of the orbit, I_i is the satellite moment of inertia along ith principal axis. $\underline{C}$ is an identity matrix.

If the UIO design algorithm is followed, without fault the residual converges to zero, as shown in figure 7.9 a. If the angular velocity estimate is wrong, i.e. $\underline{F}_y\mathbf{f_y}$ is nonzero, the residual doesn't converge to zero. Figure 7.10 a. shows the residual for an error in angular velocity estimate. The angular velocity of the satellite is estimated through and sensor fusion and filtering, the details of which is out of the scope of the present thesis.

The UIO dynamics are designed to make the residual converge to zero in the presence of unknown input $\mathbf{d}$. The fact that the disturbances and magnetorquer faults affect the same state variables ${}^{\mathbf{s}}_{\mathbf{lv}}\dot{\boldsymbol{\omega}}$ means that the system cannot distinguish the magnetorquer fault from the disturbances, thus they cannot be decoupled.

An experiment was made to investigate if ignoring the unknown torque disturbances, is it possible to distinguish magnetorquer faults through thresholding. The $\underline{E}$ was modified to a zero matrix, then the observer was redesigned accordingly. This essentially makes the observer stop being an UIO. In the test, $N_{dist}^{est\ error}$ was simulated as a constant vector with a magnitude of $1nNm$, around 2% of $\mathbf{N_{dist}}$, while the magnetorquer magnetic moment fault $\mathrm{m}_{mt,1}^{fault}$ error was a constant $10mJ/T$, a magnitude that would occur at rather high reaction wheel speed due to desaturation torque demand. Figure 7.10 a. shows the residual when only the disturbance is present, figure 7.10.b. shows the residual when a fault occurs at 800 second intervals following a square signal. The residual for the fault is orders of magnitude higher than for the disturbance, however the residual from the disturbance keeps growing and growing through many orbits. This means that thresholding is not effective for magnetorquer fault detection in the long term with this observer.

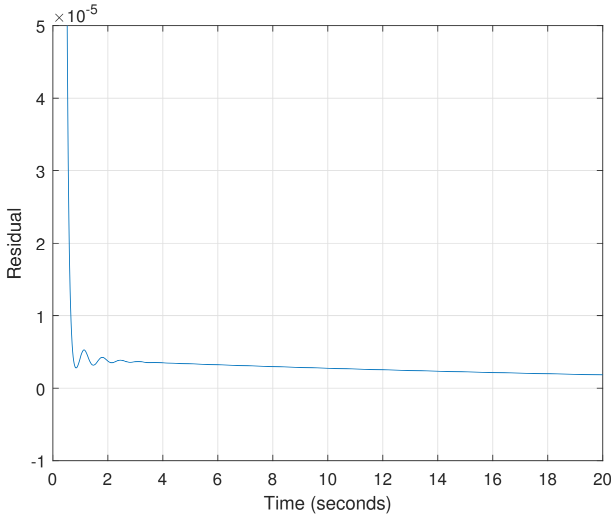

(a)

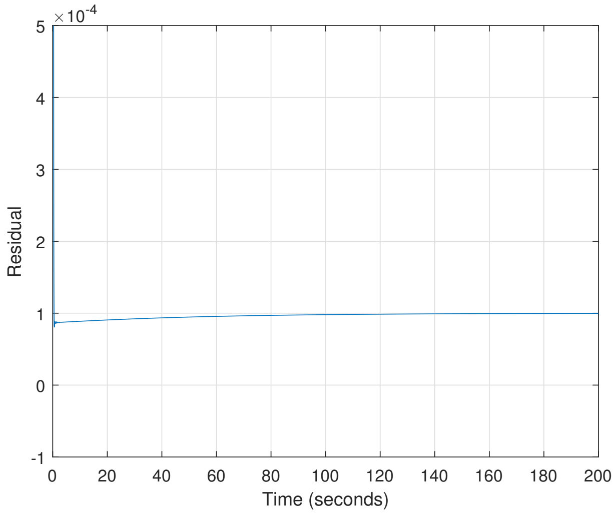

(b)

Figure 7.9: 7.9 a. presents how the residual converges to zero when disturbance is present and fault is absent. 7.9 b. presents the residual in case of a fault in angular velocity estimation.

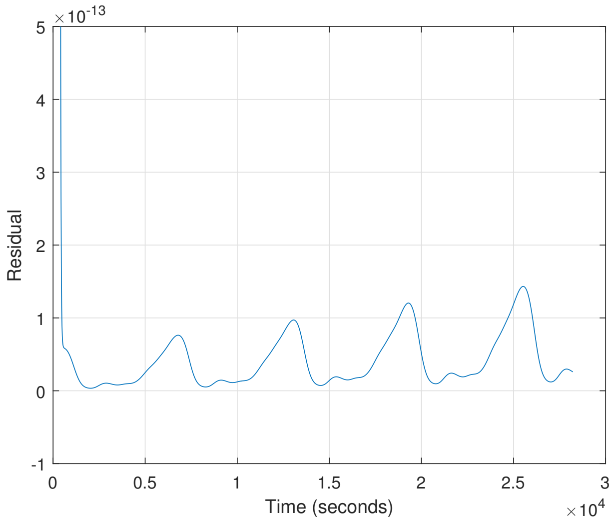

(a)

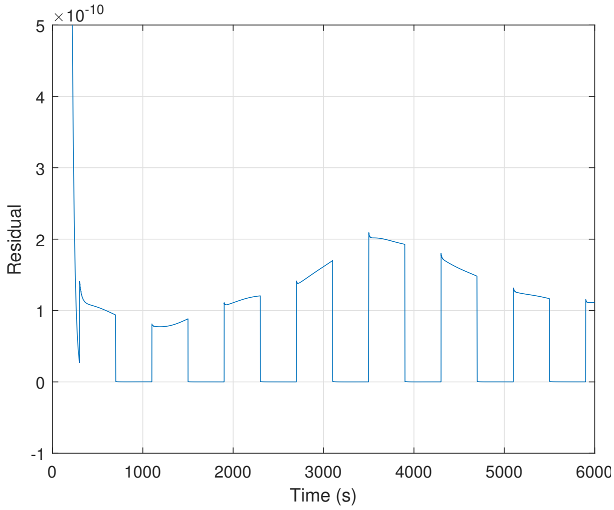

(b)

Figure 7.10: 7.10.a. presents the residual of the observer without torque disturbance convergence when only disturbance torque estimate is present. 7.10.b. presents the residual with periodically occurring magnetorquer fault. The order of magnitude of the residual in 7.10.a. is 3 times as big.

8 | Fault handling and reconfiguration

8.1 Virtual actuators and sensors

Actuators and sensors are subject to various faults. Due to these faults the system may experience drops in performance which could lead to stability loss. The objective of fault tolerant control using virtual actuators and sensors is to add a reconfiguration block which is presented as an extra layer between the faulty system and the level controller, capable of satisfying control requirements through reconfiguration. The purpose of the reconfiguration block in case of a fault is to provide fault tolerance by using the virtual actuators and sensors. As can be seen in figure 8.1 the reconfiguration of the faulty actuators is made independently of the main attitude control schemes. In the figure, u_f represents a low level control input that takes into account the faults of the system, and y_f is the faulty output.

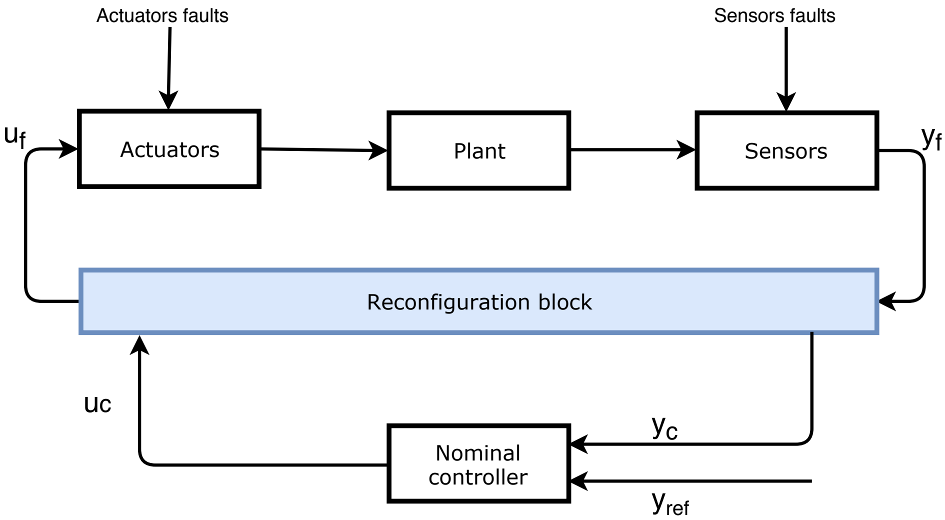

Figure 8.1: Virtual actuators and sensors scheme

The reconfiguration of the faulty actuators is made in the adequate actuator subsystems.

To keep the overall system dynamics undisturbed by reaction wheel reconfiguration, compensation schemes need to be used during reconfiguration to counteract the force occurring during the deceleration of the wheels. During magnetorquer reconfiguration, no such compensation is needed, since the magnetorquers can be shut down practically instantaneously.

8.2 Reaction Wheel Reconfiguration

Fault handling in the redundant reaction wheel configuration can be done by isolating which is the reaction wheel where the fault occurred and shutting it off and redistributing the torques to the rest of the reaction wheels. Fault signals emitted by the fault detection modules are handled by the reconfiguration logic. Section 6.1 describes the distribution of reaction wheel torque demand between the reaction wheels. When the reconfiguration system receives a fault signal, it redistributes the $\mathbf{N_{rw}^d}$ torque demand by modifying $\underline{A}_M$ matrix in equation 6.9. The torque demand for the faulty wheel becomes zero, while the sum of reaction wheel torques are controlled to follow $\mathbf{N_{rw}^d}$.

This reconfiguration/redistribution can be represented by changing the $\underline{A}_M$ columns corresponding to faulty wheels to zero vectors. For example, if a fault occurs in the 3rd reaction wheel, the transformation matrix becomes $\underline{A}_{M,f3}$, as presented in equation 8.1.

$$\underline{A}_{M,f3} = \begin{bmatrix} \mathbf{Axis_1^M} & \mathbf{Axis_2^M} & \mathbf{0} & \mathbf{Axis_4^M} \end{bmatrix} \tag{8.1}$$

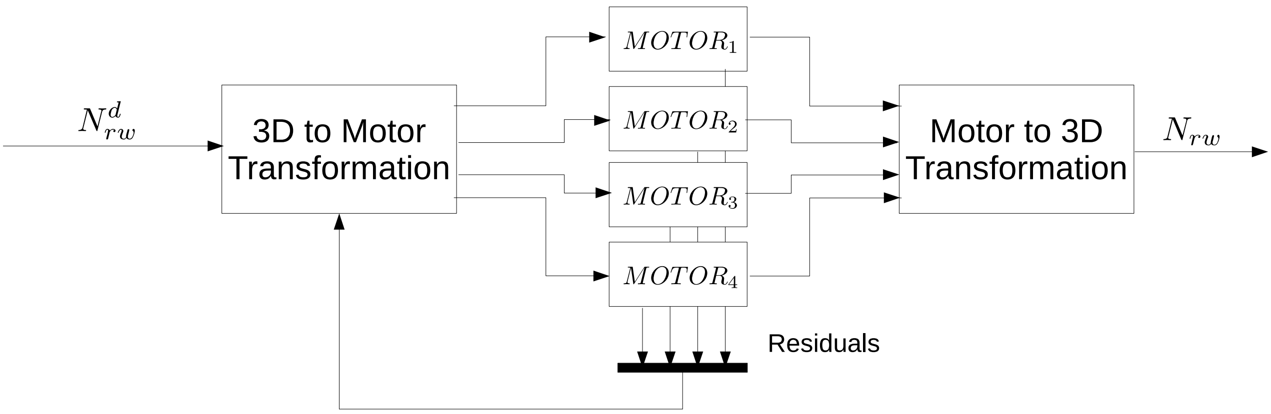

Figure 8.2: Reconfiguration Control Scheme for Reaction Wheels

The pseudo inverse used for transformation between 3D to motor torque is calculated in the same manner as presented in equation 6.11, see equation 8.2. The torque distribution controller scheme which checks for faults in the motors, is presented in Figure 8.2

$$\underline{A}_{M,f3}^{\dagger} = \underline{A}_{M,f3}^T(\underline{A}_{M,f3}\underline{A}_{M,f3}^T)^{-1} \tag{8.2}$$

Equation 8.3 presents the reconfigured torque distribution equation.

$$\mathbf{N_M^d} = \underline{A}^{\dagger}_{M,f3}\mathbf{N_{rw}^d} \tag{8.3}$$

Reconfiguration with compensation in case of angular velocity sensor fault

A reconfiguration scheme using anomaly detection in angular velocity sensors has been implemented in the simulation. The detection checks the magnitude of the angular velocity gradient, and if it's above the threshold, the supervisor shuts down the corresponding wheel and distributes the torque demand to the remaining wheels. This is necessary, since the reaction wheel control scheme relies on angular velocity measurements.

It is imperative to compensate for the torque output of the faulty wheel for the satellite dynamics not to be affected by the fault. The torque output of the faulty wheel can not be derived from angular velocity measurements in the presence of an angular velocity sensor fault. In order to be able to compensate for the deceleration torque, using the assumption that the only fault is in the sensor, wheel deceleration can be simulated based on the model, and compensation can be done for the simulated torque output of the wheel. This concept is illustrated in figure 8.3.

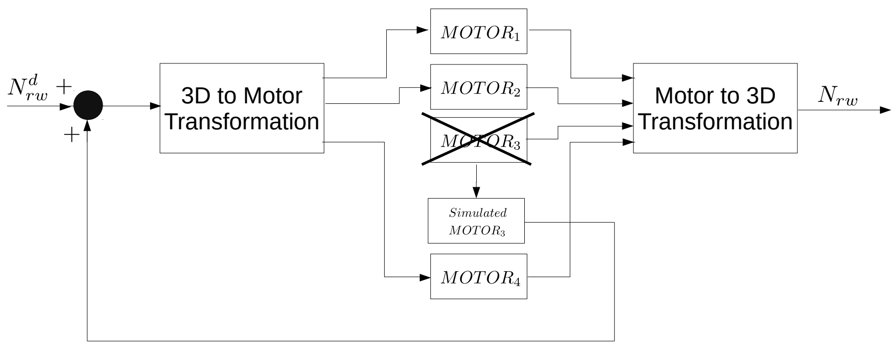

Figure 8.3: Shutdown torque compensation in case of angular velocity sensor fault.

The shut down happens as follows: when the sensor fault is detected, the system registers the last measure angular velocity and a simulation starts for wheel deceleration with the angular velocity initial value being the last non-faulty value. The control voltage is zero, the wheel is decelerated by the friction. As the fault occurs, the reaction wheel torque distribution is changed to omit the faulty wheel. The simulated torque output of the faulty wheel is fed to the reaction wheel torque distributor for compensation. The resulting graphs are presented in figures 8.4 - 8.5.

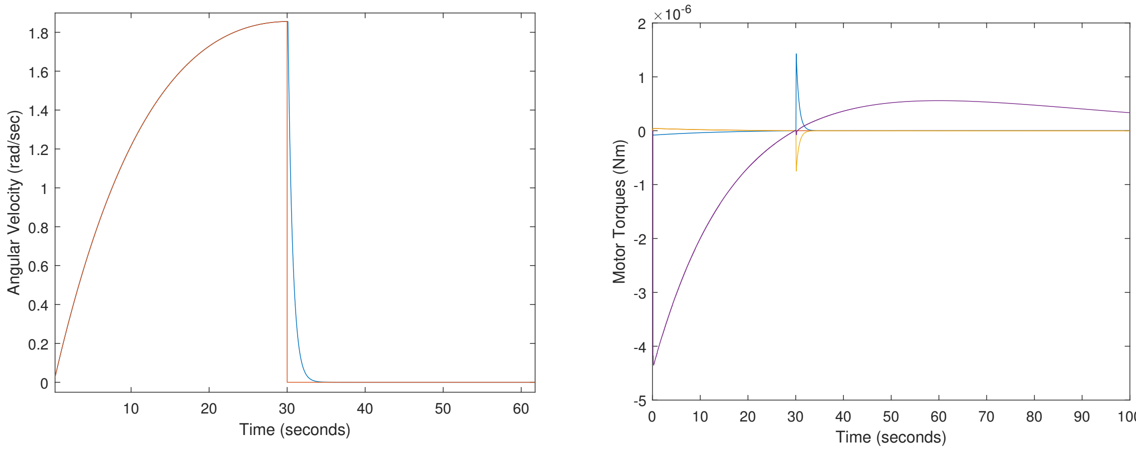

Figure 8.4: Figure 8.4a: $\omega_{M,i}$ sensor signal and actual value with fault occuring at 30 seconds. Figure 8.4b: N_M with ω sensor fault occuring at 30 seconds

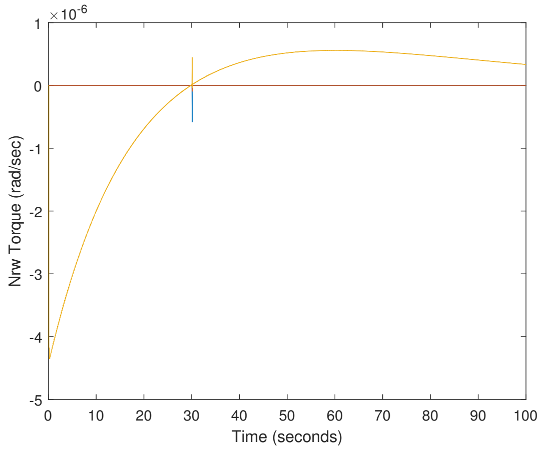

Figure 8.5: N_{rw} with ω sensor fault occuring at 30 seconds. The peak corresponds to the one control step it takes to reconfigure the system.

Reconfiguration with compensation in case of residual fault detection

If the structural analysis based motor fault detector discussed in section 7.2 sends a fault signal, $\mathrm{N}_{\mathbf{rw}}$ is redistributed while the faulty wheel undergoes a controlled deceleration. The torque output of the faulty wheel is compensated for as shown in figure 8.6. One type of fault that the residual can detect is the change of the bearing friction. If the friction increases and the wheel is shutdown by cutting the control voltage to zero, the deceleration torque could become too large to compensate for. Instead, the reference angular velocity of the faulty wheel is smoothly decreased to zero, so that the faulty torque output stays small. Figures 8.7 - 8.8 present the behaviour of the system during reconfiguration.

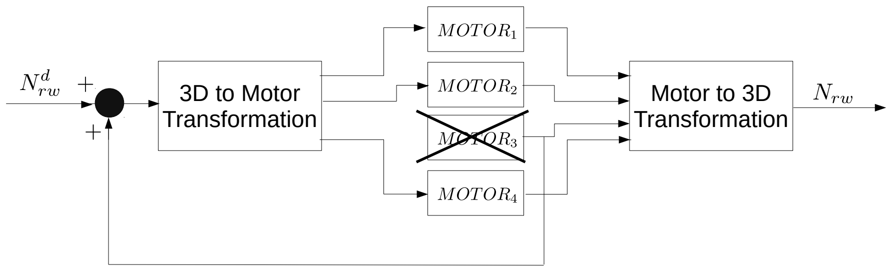

Figure 8.6: Shutdown torque compensation in case of fault detected through residual.

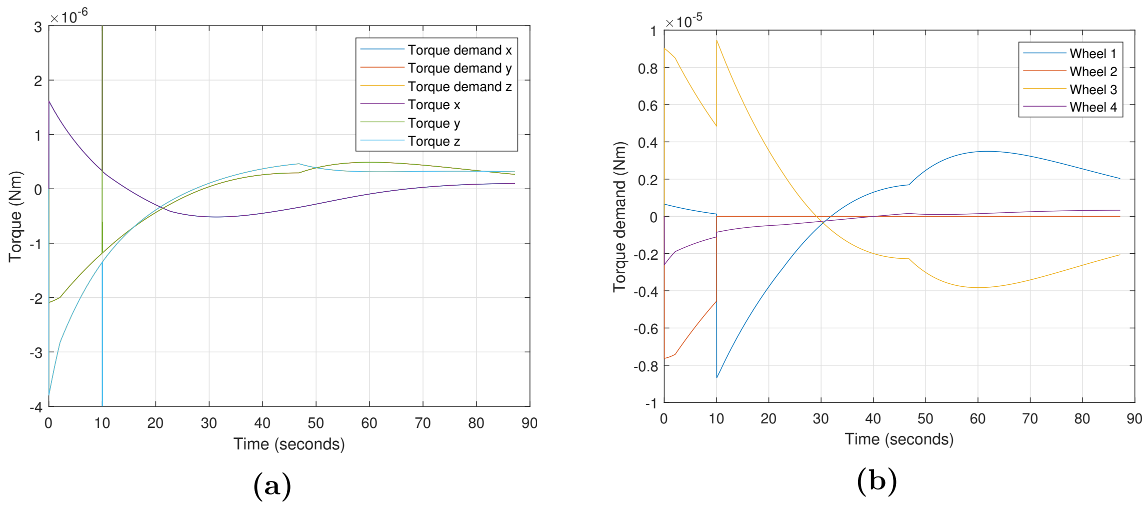

Figure 8.7: Figure 8.7a: N_{rw} with fault occuring at 10 seconds. Figure 8.7b: N_M with fault occuring at 10 seconds.

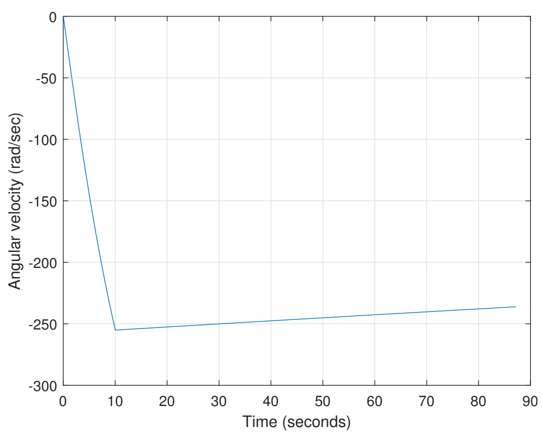

Figure 8.8: $\omega_{M,i}$ with fault occuring at 10 seconds

8.3 Magnetorquer Reconfiguration

Reconfiguration with compensation in case of Luenberger-like Observer residual fault detection

Similarly to the reaction wheel reconfiguration *section 8.2*, fault handling in the redundant magnetorquer scheme can be done by isolating the faulty magnetic component, shutting it off and at the same time turn on the redundant magnetorquer at the same axis. As it has been discussed in *section 7.2* the Luenberger-like Observer is not robust in the sense of isolating which component is faulty. Therefore, a combination with the structural analysis method *section 7.2* can be made in order to isolate the faulty component. Each method give a flag, commonly a binary input, such that when a fault is present each method indicate 1 and when a fault is absent indicate 0. Moreover, the structural analysis method is also limited on the faults which can detect. Therefore, the binary flags from both methods are inputs to a block which emulates the logic operator OR, so if the flags from each method give binary indicator 1, all the magnetorquers are switched which gives robustness in a manner of fault handling. In the *figure 8.9* it can be seen how the main magnetorquers shutting off in the presence of a fault in the power supply at time 150 and their corresponding pair takes action. Moreover, it is worth mentioning that isolation and configuration of only the faulty component can achieved by replacing the OR by AND logic operator, but this will lead in a reduced number of the family of faults that can be handled.

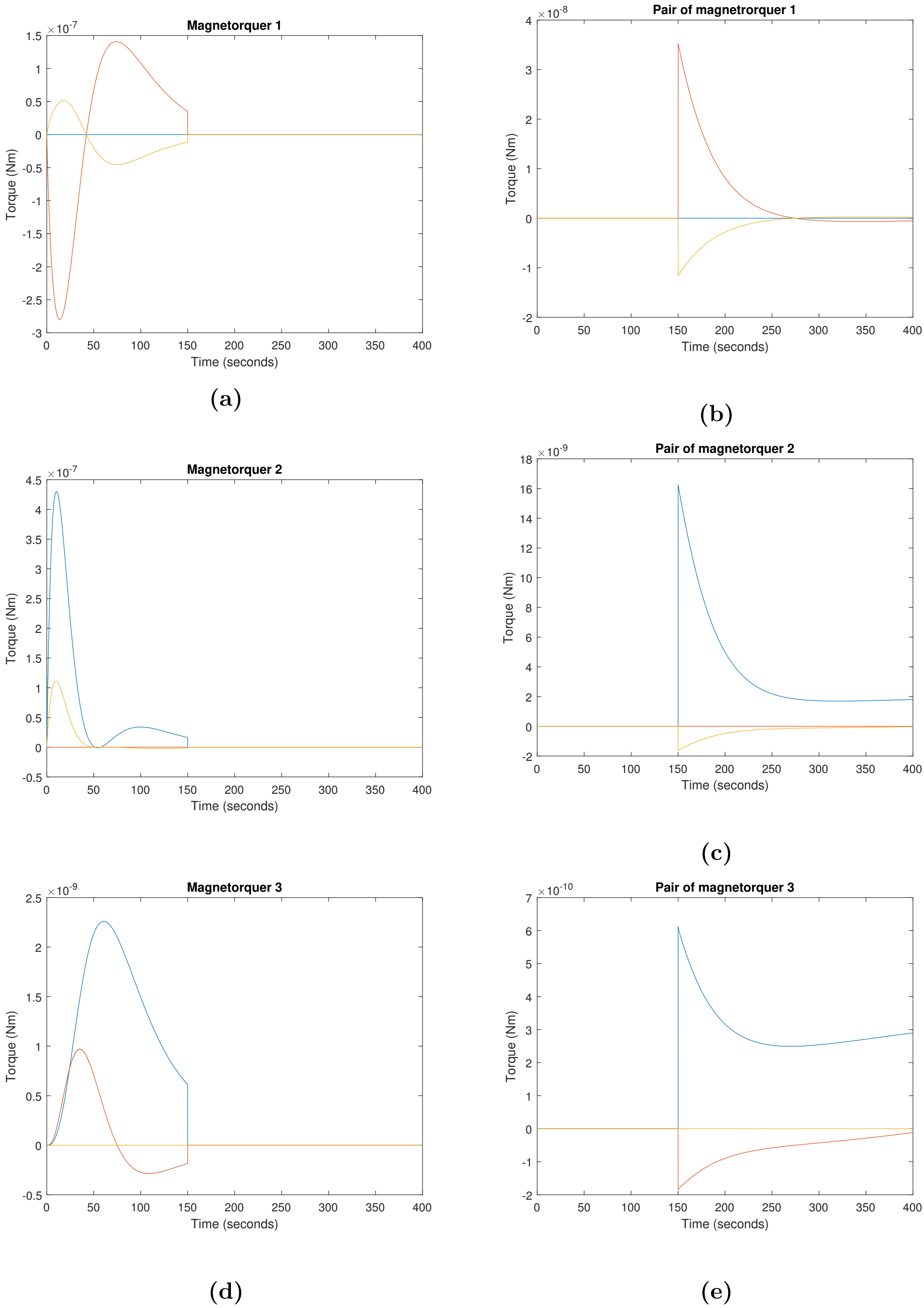

Figure 8.9: To the left are depicted the magnetorquers of each axis subjected to a fault in the voltage supply and to the right the redundant magnetorquer pairs.

Figure 8.10

9 | Acceptance test

The system is tested to see if it fulfills the requirements put up (*chapter 3*).

1. The satellite shall track the nadir within 1°.

Nadir pointing capability is tested by turning on the linear attitude controller of a satellite with initial attitude and angular velocity deviating from the reference. After reducing the initial error, the tracking error stays below 1^o, as shown in figure 9.1.

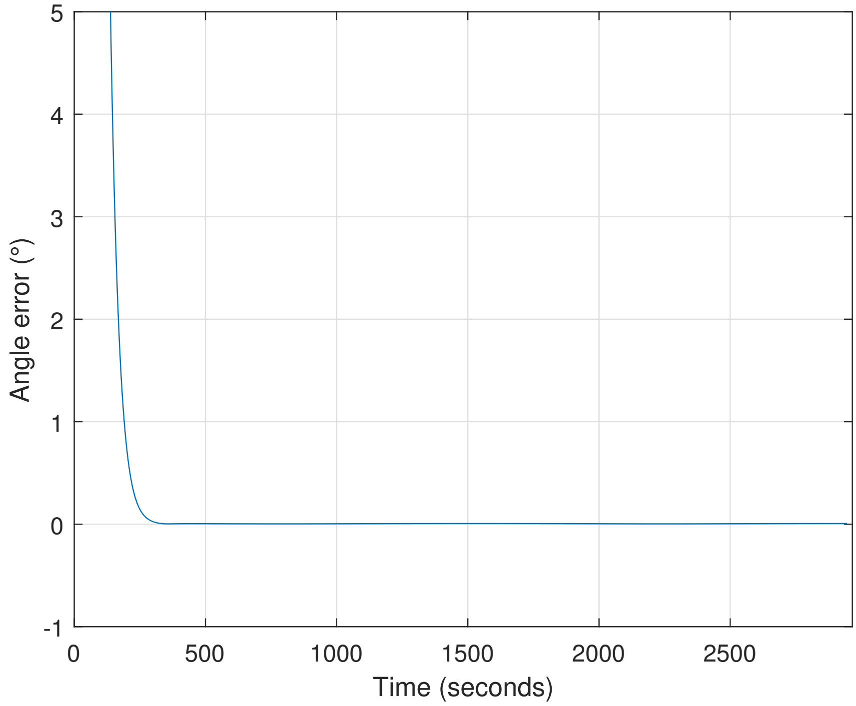

Figure 9.1: Tracking error during nadir pointing

2. The satellite should be able to track the Earth station within 1°.

Earth station tracking is tested in a scenario where the satellite flies right over the station. This is the closest the satellite in orbit can get to the Earth station, leading to maximum torque demand. The tracking error is kept below 1^o, with error peaks appearing during flyover. Figures 9.4 and 9.3 present the tracking error and torque demand arising during station tracking.

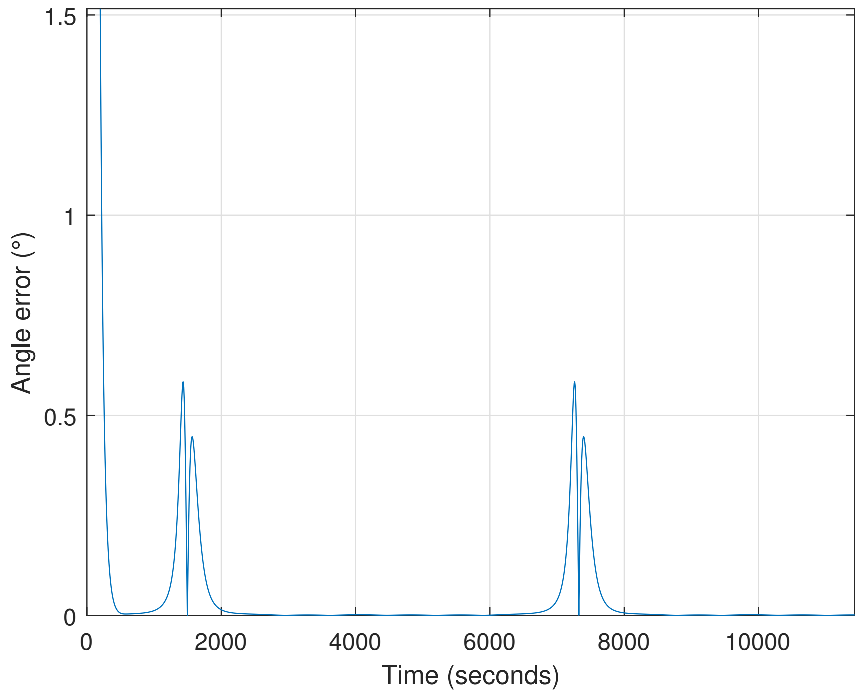

Figure 9.2: Tracking error during Earth station pointing. The satellite flies over the station.

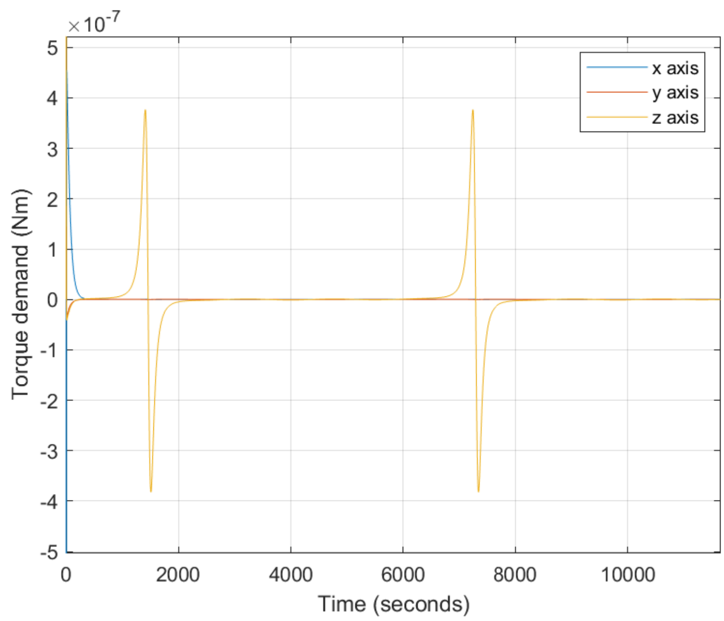

Figure 9.3: Torque demand **u** during Earth station pointing. The satellite flies over the station.

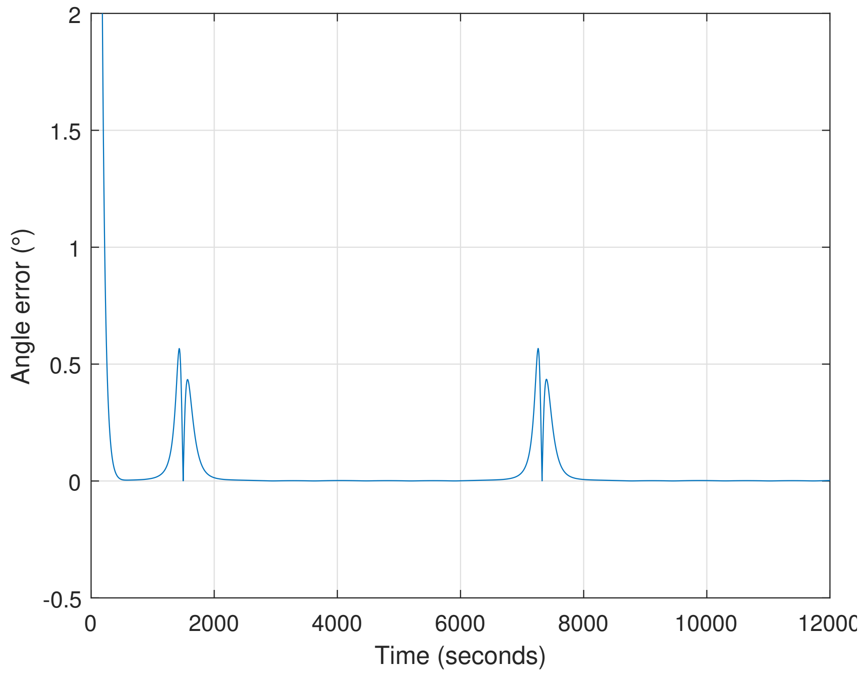

Figure 9.4: Tracking error during Earth station pointing using the linear controller. The satellite flies over the station. The 3rd reaction wheel is faulty and switched off.

3. The satellite shall detect certain actuator faults.

The system is able to detect a family of faults that may occur during a mission. For the purpose of fault tolerant control, it was not necessary to find the exact source of the fault, however finding the actuator where the fault has occurred has proven sufficient.

4. The satellite should be able to reconfigure the control scheme in order to handle faults.

The system is able to reconfigure the control scheme in order to accommodate for possible faults.

10 | Closure

10.1 Results

A satellite attitude control scheme for two cooperating actuator subsystems was implemented in a simulation environment for a fault-free system. The two subsystems supplement each other by eliminating each other's weaknesses. The reaction wheel is capable of arbitrary torque exertion at any given moment, however is susceptible to saturation, the magnetorquer can only exert torques in 2 dimensions at any given moment, but is capable of desaturating the reaction wheels. The attitude control system was designed to be modular in order to be able to implement parallel control loops. Nadir pointing capability of these control methods were proven. The control scheme can also satisfy the more difficult problem of Earth station tracking. Earth station tracking is a benchmark of great attitude control ability. The simulation environment included environmental disturbances, but signal disturbances were not considered.

The system was designed to be fault-tolerant, keeping satisfactory controllability even when actuator faults occur. In order to implement a fault-tolerant control scheme, the problem of fault detection had to be addressed. It was shown that certain type of faults can be detected using methods that have low computation requirements. Detecting other faults, such as axis misalignment proved to be more problematic. Non-observer based fault detection methods in real-life applications require filtering, which is out of the scope of the thesis. Using observers eliminate the need for filtering, thus if an observer works in the simulation environment neglecting signal disturbances, their real-life implementation can prove successful with a higher probability. Experiments were made using unknown input observer based fault detection. It proved useful for detecting fault in attitude estimation. It was shown however that the using UIO for actuator fault detection is problematic due to the fact that environmental disturbances have similar effect as actuator faults.

Based on fault detector signals, faults have been handled by shutting down the adequate member of the redundant actuator subsystem and redistributing the control demand for the functioning actuators. For reaction wheels, smooth reconfiguration was guaranteed using special transition controllers. Reaction wheel reconfiguration resulted in increased power consumption for certain maneuvers, but the reconfigured control system still managed to satisfy the control requirements.

10.2 Discussion

State of the art control schemes have been implemented and combined in the simulation environment, adjusted to the specific requirements of fault tolerant control.

The limitation of unknown input observers has been reached with the torque disturbance not being distinguishable from actuator fault. Literature research has shown how observer design becomes significantly more difficult for nonlinear systems.

The thesis has shown that exact identification of the fault source is not required to perform fault tolerant control for redundant actuator system, isolating the actuator where the fault occurred proved sufficient. This relaxes the amount of 'detective work' required in the system.

10.3 Conclusion

In this thesis actuator fault detection and fault tolerant control was examined for a pico-satellie. For fulfilling the requirements, various control schemes were developed and tested in a simulation environment. The simulated satellite was able to accommodate faults autonomously.

A | Quaternions

This appendix is based on sources from [28] and [17].

There are several possible mathematical representations for rotation. In physics, rotation matrices, Euler angles (eg. pitch-roll-yaw) and quaternions. In satellite engineering, quaternions are the preferred representations, since they are more compact than rotation matrices and lack singularities. Their only drawback is the double coverage property.

Quaternions include four values, three of them represent a vector ϵ, the fourth a scalar η.

$$\mathbf{q} = \begin{bmatrix} q_1 \\ q_2 \\ q_3 \\ q_4 \end{bmatrix} = \begin{bmatrix} \mathbf{q}_{1:3} \\ q_4 \end{bmatrix} = \begin{bmatrix} \epsilon \\ \boldsymbol{\eta} \end{bmatrix} \tag{A.1}$$

A rotation of Φ around the unit vector $\mathbf{q_{1:3}}$ can be described according to Euler's formula.

$$\mathbf{q} = e^{\frac{\Phi}{2}(e_1\mathbf{i}+e_2\mathbf{j}+e_3\mathbf{k}+e_4)} = \cos\frac{\Phi}{2} + (e_1\mathbf{i} + e_2\mathbf{j} + e_3\mathbf{k} + e_4)\sin\frac{\Phi}{2} \tag{A.2}$$

Consequently

$$\mathbf{q} = \begin{bmatrix} q_1 \\ q_2 \\ q_3 \\ q_4 \end{bmatrix} = \begin{bmatrix} e_1 \sin\frac{\Phi}{2} \\ e_2 \sin\frac{\Phi}{2} \\ e_3 \sin\frac{\Phi}{2} \\ \cos\frac{\Phi}{2} \end{bmatrix} \tag{A.3}$$

Rotation matrix corresponding to a quaternion can be calculated as

$$\underline{R}({}^{\mathbf{s}}_{\mathbf{i}}\mathbf{q}(\mathbf{t})) = (q_4^2 - \mathbf{q_{1:3}}^T\mathbf{q_{1:3}})\underline{1} + 2\mathbf{q_{1:3}}\mathbf{q_{1:3}}^T - 2q_4\underline{q}_{1:3}^{\times} \tag{A.4}$$

Quaternion multiplication

Let $\mathbf{q}$ represent the unit rotation quaternion, with $\mathbf{i}$, $\mathbf{j}$, $\mathbf{k}$ being the base vectors in Euclidean space and q_4 as the scalar part:

$$\mathbf{q} = q_1\mathbf{i} + q_2\mathbf{j} + q_3\mathbf{k} + q_4 \tag{A.5}$$

where $\mathbf{i}, \mathbf{j}, \mathbf{k}$ represent the hyper imaginary parts and satisfying the rules introduced by Hamilton:

$$\begin{aligned}
\mathbf{i^2} = \mathbf{j^2} = \mathbf{k^2} &= -1 \\
\mathbf{ij} = -\mathbf{ji} &= \mathbf{k} \\
\mathbf{jk} = -\mathbf{kj} &= \mathbf{i} \\
\mathbf{ki} = -\mathbf{ik} &= \mathbf{j}
\end{aligned}$$

Next a product of two quaternions $\mathbf{q}_A$ and $\mathbf{q}_B$ is illustrated:

$$\mathbf{q}_C = \mathbf{q}_A \otimes \mathbf{q}_B = (q_{A_1}\mathbf{i} + q_{A_2}\mathbf{j} + q_{A_3}\mathbf{k} + q_{A_4}) \otimes (q_{B_1}\mathbf{i} + q_{B_2}\mathbf{j} + q_{B_3}\mathbf{k} + q_{B_4}) \tag{A.6}$$

After rearranging terms and using the rules above, equation A.6 becomes:

$$\begin{aligned}
\mathbf{q}_C = &(q_{A_1}q_{B_4} + q_{A_2}q_{B_3} - q_{A_3}q_{B_2} + q_{A_4}q_{B_1})\mathbf{i}+ &\text{(A.7)}\\
&+(-q_{A_1}q_{B_3} + q_{A_2}q_{B_4} - q_{A_3}q_{B_1} + q_{A_4}q_{B_2})\mathbf{j}+ &\text{(A.8)}\\
&+(q_{A_1}q_{B_2} - q_{A_2}q_{B_1} - q_{A_3}q_{B_4} + q_{A_4}q_{B_3})\mathbf{k}+ &\text{(A.9)}\\
&+(-q_{A_1}q_{B_1} - q_{A_2}q_{B_2} - q_{A_3}q_{B_3} + q_{A_4}q_{B_4}) &\text{(A.10)}
\end{aligned}$$

The product quaternion can be expressed in a matrix form:

$$\begin{bmatrix} q_{C_1} \\ q_{C_2} \\ q_{C_3} \\ q_{C_4} \end{bmatrix} = \underbrace{\begin{bmatrix} q_{A_4} & q_{A_3} & -q_{A_2} & q_{A_1} \\ -q_{A_3} & q_{A_4} & q_{A_1} & q_{A_2} \\ q_{A_2} & -q_{A_1} & q_{A_4} & q_{A_3} \\ -q_{A_1} & -q_{A_2} & -q_{A_3} & q_{A_4} \end{bmatrix}}_{\underline{C}_A} \begin{bmatrix} q_{B_1} \\ q_{B_2} \\ q_{B_3} \\ q_{B_4} \end{bmatrix} \tag{A.11}$$

A skew-symmetric matrix is given as $\underline{q}^{\times}$ and defined as

$$\underline{q}^{\times} = \begin{bmatrix} 0 & -q_{A_3} & q_{A_2} \\ q_{A_3} & 0 & -q_{A_1} \\ -q_{A_2} & q_{A_1} & 0 \end{bmatrix} \tag{A.12}$$

Moreover equation A.11 can be written as

$$\mathbf{q}_C = \mathbf{q}_A\mathbf{q}_B = \underline{C}_A\mathbf{q}_B = \begin{bmatrix} -\underline{q}^{\times} + \underline{\mathbf{1}}q_{C_4} & \mathbf{q} \\ -\mathbf{q}^{\mathsf{T}} & q_{C_4} \end{bmatrix} \mathbf{q}_B \tag{A.13}$$

Properties of quaternions

The *complex conjugate* of a quaternion $\mathbf{q}$ is given by

$$\mathbf{q}^* = -q_1\mathbf{i} - q_2\mathbf{j} - q_3\mathbf{k} + q_4 \tag{A.14}$$

Thus

$$(\mathbf{q}_A\mathbf{q}_B) = \mathbf{q}_B^*\mathbf{q}_A^* \tag{A.15}$$

The *norm* of a quaternion $\mathbf{q}$, denoted by $|\mathbf{q}|$ is

$$|\mathbf{q}| = \mathbf{q}\mathbf{q}^* = \mathbf{q}^*\mathbf{q} = |\mathbf{q}|^2 = \sqrt{q_1^2 + q_2^2 + q_3^2 + q_4^2} \tag{A.16}$$

The *inverse* of a quaternion $\mathbf{q}$ is defined as

$$\mathbf{q}^{-1} = \frac{\mathbf{q}^*}{|\mathbf{q}|^2} \tag{A.17}$$

It can be verified that

$$\mathbf{q}^{-1}\mathbf{q} = \mathbf{q}\mathbf{q}^{-1} = 1 \tag{A.18}$$

where $\mathbf{q}$ is the unit quaternion and the inverse is its conjugate $\mathbf{q}^{-1}$

B | Reaction wheel motors

B.1 Motor characteristics

The manufacturer data-sheet contains basic characteristics of the motor as it can be seen in the B.1. There are some parameters that are required for simulation purposes and are not listed in the table bellow and consequently have to be addressed. The parameters are the friction torque T_{fric} which give rise to the calculation of the friction coefficient b, and the back Electromotive Force (EMF) constant k_e. The motor given in [4] is used as a reference.

Characteristics	***Value***
No load speed	20000 $[rpm]$
No load current	156 $[mA]$
Nominal speed	9600$[rpm]$
Nominal torque	1.8 $[mNm]$
Nominal current	0.794 $[A]$
stall torque	3.79 $[mNm]$
stall current	1.5 $[A]$
Terminal resistance	4.1 $[Ohm]$
Terminal inductance	0.107 $[mH]$
speed constant	3770 $[rpm/V]$
Rotor inertia	1.1 $[gcm^2]$
Max speed	22000 $[rpm]$
weight	8 $[g]$

Table B.1: Flat motor ‰ 13.6 mm, brushless, 1.5 Watt, sensorless with 6V nominal voltage

Some of the torque in the mechanical part of the motors is used to overcome the friction and the rest is used in the motor shaft. An expression can be derived as

$$T_m = T_{shaft} - T_{fric}$$

where T_m is the nominal torque. Using the motor torque constant from the data sheet, T_{fric} can be calculated as

$$T_{fric} = k_t I_{nom} - T_m$$

where I_{nom}[A] is the nominal current. Viscous friction coefficient b can now be calculated as

$$b = \frac{T_{fric}}{\omega_{no-load}}$$

and $\omega_{no-load}$ is expressed in rad/sec. Finally, the back emf constant is calculated as

$$k_e = \frac{V_{nom} - I_{nom}R}{\omega_{no-load}}$$

where V_{nom} is the nominal voltage and is equal to 6[V] and R[Ohm] is the terminal resistance.

Torque control, an alternative reaction wheel controller

An alternative, torque motor controller was implemented in the simulation environment. Since the torque control is done through current control, the dynamics time constant is rather small, thus the simulation became quite computation demanding. For controlling the current, the motor inductance needs to be taken into account. Even though torque control is more appropriate than angular velocity control, since it does not have torque delay, the simulations proved that the angular velocity controller can track the torque demand sufficiently. This is due to the fact that the satellite does not require sudden high speed attitude changes.

The torque control scheme works as follows: the main attitude controller sends a torque demand to the actuators, which is then distributed between the actuators. Each of the reaction wheels get their own individual torque demand signals. Two methods have been implemented for tracking this torque demand. One is by transforming the torque to angular velocity demand, which the motor has to track, the other is directly controlling for actuator error.

As shown on Figure B.1 , the torque controller controls the torque error signal using a PD controller. Since the torque has a $10^{-5}Nm$ magnitude, while the voltage has $10^{1}V$, numerically the PD gains are quite large. The control signal is the input voltage for the DC motor. The subsystem is second order, including an integrator for current and one for angular velocity.

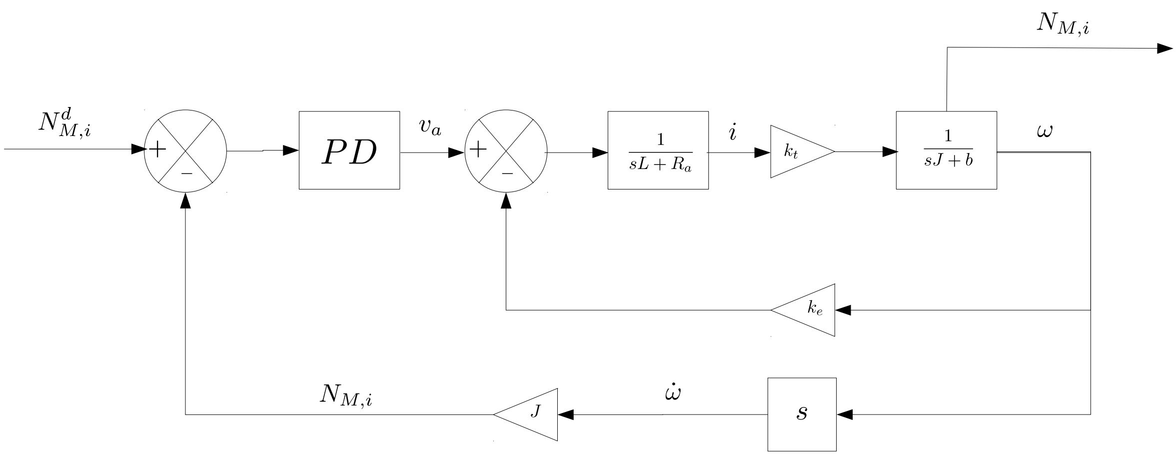

Figure B.1: Torque control scheme.

C | Derivation of the satellite equations of motion

This section describes the derivation of the mathematical model of the satellite which contains the attitude dynamic and kinematic model, based on the rigid body dynamics and kinematics.

Kinematic equation

In this subsection, the focus will be on describing the attitude kinematics of the satellite. Quaternion representation is used for describing the satellite attitude. It was decided to choose quaternion representation, because they provide a way to deal with singularities that would occur in Euler angle representation.

The quaternion $\mathbf{q}(t)$ is defined as the attitude quaternion of a rigid body at time t with respect to the inertial frame and at time $t + \Delta t$, the quaternion $\mathbf{q}(t + \Delta t)$ is defined. The orientation quaternion can be divided into the quaternion at time t and performing a quaternion multiplication with the rotation in the interval Δt as follows:

$$ {}^{\mathbf{s}}_{\mathbf{i}}\mathbf{q}(t + \Delta t) = \mathbf{q}(\Delta t) \otimes {}^{\mathbf{s}}_{\mathbf{i}}\mathbf{q}(t) \tag{C.1} $$

where the orientation quaternion ${}^{\mathbf{s}}_{\mathbf{i}}\mathbf{q}(t+\Delta t)$ represents the rotation of the spacecraft body frame with respect to the inertial frame

The quaternion at time Δt can be express using the triad u, v, w, that represent the axis of the spacecraft as:

$$ q_1(\Delta t) = e_u \sin \frac{\Delta\Phi}{2} \tag{C.2} $$

$$ q_2(\Delta t) = e_v \sin \frac{\Delta\Phi}{2} \tag{C.3} $$

$$ q_3(\Delta t) = e_w \sin \frac{\Delta\Phi}{2} \tag{C.4} $$

$$ q_4(\Delta t) = \cos \frac{\Delta\Phi}{2} \tag{C.5} $$

where $\Delta\Phi$ is the rotation at time Δt and e_u, e_v, e_w are the components along the triad u, v, w at time Δt.

Using equation C.2 and equation C.5 and insert them into equation C.1 which yields:

$$
{}^{\mathbf{s}}_{\mathbf{i}}\mathbf{q}(t+\Delta t) = \left\{ \cos\frac{\Delta\Phi}{2}\underline{1}_{(4\times4)} + \sin\frac{\Delta\Phi}{2}\begin{bmatrix} 0 & e_z & -e_y & e_x \\ -e_z & 0 & e_x & e_y \\ e_y & -e_x & 0 & e_z \\ -e_x & e_y & -e_z & 0 \end{bmatrix} \right\} {}^{\mathbf{s}}_{\mathbf{i}}\mathbf{q}(t) \tag{C.6}
$$

where $\underline{1}$ is the identity matrix with the dimensions of 4×4.

In order to turn equation C.6 into a differential equation, a small angle approximation it is used:

$$
\Delta\phi = \omega\ \Delta t \tag{C.7}
$$

$$
\cos\frac{\Delta\Phi}{2} \approx 1 \tag{C.8}
$$

$$
\sin\frac{\Delta\Phi}{2} \approx \frac{\omega\Delta t}{2} \tag{C.9}
$$

$$
\tag{C.10}
$$

After using the approximation and substitute the terms into C.6, the following equation is obtained:

$$
{}^{\mathbf{s}}_{\mathbf{i}}\mathbf{q}(\mathbf{t}+\mathbf{\Delta t}) \approx \left[1 + \frac{1}{2}\underline{\omega}^{\times}\Delta(t)\right] {}^{\mathbf{s}}_{\mathbf{i}}\mathbf{q}(\mathbf{t}) \tag{C.11}
$$

where $\underline{\Omega}$ is the skew symmetric matrix written in form:

$$
\underline{\omega}^{\times} = \begin{bmatrix} 0 & \omega_w & -\omega_v & \omega_u \\ -\omega_w & 0 & \omega_u & \omega_v \\ \omega_v & -\omega_u & 0 & \omega_w \\ -\omega_u & -\omega_v & -\omega_w & 0 \end{bmatrix} \tag{C.12}
$$

where the terms $\omega_u, \omega_v, \omega_w$ are the angular velocities components.

The rate of change in the orientation of the spacecraft ${}^{\mathbf{s}}_{\mathbf{i}}\mathbf{q}(\mathbf{t})$ can be found:

$$
{}^{\mathbf{s}}_{\mathbf{i}}\dot{\mathbf{q}}(\mathbf{t}) = \lim_{\Delta t\to 0}\frac{\mathbf{q}(t+\Delta t) - \mathbf{q}(t)}{\Delta t} = \frac{1}{2}\underline{\omega}^{\times}{}^{\mathbf{s}}_{\mathbf{i}}\mathbf{q}(\mathbf{t}) \tag{C.13}
$$

Dynamic equation

The satellite dynamics are described using Euler's equation of motion and Newton's laws of motion. Using Euler's equation of motion, the relation between the change in angular momentum and the external torques that affect the satellite is given as follows:

$$
\dot{\mathbf{h}}_T = \mathbf{N_{mt}} + \mathbf{N_{dist}} \tag{C.14}
$$

where h_T is the angular momentum of a rigid body, N_{mt} is the torque from the magnetorquers and N_{dist} is the torque from the disturbances.

The change in angular momentum of the satellite can be expressed as the product between the angular acceleration and the moment of inertia:

$$\dot{\mathbf{h}}_{\mathbf{sat}} = \underline{I}_s\dot{\boldsymbol{\omega}} \tag{C.15}$$

where h_{sat} is the angular momentum of the satellite, $\underline{I}_s$ is the moment of inertia of the satellite and $\boldsymbol{\omega}$ is the angular velocity.

Including the momentum wheels, the total angular momentum is given by:

$$\mathbf{h_T} = \mathbf{h_{sat}} + \mathbf{h_{rw}} \tag{C.16}$$

where $\mathbf{h_{rw}}$ is the angular momentum of the reaction wheels. Therefore, the total angular momentum is described by:

$$\mathbf{h_T} = \underline{I}_s\boldsymbol{\omega} + \mathbf{h_{rw}} \tag{C.17}$$

By rearranging terms, equation C.17 becomes:

$$\boldsymbol{\omega} = \underline{I}_s^{-1}(\mathbf{h_T} - \mathbf{h_{rw}}) \tag{C.18}$$

Using Euler's equation of motion, the time derivative of $\mathbf{h_T}$ expressed in the SBRF frame is:

$$\dot{\mathbf{h}}_{\mathbf{T}} = \dot{\mathbf{h}}_{\mathbf{sat}} + \boldsymbol{\omega} \times \mathbf{h}_T = \mathbf{N_{mt}} + \mathbf{N_{dist}} \tag{C.19}$$

$$\underline{I}_s\dot{\boldsymbol{\omega}} + \dot{\mathbf{h}}_{\mathbf{rw}} + \boldsymbol{\omega} \times \mathbf{h}_T = \mathbf{N_{mt}} + \mathbf{N_{dist}} \tag{C.20}$$

Subsequently, the angular velocity is separated and expressed as:

$$\dot{\boldsymbol{\omega}} = -\underline{I}_s^{-1}\boldsymbol{\omega} \times \mathbf{h}_T - \underline{I}_s^{-1}\dot{\mathbf{h}}_{\mathbf{rw}} + \underline{I}_s^{-1}(\mathbf{N_{mt}} + \mathbf{N_{dist}}) \tag{C.21}$$

Next, by replacing the cross product with a skew-symmetric matrix $\boldsymbol{\omega}^{\times}$, *equation (C.21)* becomes:

$$\dot{\boldsymbol{\omega}} = -\underline{I}_s^{-1}\boldsymbol{\omega}^{\times}\underline{I}_s\boldsymbol{\omega} - \underline{I}_s^{-1}\boldsymbol{\omega}^{\times}\mathbf{h}_{rw} + \underline{I}_s^{-1}\mathbf{N_{rw}} + \underline{I}_s^{-1}(\mathbf{N_{mt}} + \mathbf{N_{dist}}) \tag{C.22}$$

where N_{mt} is the torque from the magnetorquers, N_{rw} is the torque from the momentum wheels and the skew-symmetric matrix is:

$$\boldsymbol{\omega}^{\times} \triangleq \begin{bmatrix} 0 & -\omega_3 & \omega_2 \\ \omega_3 & 0 & -\omega_1 \\ -\omega_2 & \omega_1 & 0 \end{bmatrix} \tag{C.23}$$

Moreover, the torque set to the momentum wheels is equal to the time derivative of the angular momentum:

$$\mathbf{N_{rw}} = -\dot{\mathbf{h}}_{\mathbf{rw}} \tag{C.24}$$

Linearization of satellite equations

Due to the non-linear equations of motion of the satellite derived in the above sections, a linearization of these equations around an operating point is made, which will serve for designing a linear controller.

Kinematic equation

Starting with the non-linear kinematic equation which is given by:

$$\dot{\mathbf{q}}(\mathbf{t}) = \frac{1}{2}\underline{\omega}^{\times}\mathbf{q}(\mathbf{t}) \tag{C.25}$$

Consequently, the quaternion can be expressed in a different form by dividing the initial quaternion $\mathbf{q}(\mathbf{t})$ into a quaternion that represents the operating point and a quaternion error which represent a variation around the operating point:

$$\mathbf{q}(t + \Delta t) = \mathbf{q}(\Delta t) \otimes \mathbf{q}(t) = \bar{\mathbf{q}} \otimes \tilde{\mathbf{q}} \tag{C.26}$$

where,
$\bar{\mathbf{q}}$ is the operating point
$\tilde{\mathbf{q}}$ is the quaternion error

By applying quaternion properties, the quaternion error can be written as:

$$\tilde{\mathbf{q}} = \bar{\mathbf{q}}^{-1} \otimes \mathbf{q} = \bar{\mathbf{q}}^{*} \otimes \mathbf{q} \tag{C.27}$$

where $\mathbf{q}^{-1} = \mathbf{q}^{*}$

Equation C.25 can be expanded by using a two quaternion multiplication, where the properties of these multiplication can be seen in appendix B, therefore equation C.25 becomes:

$$\dot{\mathbf{q}} = \frac{1}{2}\mathbf{q} \otimes \mathbf{q}_{\omega} \tag{C.28}$$

where $\mathbf{q}_{\omega}$ is the angular velocity quaternion and is given by: $\mathbf{q}_{\omega} = \bar{\mathbf{q}} + \tilde{\mathbf{q}}$

Taking the time derivative of equation C.27 and using the product rule, the equation becomes:

$$\dot{\tilde{\mathbf{q}}} = \dot{\bar{\mathbf{q}}}^{*} \otimes \mathbf{q} + \bar{\mathbf{q}}^{*} \otimes \dot{\mathbf{q}} \tag{C.29}$$

Inserting equation C.28 into equation C.29 and using the following properties of quaternions $\mathbf{q}_{\omega}^{*} = -\mathbf{q}_{\omega}$ and $(\mathbf{q}\mathbf{q}_{\omega}{}^{*}) = \mathbf{q}_{\omega}^{*}\mathbf{q}^{*}$, the equation C.28 result in:

$$\dot{\tilde{\mathbf{q}}} = \frac{1}{2}\Big[- \bar{\mathbf{q}}_{\omega} \otimes \tilde{\mathbf{q}} + \tilde{\mathbf{q}} \otimes \bar{\mathbf{q}}_{\omega} + \tilde{\mathbf{q}} \otimes \tilde{\mathbf{q}}_{\omega}\Big] \tag{C.30}$$

In order to express the products quaternion from the previous equation, the product of these quaternion can be written as a matrix that have the real and the complex part and one quaternion, which will end up as a product between a matrix and a vector. Therefore, the product quaternion between $\bar{\mathbf{q}}_\omega \otimes \tilde{\mathbf{q}}$ can be rewritten as:

$$\bar{\mathbf{q}}_\omega \otimes \tilde{\mathbf{q}} = \begin{bmatrix} -\tilde{\mathbf{q}}^\times + \underline{\mathbf{1}}\tilde{q}_4 & \tilde{\mathbf{q}} \\ -\tilde{\mathbf{q}}^\mathsf{T} & \tilde{q}_4 \end{bmatrix} \begin{bmatrix} \bar{\boldsymbol{\omega}} \\ 0 \end{bmatrix} = \begin{bmatrix} -\underline{\bar{\omega}}^\times \tilde{\mathbf{q}} + \underline{\mathbf{1}}\tilde{q}_4 \bar{\boldsymbol{\omega}} \\ -\tilde{\mathbf{q}}^\mathsf{T} \bar{\boldsymbol{\omega}} \end{bmatrix} \tag{C.31}$$

where the following property is used ($\bar{\boldsymbol{\omega}}^\times \tilde{\mathbf{q}} = -\tilde{\mathbf{q}}^\times \bar{\boldsymbol{\omega}}$ and $S(\boldsymbol{\omega})^\times$ is the skew symmetric matrix.

Similarly, the product quaternion between $\tilde{\mathbf{q}} \otimes \bar{\mathbf{q}}_\omega$ is found:

$$\tilde{\mathbf{q}} \otimes \bar{\mathbf{q}}_\omega = \begin{bmatrix} -\bar{\boldsymbol{\omega}}^\times & \bar{\boldsymbol{\omega}} \\ -\bar{\boldsymbol{\omega}}^\mathsf{T} & 0 \end{bmatrix} \begin{bmatrix} \tilde{\mathbf{q}} \\ \tilde{q}_4 \end{bmatrix} = \begin{bmatrix} -\bar{\boldsymbol{\omega}}^\times \tilde{\mathbf{q}} + \bar{\boldsymbol{\omega}}\tilde{q}_4 \\ -\tilde{\boldsymbol{\omega}}^\mathsf{T} \tilde{\mathbf{q}} \end{bmatrix} \tag{C.32}$$

The last product quaternion can be found in the same manner:

$$\tilde{\mathbf{q}} \otimes \tilde{\mathbf{q}}_\omega = \begin{bmatrix} -\tilde{\boldsymbol{\omega}}^\times & \tilde{\boldsymbol{\omega}} \\ -\tilde{\boldsymbol{\omega}}^\mathsf{T} & 0 \end{bmatrix} \begin{bmatrix} \tilde{\mathbf{q}} \\ \tilde{q}_4 \end{bmatrix} = \begin{bmatrix} -\tilde{\boldsymbol{\omega}}^\times \tilde{\mathbf{q}} + \tilde{\boldsymbol{\omega}}\tilde{q}_4 \\ -\tilde{\boldsymbol{\omega}}^\mathsf{T} \tilde{\mathbf{q}} \end{bmatrix} \tag{C.33}$$

Using the following property, a small approximation for the angle is made

$$\lim_{\theta \to 0} \mathbf{q} = \lim_{\theta \to 0} \begin{bmatrix} \mathbf{q} \\ q_4 \end{bmatrix} = \lim_{\theta \to 0} \begin{bmatrix} e_u \sin(\frac{\theta}{2}) \\ e_v \sin(\frac{\theta}{2}) \\ e_w \sin(\frac{\theta}{2}) \\ \cos(\frac{\theta}{2}) \end{bmatrix} \tag{C.34}$$

where $\tilde{\mathbf{q}} \to 0$ and $\tilde{q}_4 \to 1$

Therefore, equation C.33 can be rewritten by using this property as:

$$\tilde{\mathbf{q}} \otimes \tilde{\mathbf{q}}_\omega = \begin{bmatrix} -\tilde{\boldsymbol{\omega}}^\times \tilde{\mathbf{q}} + \tilde{\boldsymbol{\omega}}\tilde{q}_4 \\ -\tilde{\boldsymbol{\omega}}^\mathsf{T} \tilde{\mathbf{q}} \end{bmatrix} = \tilde{\mathbf{q}}_\omega \tag{C.35}$$

Collecting terms and inserting equation C.31, C.32, C.35 into equation C.30 yields the following form:

$$\dot{\tilde{\mathbf{q}}} \approx -\frac{1}{2} \begin{bmatrix} -\bar{\boldsymbol{\omega}}^\times \tilde{\mathbf{q}} + \underline{\mathbf{1}}\tilde{q}_4 \bar{\boldsymbol{\omega}} \\ -\tilde{\mathbf{q}}^\mathsf{T} \bar{\boldsymbol{\omega}} \end{bmatrix} + \frac{1}{2} \begin{bmatrix} -\bar{\boldsymbol{\omega}}^\times \tilde{\mathbf{q}} + \bar{\boldsymbol{\omega}}\tilde{q}_4 \\ -\tilde{\boldsymbol{\omega}}^\mathsf{T} \tilde{\mathbf{q}} \end{bmatrix} + \frac{1}{2}\tilde{\mathbf{q}}_\omega \approx \begin{bmatrix} -\bar{\boldsymbol{\omega}}^\times \\ 0 \end{bmatrix} \tilde{\mathbf{q}} + \frac{1}{2}\tilde{\mathbf{q}}_\omega \tag{C.36}$$

Dynamic equation

Next, the non-linear dynamic equation is given by:

$$\begin{aligned}\dot{\boldsymbol{\omega}} &= -\underline{I}_s^{-1}\underline{\omega}^{\times}\underline{I}_s\boldsymbol{\omega} - \underline{I}_s^{-1}\underline{\omega}^{\times}\mathbf{h}_{rw} + \underline{I}_s^{-1}\mathbf{N_{rw}} + \underline{I}_s^{-1}(\mathbf{N_{mt}} + \mathbf{N_{dist}}) = \\ &= \underline{I}_s^{-1}[\mathbf{N_{dist}} + \mathbf{N_{ctrl}} - \underline{\omega}^{\times}(\underline{I}_s\omega + \mathbf{h}_{rw})]\end{aligned}$$

An operating point is introduce as:

$$\boldsymbol{\omega} = \bar{\boldsymbol{\omega}} + \tilde{\boldsymbol{\omega}} \tag{C.37}$$

where the angular velocity $\boldsymbol{\omega}$ is separated into a operating point $\bar{\boldsymbol{\omega}}$ and the error around this operating point $\tilde{\boldsymbol{\omega}}$.

The next step is to use a a first order Taylor expansion for linearizing the time derivative of the angular velocity, with the mention of neglecting the $\mathbf{N_{dist}}$ which is assumed to be insignificant.

$$\dot{\boldsymbol{\omega}} \approx -\underline{I}_s^{-1}\frac{d\dot{\boldsymbol{\omega}}}{d\boldsymbol{\omega}}\bigg|_{\boldsymbol{\omega}=\bar{\boldsymbol{\omega}}}\tilde{\boldsymbol{\omega}} - \underline{I}_s^{-1}\frac{d\dot{\boldsymbol{\omega}}}{d\mathbf{h_{rw}}}\bigg|_{\mathbf{h_{rw}}=\bar{\mathbf{h}}_{\mathbf{rw}}}\tilde{\mathbf{h}}_{\mathbf{rw}} + \underline{I}_s^{-1}\frac{d\dot{\boldsymbol{\omega}}}{d\mathbf{N_{ctrl}}}\bigg|_{\mathbf{N_{ctrl}}=\bar{\mathbf{N}}_{\mathbf{ctrl}}}\tilde{\mathbf{N}}_{\mathbf{ctrl}} \tag{C.38}$$

By using the property $\boldsymbol{\omega}^{\times}\underline{I}_s\bar{\boldsymbol{\omega}} = -\underline{I}_s\bar{\boldsymbol{\omega}}^{\times}\boldsymbol{\omega}$ and rewriting the C.38 by expanding the terms, will result the linearized dynamic equation:

$$\dot{\boldsymbol{\omega}} = \underline{I}_s(\underline{I}_s\bar{\boldsymbol{\omega}}^{\times} - \bar{\boldsymbol{\omega}}^{\times}\underline{I}_s + \bar{\mathbf{h}}_{\mathbf{rw}}{}^{\times})\tilde{\boldsymbol{\omega}} - \underline{I}_s\bar{\boldsymbol{\omega}}^{\times}\tilde{\mathbf{h}}_{\mathbf{rw}} + \underline{I}_s\tilde{\mathbf{N}}_{\mathbf{ctrl}} \tag{C.39}$$

D | Maximum Torque Demand

In order to be able to choose actuators that are able to satisfy the control demands, the maximum torque demand for Earth station tracking needs to be calculated. As a first step, the maximum angular acceleration is calculated for a scenario where the satellite always points towards the Earth station. Figure D.1a shows the angular velocity of the satellite orbiting at 600 km on a circular orbit, while the station is at sea level. When the satellite is closest to the Earth station, the station is on the nadir of the satellite. The angular velocity is the highest when the satellite flies above the station. Since it is an extremum, the angular acceleration in that instant is zero. By differentiating the angular velocity, the angular acceleration shown in Figure D.1b. The maximum value of angular acceleration is $1.085 \times 10^{-4} \frac{rad}{s^2}$.

If the satellite is rotating around its principal axis of inertia with the highest value, $0.0022 kg\, m^2$, the maximum angular acceleration demands $\mathbf{2.388 \times 10^{-7} \boldsymbol{Nm}}$.

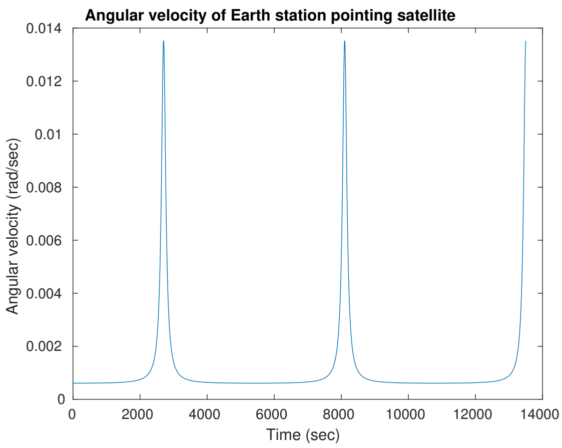

(a) Angular Velocity of Earth station pointing satellites.

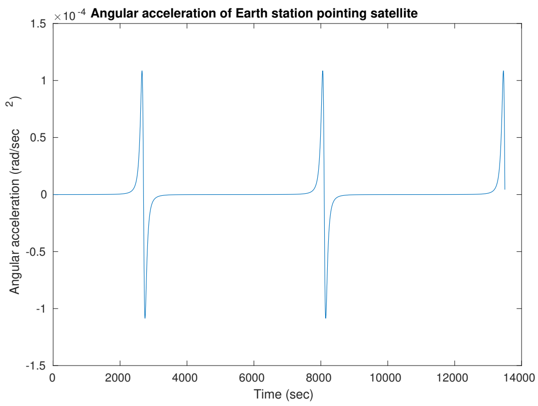

(b) Angular Acceleration of Earth station pointing satellites.

E | Alternative method for identifying reaction wheel fault

With enough on-board computational power the faulty reaction wheel can be detected through the calculated reaction wheel output torque, assuming only one reaction wheel is faulty. It is done by calculating the difference between 3D torque demand and actual 3D torque output. In order for this residual based fault detection to work, the model needs to precisely reflect the satellite dynamics and the signals need to be filtered properly.

$$\mathbf{N}_{rw} = \underline{\boldsymbol{I}}_s\dot{\boldsymbol{\omega}} + \boldsymbol{\omega} \times \mathbf{h_{rw}} - \mathbf{N_{mt}} - \mathbf{N_{dist}} \tag{E.1}$$

Then the difference between torque demand and torque output is calculated. The reaction wheel that has the most similar axis orientation to the torque difference is deemed as faulty.

$$\mathbf{N}_{rw}^{d} - \mathbf{N}_{rw} = \mathbf{N}_{rw}^{diff} \tag{E.2}$$

$$\pm\, \mathbf{N}_{rw}^{diff} \overset{?}{\approx} \mathbf{axis} \tag{E.3}$$

If the torque error exceeds a certain threshold, then the faulty wheel index can be identified.

$$\boldsymbol{faultyWheelIndex} = \mathbf{arg}\,\min_{i}(\pm\mathbf{N}_{rw}^{diff} - \mathbf{axis}_i) \tag{E.4}$$

Note: the lag for torque change and wheel saturation has to be taken into account separately, as those do not count as faults. Thresholds should be applied. This method has questionable applicability in presence of uncertainties, thus it was omitted from the main report.

F | Magnetorquer characteristics

The characteristics of the magnetorquers used in the satellite is inspired by [11], where two types of magnetorquers are described: one with metal core and one without core. Having an iron core increases controllable magnetic moment change at the expense of control accuracy. The parameters for one magnetorquer without core are presented in table F.1:

Parameter	***Value***
Coil size	75x75 [$\boldsymbol{mm^2}$]
Wire Thickness	0.13 [$\boldsymbol{mm}$]
Windings	250
Coil mass	0.053 [$\boldsymbol{kg}$]
Max voltage	$\pm$1.25 [$\boldsymbol{V}$]
Max current	15.78 [$\boldsymbol{mA}$]
Actuator on time	88%
Max power consumption pr. coil	17.4 [$\boldsymbol{mW}$]
Total power consumption	134.2 [$\boldsymbol{mW}$]
Coil Discharge time:	0.33481 [$\boldsymbol{ms}$] (99% discharged)
Available time for measurements	11.67 [$\boldsymbol{ms}$]

Table F.1: Parameters for magnetorqer without metal core

For this type of magnetorqer, one magnetorqer will generate around 200 [$\boldsymbol{nNm}$] at low magnetic field strength (18000 [$\boldsymbol{nT}$), which is perpendicular to the area of the coil. (thesis)

A second alternative is to choose a magnetorqer with metal core, because the power consumption, the size and weight are considered superior compared with a magnetorqer without cores. Moreover, because the interest in redundancy is important and four magnetorqers will be placed inside the satellite, the magnetorqer with metal core is preferable because of their weight and size. The parameters for the magnetorqer with metal core is illustrated in the following table:

Parameter	***Value***
Core diameter:	10 [$\boldsymbol{mm}$]
Core length	10 [$\boldsymbol{mm}$]
Permeability	1000
Wire Thickness	0.13 [$\boldsymbol{mm}$]
Windings	200
Coil mass	0.019 [$\boldsymbol{kg}$]
Max voltage	±1.25 [$\boldsymbol{V}$]
Max current	20 [$\boldsymbol{mA}$]
External resistance needed	62.5 [$\boldsymbol{\Omega}$]
Actuator on time	27 % [$\boldsymbol{mW}$]
Max power consumption pr. coil	6.75[$\boldsymbol{mW}$]
Total power consumption	35.3 [$\boldsymbol{mW}$]

Table F.2: Parameters for magnetorqer with metal core

In this case, one magnetorqer will generate around 400 [$\boldsymbol{nNm}$] at low magnetic field strength (18000 [$\boldsymbol{nT}$]). Besides the advantage of having a reduced dimension and a better power consumption, the magnetorqer with core, generates a magnetic moment higher than expected. On the other hand, the magnetorquer without core was already tested on the AAUSAT and can be seen as a safe choice of actuator.

G | Simulation framework

This chapter gives an overview and development notes about the simulation environment.

The simulation environment is created in Simulink and MATLAB. Some elements were reused from AAUSAT team's Simulink library created for LEO satellites, The library incorporates building blocks containing satellite kinematics and dynamics, orbit propagation model, environmental perturbations, orbit propagation, models for the sensors and actuatuors and also different functionalities such as quaternions multiplications, vectors or matrices operations. Even if the AAUSAT library was proven to work well, a few adjustments were made for the this thesis. Among these adjustments was modifying the S-function written in C code that is responsible for handling the satellite dynamics and kinematics. The C-code is compiled using mex compiler and the compiled blocks can function at similar speeds as Simulinks blocks.

A convenient way to program in Simulink is by using MATLAB code blocks. In the beginning these were used in abundance, however soon it became obvious that they slow down the simulation. Even Mathwork's website states that getting rid of MATLAB blocks can lead to significant speed increase. Thus, from the middle of the development the usage of MATLAB blocks was minimized, the ones used before were mostly recreated by using Simulink blocks.

The simulation environment got really complex during the development. To handle this complexity, blocks were grouped together in subsystems, according to their functionalities. Then a hierarchy was introduced between some of the blocks as a further step in keeping the complexity manageable. This also helped in making the system modular. Modules such as reaction wheel control schemes and models could be changed much easier. When long simulation times were necessary, this made swapping to less computation heavy components easier.

Algebraic loops in the Simulink model lead to significant simulation speed decrease. To avoid algebraic loops in the feedbacks, unit delays were used when necessary. In the case of controller feedback, this is justified, since the digital controllers have a discrete sampling time. Using unit delays to speed up simulation of continuous dynamics do not affect the simulation result in any significant way, especially when using small simulation step sizes.

The complexity was also managed by using *From* and *Goto* blocks. These blocks offer virtual connection and provide a way to send a signal between different blocks without connecting them. This means that the huge amount of connections do not pollute the block structure.

The default Simulink libraries lack many essential blocks. In order to avoid having to implement things such as quaternion calculations, risking slowdowns, Aerospace Toolbox was utilized in the environment.

The maximum step size for most simulations were set to 10 ms, but if fast dynamics were simulated such as torque controlled reaction wheel, the actual automatically adjusted step size was decreased to much smaller values. Many signals are rather small, some of are in the order of magnitude of $\mathbf{10-12}$. To make sure that Simulink calculates these signals properly, the tolerance needed to be decreased accordingly.

The *igrf2005.d* file is a collection of data gather from different magnetic observatories placed around the world. It is a reliable source of comparing the Earth magnetic field with the magnetic field measured by the magnetometer. In Simulink, a block that have as input the satellite position and the rotation of Earth, gives as output a vector with the magnetic field taking into account the satellite position.

H | Severity and occurrence evaluation

The importance of dealing with certain faults can be decided using severity and occurrence evaluation. Faults described in 7 are evaluated using intuitive severity and occurrence values. The severity and occurence index is computed using the following formula:

$$\boldsymbol{SO_{index} = severity \cdot occurrence} \tag{H.1}$$

The following table presents the evaluation findings. (OI)

Magnetorquer			
Reference	Severity	Occurrence	SO Index
$\boldsymbol{MT1}$	7	5 4	35 28
$\boldsymbol{MT2}$	10	3	30
$\boldsymbol{MT3}$	3	2 1	6 3
$\boldsymbol{MT4}$	4	6	24

Table H.1: SO for magnetorquer

The same procedure is done for reaction wheels as follows:

Reaction wheels			
Reference	Severity	Occurrence	SO Index
$\boldsymbol{RW1}$	7	3	21
$\boldsymbol{RW2}$	10	3	30
$\boldsymbol{RW3}$	6	2	12
$\boldsymbol{RW4}$	5	3	15

Table H.2: SO for reaction wheels

I | UIO

$$
\begin{aligned}
\begin{bmatrix} {}^{\mathrm{s}}_{\mathrm{lv}}\dot{\omega} \\ \dot{\omega}_{\mathrm{rw}} \\ \dot{\mathrm{q}}_{1:3} \end{bmatrix} = {} &
\begin{bmatrix}
0 & 0 & \omega_o \frac{I_1 - I_2 + I_3}{-I_1} & 0 & 0 & \omega_o \frac{I_w}{-I_1} & 8\omega_o^2 \frac{I_3 - I_2}{I_1} & 0 & 0 \\
0 & 0 & 0 & 0 & 0 & 0 & 0 & 6\omega_o^2 \frac{I_3 - I_1}{I_2} & 0 \\
\omega_o \frac{I_1 - I_2 + I_3}{I_3} & 0 & 0 & \omega_o \frac{I_w}{I_3} & 0 & 0 & 0 & 0 & 2\omega_o^2 \frac{I_1 - I_2}{I_3} \\
0 & 0 & 0 & 0 & 0 & 0 & 0 & 0 & 0 \\
0 & 0 & 0 & 0 & 0 & 0 & 0 & 0 & 0 \\
0 & 0 & 0 & 0 & 0 & 0 & 0 & 0 & 0 \\
0.5 & 0 & 0 & 0 & 0 & 0 & 0 & 0 & 0 \\
0 & 0.5 & 0 & 0 & 0 & 0 & 0 & 0 & 0 \\
0 & 0 & 0.5 & 0 & 0 & 0 & 0 & 0 & 0
\end{bmatrix}
\begin{bmatrix} {}^{s}_{lv}\omega_1 \\ {}^{s}_{lv}\omega_2 \\ {}^{s}_{lv}\omega_3 \\ \omega_{rw,1} \\ \omega_{rw,2} \\ \omega_{rw,3} \\ q_1 \\ q_2 \\ q_3 \end{bmatrix} \\
& + \begin{bmatrix}
I_1^{-1} & 0 & 0 & 0 & \frac{b_3}{I_1} & -\frac{b_2}{I_1} & I_1^{-1} & 0 & 0 \\
0 & I_2^{-1} & 0 & -\frac{b_3}{I_2} & 0 & \frac{b_1}{I_2} & 0 & I_2^{-1} & 0 \\
0 & 0 & I_3^{-1} & \frac{b_2}{I_3} & -\frac{b_1}{I_3} & 0 & 0 & 0 & I_3^{-1} \\
I_w^{-1} & 0 & 0 & 0 & 0 & 0 & 0 & 0 & 0 \\
0 & I_w^{-1} & 0 & 0 & 0 & 0 & 0 & 0 & 0 \\
0 & 0 & I_w^{-1} & 0 & 0 & 0 & 0 & 0 & 0 \\
0 & 0 & 0 & 0 & 0 & 0 & 0 & 0 & 0 \\
0 & 0 & 0 & 0 & 0 & 0 & 0 & 0 & 0 \\
0 & 0 & 0 & 0 & 0 & 0 & 0 & 0 & 0
\end{bmatrix}
\begin{bmatrix} N_{rw,1} \\ N_{rw,2} \\ N_{rw,3} \\ \mathrm{m}_{mt,1} \\ \mathrm{m}_{mt,2} \\ \mathrm{m}_{mt,3} \\ N_{dist,1}^{est} \\ N_{dist,2}^{est} \\ N_{dist,3}^{est} \end{bmatrix}
+ \begin{bmatrix}
I_1^{-1} & 0 & 0 \\
0 & I_2^{-1} & 0 \\
0 & 0 & I_3^{-1} \\
0 & 0 & 0 \\
0 & 0 & 0 \\
0 & 0 & 0 \\
0 & 0 & 0 \\
0 & 0 & 0 \\
0 & 0 & 0
\end{bmatrix}
\begin{bmatrix} N_{dist,1}^{est\ error} \\ N_{dist,2}^{est\ error} \\ N_{dist,3}^{est\ error} \end{bmatrix} \\
& + \begin{bmatrix}
I_1^{-1} & 0 & 0 & 0 & \frac{b_3}{I_1} & -\frac{b_2}{I_1} \\
0 & I_2^{-1} & 0 & -\frac{b_3}{I_2} & 0 & \frac{b_1}{I_2} \\
0 & 0 & I_3^{-1} & \frac{b_2}{I_3} & -\frac{b_1}{I_3} & 0 \\
I_w^{-1} & 0 & 0 & 0 & 0 & 0 \\
0 & I_w^{-1} & 0 & 0 & 0 & 0 \\
0 & 0 & I_w^{-1} & 0 & 0 & 0 \\
0 & 0 & 0 & 0 & 0 & 0 \\
0 & 0 & 0 & 0 & 0 & 0 \\
0 & 0 & 0 & 0 & 0 & 0
\end{bmatrix}
\begin{bmatrix} N_{rw,1}^{fault} \\ N_{rw,2}^{fault} \\ N_{rw,3}^{fault} \\ \mathrm{m}_{mt,1}^{fault} \\ \mathrm{m}_{mt,2}^{fault} \\ \mathrm{m}_{mt,3}^{fault} \end{bmatrix}
\end{aligned}
\tag{I.1}
$$

Modified equations for tetrahedral reaction wheel configuration and gravity gradient torque given as an input:

$$\dot{\mathbf{x}} = \underline{\boldsymbol{A}}\mathbf{x} + \underline{\boldsymbol{B}}(\boldsymbol{t})\mathbf{u} + \underline{\boldsymbol{E}}\mathbf{d} + \underline{\boldsymbol{F}}_x\mathbf{f}_{\mathbf{y}} \tag{I.2}$$

$$\mathbf{y} = \underline{\boldsymbol{C}}\mathbf{x} + \underline{\boldsymbol{F}}_y\mathbf{f}_{\mathbf{y}} \tag{I.3}$$

$$\begin{bmatrix} {}^{\mathrm{s}}_{\mathrm{lv}}\dot{\omega} \\ \dot{\omega}_{\mathrm{rw}} \\ \dot{\mathrm{q}}_{1:3} \end{bmatrix}$$

$$= \begin{bmatrix} 0 & 0 & \omega_o \frac{I_1 - I_2 + I_3}{-I_1} & 0.58\omega_o \frac{I_w}{I_1} & 0.58\omega_o \frac{I_w}{I_1} & 0.58\omega_o \frac{I_w}{I_1} & -\omega_o \frac{I_w}{I_1} & 2\omega_o^2 \frac{I_3 - I_2}{I_1} & 0 & 0 \\ 0 & 0 & 0 & 0 & 0 & 0 & 0 & 0 & 0 & 0 \\ \omega_o \frac{I_1 - I_2 + I_3}{I_3} & 0 & 0 & 0.81\omega_o \frac{I_w}{I_3} & 0.77\omega_o \frac{I_w}{I_3} & 0.77\omega_o \frac{I_w}{I_3} & 0 & 0 & 0 & 2\omega_o^2 \frac{I_1 - I_2}{I_3} \\ 0 & 0 & 0 & 0 & 0 & 0 & 0 & 0 & 0 & 0 \\ 0 & 0 & 0 & 0 & 0 & 0 & 0 & 0 & 0 & 0 \\ 0 & 0 & 0 & 0 & 0 & 0 & 0 & 0 & 0 & 0 \\ 0 & 0 & 0 & 0 & 0 & 0 & 0 & 0 & 0 & 0 \\ 0.5 & 0 & 0 & 0 & 0 & 0 & 0 & 0 & 0 & 0 \\ 0 & 0.5 & 0 & 0 & 0 & 0 & 0 & 0 & 0 & 0 \\ 0 & 0 & 0.5 & 0 & 0 & 0 & 0 & 0 & 0 & 0 \end{bmatrix} \begin{bmatrix} {}^{s}_{lv}\omega_1 \\ {}^{s}_{lv}\omega_2 \\ {}^{s}_{lv}\omega_3 \\ \omega_{rw,1} \\ \omega_{rw,2} \\ \omega_{rw,3} \\ \omega_{rw,4} \\ q_1 \\ q_2 \\ q_3 \end{bmatrix} \tag{I.4}$$

$$+ \begin{bmatrix} 0.81I_1^{-1} & 0.77I_1^{-1} & 0.77I_1^{-1} & 0 & 0 & \frac{b_3}{I_1} & -\frac{b_2}{I_1} & I_1^{-1} & 0 & 0 \\ 0 & 0.125I_2^{-1} & -0.125I_2^{-1} & 0 & -\frac{b_3}{I_2} & 0 & \frac{b_1}{I_2} & 0 & I_2^{-1} & 0 \\ -0.58I_3^{-1} & -0.58I_3^{-1} & -0.58I_3^{-1} & I_3^{-1} & \frac{b_2}{I_3} & -\frac{b_1}{I_3} & 0 & 0 & 0 & I_3^{-1} \\ I_w^{-1} & 0 & 0 & 0 & 0 & 0 & 0 & 0 & 0 & 0 \\ 0 & I_w^{-1} & 0 & 0 & 0 & 0 & 0 & 0 & 0 & 0 \\ 0 & 0 & I_w^{-1} & 0 & 0 & 0 & 0 & 0 & 0 & 0 \\ 0 & 0 & 0 & I_w^{-1} & 0 & 0 & 0 & 0 & 0 & 0 \\ 0 & 0 & 0 & 0 & 0 & 0 & 0 & 0 & 0 & 0 \\ 0 & 0 & 0 & 0 & 0 & 0 & 0 & 0 & 0 & 0 \\ 0 & 0 & 0 & 0 & 0 & 0 & 0 & 0 & 0 & 0 \end{bmatrix} \begin{bmatrix} N_{rw,1} \\ N_{rw,2} \\ N_{rw,3} \\ N_{rw,4} \\ \mathrm{m}_{mt,1} \\ \mathrm{m}_{mt,2} \\ \mathrm{m}_{mt,3} \\ N^{est}_{dist,1} \\ N^{est}_{dist,2} \\ N^{est}_{dist,3} \end{bmatrix} +$$

$$\begin{bmatrix} I_1^{-1} & 0 & 0 \\ 0 & I_2^{-1} & 0 \\ 0 & 0 & I_3^{-1} \\ 0 & 0 & 0 \\ 0 & 0 & 0 \\ 0 & 0 & 0 \\ 0 & 0 & 0 \\ 0 & 0 & 0 \\ 0 & 0 & 0 \end{bmatrix} \begin{bmatrix} N^{est\ error}_{dist,1} \\ N^{est\ error}_{dist,2} \\ N^{est\ error}_{dist,3} \end{bmatrix}$$

$$+ \begin{bmatrix} 0.81I_1^{-1} & 0.77I_1^{-1} & 0.77I_1^{-1} & 0 & 0 & \frac{b_3}{I_1} & -\frac{b_2}{I_1} \\ 0 & 0.125I_2^{-1} & -0.125I_2^{-1} & 0 & -\frac{b_3}{I_2} & 0 & \frac{b_1}{I_2} \\ -0.58I_3^{-1} & -0.58I_3^{-1} & -0.58I_3^{-1} & I_3^{-1} & \frac{b_2}{I_3} & -\frac{b_1}{I_3} & 0 \\ I_w^{-1} & 0 & 0 & 0 & 0 & 0 & \\ 0 & I_w^{-1} & 0 & 0 & 0 & 0 & \\ 0 & 0 & I_w^{-1} & 0 & 0 & 0 & 0 \\ 0 & 0 & 0 & I_w^{-1} & 0 & 0 & 0 \\ 0 & 0 & 0 & 0 & 0 & 0 & 0 \\ 0 & 0 & 0 & 0 & 0 & 0 & 0 \end{bmatrix} \begin{bmatrix} N^{fault}_{rw,1} \\ N^{fault}_{rw,2} \\ N^{fault}_{rw,3} \\ N^{fault}_{rw,4} \\ \mathrm{m}^{fault}_{mt,1} \\ \mathrm{m}^{fault}_{mt,2} \\ \mathrm{m}^{fault}_{mt,3} \end{bmatrix} \tag{I.5}$$

For more details please refer to [33].

Bibliography

[1] AAU. *AAU STUDENT SPACE*. Mar. 18, 2018. URL: http://www.space.aau.dk/.

[2] "Andy". *How many satellites are orbiting the Earth in 2017?* Oct. 15, 2017. URL: https://www.pixalytics.com/sats-orbiting-earth-2017/.

[3] József Bokor and Zoltán Szabó. “Fault detection and isolation in nonlinear systems”. In: *Annual Reviews in Control* 33.2 (2009), pp. 113–123. ISSN: 1367-5788. DOI: https://doi.org/10.1016/j.arcontrol.2009.09.001. URL: http://www.sciencedirect.com/science/article/pii/S136757880900056X.

[4] directory.eoportal.org. *AAUSAT*. URL: directory.eoportal.org (visited on 03/15/2018).

[5] Reid G. Reynolds and Landis Markley. “Maximum Torque and Momentum Envelopes for Reaction Wheel Arrays”. In: 33 (July 2001).

[6] Angel Mario Cano Garza. “Reaction Wheels for Picosatellites”. In: 23.2 (Dec. 2008), p. 75.

[7] Chris Hall. *Reference Frames for Spacecraft Dynamics and Control*. URL: http://www.dept.aoe.vt.edu/~cdhall/courses/aoe4140/refframes.pdf (visited on 03/15/2018).

[8] Flemming Hansen. *CubeSats*. Aug. 13, 2001. URL: http://www.space.aau.dk/cubesat/documents/CubeSat_Presentation.pdf (visited on 03/18/2018).

[9] Rasmus Holst. *Satellite Attitude Control Using Magnetorquers With Magnetic Dipole Moment Cancellation*. Aalborg University, 2014.

[10] Zuliana Ismail and Renuganth Varatharajoo. “Satellite Attitude Control Using Only Electromagnetic Actuationl”. In: *phdThesis* (2010), pp. 20–22. ISSN: 0273-1177. DOI: https://doi.org/10.1016/j.asr.2009.11.004. URL: http://www.sciencedirect.com/science/article/pii/S0273117709007078.

[11] Kasper Fuglsang Jensen and Kasper Vinther. *Attitude Determination and Control System for AAUSAT3*. Aalborg University, 2010.

[12] jie-chen. *ROBUST RESIDUAL GENERATOR FOR MODEL-BASED FAULT DIAGNOSIS OF DYNAMIC SYSTEMS*. 1st ed. 1995.

[13] Tor A. Johansen and Thor I. Fossen. “Control allocation—A survey”. In: *Automatica* 49.5 (2013), pp. 1087–1103. ISSN: 0005-1098. DOI: https://doi.org/10.1016/j.automatica.2013.01.035. URL: http://www.sciencedirect.com/science/article/pii/S0005109813000368.

[14] Dr. T.S. Kelso. *Orbital Coordinate Systems*. URL: https://www.celestrak.com/columns/v02n01/ (visited on 03/15/2018).

[15] Ibrahim Kök. *Comparison and Analysis of Attitude Control Systems of a Satellite Using Reaction Wheel Actuators*. URL: http://www.diva-portal.org/smash/get/diva2:1020537/FULLTEXT02.

[16] İbrahim Kök. “LOW NOISE FIVE-AXIS MAGNETIC BEARING REACTION WHEEL”. In: *A Thesis Presented to University of Würzburg and Lulea University of Technology* (2012). URL: http://www.diva-portal.org/smash/get/diva2:1020537/FULLTEXT02.pdf.

[17] Jack B. Kuipers. “Quaternions and rotation sequencest”. In: (Sept. 2007), p. 7.

[18] Saroj Kumar et al. “Design and development of 3-axis reaction wheel for STUDSAT-2”. In: *2015 IEEE Aerospace Conference* (2015), pp. 1–13.

[19] F. Landis Markley and John L. Crassidis. *Fundamentals of Spacecraft Attitude Determination and Control*. 1st ed. Springer, 2014.

[20] C. G. Mayhew, R. G. Sanfelice, and A. R. Teel. “Robust global asymptotic attitude stabilization of a rigid body by quaternion-based hybrid feedback”. In: *Proceedings of the 48h IEEE Conference on Decision and Control (CDC) held jointly with 2009 28th Chinese Control Conference*. Dec. 2009, pp. 2522–2527. DOI: 10.1109/CDC.2009.5400431.

[21] Thibaud Peers, Nikolaos Biniakos, and Alexandru-Cosmin Nicolae. *Formation flying of pico-satellites*. Aalborg University, 2017.

[22] Jeff Root. *ORBITAL SPEED*. URL: http://www.freemars.org/jeff/speed/index.htm.

[23] Izadi-Zamanabadi Roozbeh and Larsen Jesper Abildgaard. “Fully magnetic attitude control for spacecraft subject to gravity gradient”. In: (1999), p. 7.

[24] Peter B. de Selding. *SpaceX’s new price chart illustrates performance cost of reusability*. May 2, 2016. URL: http://spacenews.com/spacexs-new-price-chart-illustrates-performance-cost-of-reusability/ (visited on 03/18/2018).

[25] Raymond A. Serway and John W. Jewett. *Physics for Scientists and Engineers*. 6th ed. Thomson Brooks/Cole, 2004.

[26] Marcel J. Sidi. *Spacecraft dynamics and control*. 1st ed. Press Syndicate of the University of Cambridge, 1997.

[27] J. F. Trégouët et al. “Reaction Wheels Desaturation Using Magnetorquers and Static Input Allocation”. In: *IEEE Transactions on Control Systems Technology* 23.2 (Mar. 2015), pp. 525–539. ISSN: 1063-6536. DOI: 10.1109/TCST.2014.2326037.

[28] James R. Wertz. *Spacecraft attitude determination and control*. 7th ed. KluwerAcademicPublisher, 1994.

[29] James R. Wertz and Wiley J. Larson. *Space Mission Analysis and Design*. 3rd ed. Microcosm Press, 1999.

[30] Rafal Wisniewski. “A study of reaction wheel configurations for a 3-axis satellite attitude control”. In: *Advances in Space Research* 45.6 (1997), pp. 750–759. DOI: http://vbn.aau.dk/files/107993/fulltext. URL: http://vbn.aau.dk/files/107993/fulltext.

[31] Rafal Wisniewski and Mogens Blanke. "Fully magnetic attitude control for spacecraft subject to gravity gradient". In: (July 1998).

[32] Chang-liang Xia. *PERMANENT MAGNET BRUSHLESS DC MOTOR DRIVES AND CONTROLS*. 1st ed. Press Syndicate of the University of Cambridge, 2012.

[33] Y. Yang. "Spacecraft Attitude and Reaction Wheel Desaturation Combined Control Method". In: *IEEE Transactions on Aerospace and Electronic Systems* 53.1 (Feb. 2017), pp. 286–295. ISSN: 0018-9251. DOI: 10.1109/TAES.2017.2650158.